ENTHALPY-MASS FLUX-IMPACT PRESSURE-PROBE SYSTEM DESIGN FOR NASA ARMSEF FACILITY

T. J. O'Connor

AVCO CORPORATION
Systems Division
201 Lowell Street
Wilmington, Massachusetts 01887

AVSD-0094-70-CR

February 1970

National Aeronautics and Space Administration
Manned Spacecraft Center
Houston, Texas 77058

NASA CR108295

FOREWARD

This report was prepared by the Systems Division* of Avco Corporation, Wilmington, Massachusetts under National Aeronautics and Space Administration (NASA), Manned Spacecraft Center, Contract NAS 9-7984, Task Order No. 9. The work was administered under the direction of the Structures and Mechanics Division of the NASA Manned Spacecraft Center. The NASA Project Engineers were Messrs. J. Grimaud, D. Tillian and C. Scott.

This report covers work performed between 28 October 1968 to 27 February 1970.

Dr. R. R. John was the Avco Program Director and Messrs. H. E. Hoercher and T. J. O'Connor were Project Engineers. Acknowledgement of valuable assistance is due to Messrs. L. White, J. Cote, E. Comfort, J. Connors, D. Landry, T. Bernard and D. Mitchell for design, fabrication, assembly and in-house testing.

* Formerly Applied Technology Division and Space Systems Division.

ABSTRACT

The design of a probe system capable of measuring enthalpy, impact pressure and local mass flux within the hypersonic flow field produced by the NASA/MSC Atmospheric Reentry Materials and Structures Evaluation Facility (ARMSEF) is described. The design of the enthalpy probe, the mass flow measuring system, and flow meter calibration system are included in this report. Data obtained in evaluation of the probe system in the AVCO ROVERS and the NASA ARMSEF facilities are also discussed.

TABLE OF CONTENTS

TABLE OF CONTENTS (CONCL'D)

LIST OF ILLUSTRATIONS

LIST OF ILLUSTRATIONS (CONT'D)

LIST OF ILLUSTRATIONS (CONCL'D)

LIST OF TABLES

NOMENCLATURE

A	Area, ft^2
C_p	Heat Capacity, BTU/lb ^oF
D	Diameter, ft
D_e	Equivalent diameter, ft
E	Modulus of elasticity, lb/ft^2
f	Friction factor
h	Enthalpy, BTU/lb
$\mathfrak{h}$	Heat transfer coefficient, $BTU/ft^2\text{-}hr\text{-}^oF$
ΔH_{vap}	Heat of vaporization, BTU/lb_m
k	Thermal conductivity, $BTU/ft^2\text{-}hr\text{-}(^oF/ft)$
L	Length, ft
m	Poissons ratio
$\dot{m}$	Mass flow rate, lb/hr
M	Mach number
Nu	Nusselt number
p	Pressure, lb/ft^2
Pr	Prandtl number
$\dot{q}$	Heat flux, $BTU/ft^2\text{-}hr$
$\dot{Q}$	Heating rate, BTU/hr
r	Radius, ft
R_N	Nose radius, ft
R	Gas constant, $lb\text{-}ft/lb\text{-}^oR$
$\mathfrak{R}$	Recovery factor
Re	Reynolds number
S	Stress, lb/ft^2
t	Time, sec

NOMENCLATURE (CONT'D)

T	Temperature, ^{o}R
u	Velocity, ft/hr
x	Distance along surface, ft
y	Distance perpendicular to surface, ft
z	Vertical distance, ft
α_T	Thermal expansion coefficient, $(^{o}R)^{-1}$
γ	Ratio of specific heats
ρ	Density, lb/ft^3
μ	Viscosity, lb/ft-hr
ψ	Stream function
σ	Surface tension, lb/ft
θ	Angle, degrees

SUBSCRIPTS

b	Bulk mean
e	External
g	Gas
N	Nozzle
0	Stagnation
p	Probe
sat	Saturation
w	Wall
∞	Free stream

I. INTRODUCTION

Probes of various types have been employed to determine gas enthalpy and mass flux in subsonic flow fields(1). The most successful of these thermodynamic probes for subsonic flow field diagnostic studies are the tare probes(1,2,3). Typical examples of the experimental data obtained with the tare probe are reported in References 3 and 4. The concept of a tare probe requires that the assumption be made that the total heating to the external probe surface is identical during the tare and gas sampling modes of operation. It is obvious that the error in the enthalpy determined with such a device due to this necessary assumption is simply the ratio of the difference in external heat transfer for the two modes of operation to the heat removed from the gas sample during the sampling mode. Although the errors associated with the necessity of obtaining a tare measurement may be small in a subsonic flow field, there is little or no information concerning the magnitude of these errors in supersonic flows.

The ideal enthalpy probe for use in supersonic flow fields is one which will completely eliminate the necessity of a tare measurement. Such an instrument in general would consists of two basic portions: an inner calorimetric probe, and an outer water-cooled probe to protect it from the external environment. When the calorimetric section is properly insulated from the outer water-cooled probe, the enthalpy of a gas sample drawn through an aspirating tube located on the probe axis may be determined from an energy balance on the calorimetric section cooling water and the gas sample:

$$h = (\dot{m} c_p)_{H_2O} \Delta T / \dot{m}_g + c_{p_g} (T_g - T_o) \qquad (1)$$

where ΔT is the coolant temperature rise, T_g is the temperature of gas sample as it leaves the calorimetric section and T_o is any convenient base temperature for the enthalpy computation.

In addition to its ability to accurately determine enthalpy, the ideal probe should be capable of measuring the local mass flux (ρu). Hence, the tip of the probe must be such that at supersonic and hypersonic velocities the shock at the leading edge of the sampling tube is essentially an attached shock. With this shock structure, a stream tube having a cross-sectional area equal to that of the sampling tube would enter the probe prior to passing through a system of oblique shocks downstream of the leading edge of the calorimetric probe. The probe can easily be made into an impact pressure measuring device simply by placing a pressure transducer and valve in the sampling line.

With an instrument which accurately measured gas enthalpy, mass flux, and impact pressure at hypersonic speeds the local values of density and velocity as well as enthalpy may also be determined without any assumption as to the degree of chemical equilibrium within the stream. For example, for Mach numbers in excess of 5.0, the ratio of impact pressure to free stream momentum ($p_{o_2} / \rho_\infty u_\infty^2$) has an asymptotic value in the range of 0.92-0.95 for specific heat ratios between 1.2 and 1.4(5). Successful operation of the instrument as a mass flux probe therefore implies:

$$p_{o_2} / \rho_\infty u_\infty = 0.95\, u_\infty \qquad (2)$$

and

$$\rho_\infty = 0.95\, (\rho_\infty u_\infty)^2 / p_{o_2} \qquad (3)$$

The knowledge of local density, enthalpy, and velocity provides an accurate description of the environment produced by a plasma generator. In addition, these data when employed with a chemical equilibrium program would result in additional information concerning the nature of the expansion process within the exit nozzle of the plasma generator.

The design of an enthalpy-mass flux-impact pressure probe system for use in the hypersonic exhaust jet was accomplished keeping the general requirements of an ideal probe in mind. The design of the instrument required detailed evaluation of the local heat transfer rates, the establishment of proper coolant flow rates for various facility operating conditions, stress analysis to insure the survival of the instrument. Each of these facets of the probe design are described in the remaining sections of this report.

II. DESCRIPTION

The probe system designed to measure impact pressure, mass flux, and enthalpy in the supersonic exhaust jet produced by the NASA/MSC ARMSEF facility consists of three basic subsystems: the probe system, the mass flow measuring system, and the mass flow calibrating system. Each probe sub-system is described below.

A. Probe Description

The enthalpy-mass flux-impact pressure probe designed for use in the ARMSEF facility is composed of an inner calorimetric probe, an outer probe, and a probe strut.

The inner calorimetric probe basically consists of a gas sampling tube (0.250 inch diameter) which is provided with two concentric annular cooling passages. Cooling water enters the calorimetric probe through the outer annular passage, makes a 180 degree turn at the probe tip and flows toward the rear of the probe through the inner annular channel which is adjacent to the gas aspirating tube located on the probe axis. In its path from the probe tip, the coolant flow absorbs energy from any gas being aspirated through the probe. Since an accurate measurement of gas enthalpy with energy balance techniques requires that there be little or no heat transfer between the inner and outer probe, over 95 percent of the interface between these two portions of the probe were provided with insulation in the form of either low conductivity material or dead air space. To minimize heat transfer in the remaining portion of the interface, coolant flow passages were routed so as to minimize the temperature difference between the two streams.

The external probe is similar to the inner calorimetric probe in that it consists of a 1.00 inch diameter body containing two concentric annular cooling passages. In contrast, to the inner calorimetric probe, the outer probe coolant flows through the inner annular passage to the probe tip and returns through the outer annulus. The internal configuration of this portion of the system is designed to accomodate the inner calorimetric probe. The total length of the internal and external probe bodies are such that the leading edges of the two probes lie in the same plane. When assembled, the inner and outer probe are designed to fit into a socket located on the top of the probe strut.

The water cooled strut has a total length of 36 inches making it possible for the probe to traverse a 30 inch diameter exhaust stream. The forward and trailing edges of the strut are semi-circular cylinders both of which have a diameter of 0.750 inch. The maximum width of the strut is also 0.750 inch and the length of the strut parallel to the gas stream is 3.250 inches. The cooling requirements of the strut are satisfied by cooling water flowing through 0.062 inch wide channels immediately behind the external copper shell. The interior of the strut has provisions for allowing passage of cooling water to both the external, and internal probes as well as a tube for aspirating gas through the probe. In addition, all thermocouples required for measurement of probe coolant temperature rise and the temperature of the aspirated gas sample are located within the strut.

B. Gas Sampling System Description

The gas sampling system consists of a vacuum pump required for aspirating gas through the probe and a flow meter to measure the gas sample flow rate. The vacuum pump is a commercially available item while the gas flow meters are Venturi flow meters. In addition to these basic items the sampling system includes the necessary piping, valves and instrumentation required for successful operation of the entire system as a mass flux measuring device.

C. Gas Mass Flow Calibrating System

The flow meter calibrating system provides a means of introducing accurately known flow rates through the Venturi flow meters and hence a means of calibrating the meters. Gas of any desired composition may be introduced from a series of tanks of specified volume, through sonic orifices into the gas sample lines.

III. PROBE DESIGN

EXTERNAL PROBE FLOW FIELD

A. Conical Probe Tip

In hypersonic flow, the inviscid velocity, density and pressure distributions about an open nosed, conical body of revolution may be obtained from the predictions of Chernyi[6] for the body shown in Figure 1. The results of Chernyi's analysis are

$$u = u_\infty \cos\theta + \left(\frac{\gamma-1}{\gamma+1}\right) u_1 \tag{4}$$

$$p = \rho_\infty u_\infty^2 \sin^2\theta + \left(\frac{\gamma-1}{\gamma+1}\right) p_1 \tag{5}$$

$$\rho = \left(\frac{\gamma+1}{\gamma+1}\right)\rho_0 + \rho_1 = \left(\frac{\gamma+1}{\gamma-1}\right) \frac{\rho_\infty}{1+\left(\frac{2}{\gamma-1}\right)\left(\frac{1}{M\sin\theta}\right)^2} \tag{6}$$

where

$$u_1 = -u_\infty\left(\frac{\sin^2\theta}{\cos\theta}\right)\left(1+\frac{2}{\gamma-1}\cdot\frac{1}{M^2\sin^2\theta}\right)\cdot\frac{\psi+\rho_\infty u_\infty r_0^2}{2\psi+\rho_\infty u_\infty r_0^2} \tag{7}$$

$$p_1 = \rho_\infty u_\infty^2 \sin^2\theta\left(1+\frac{2}{\gamma-1}\cdot\frac{1}{M^2\sin^2\theta}\right)\left(1+\frac{1}{4}\left[1+\frac{r_0^2}{r^2}\right]^2-\left[\frac{\psi}{\rho_\infty u_\infty r^2}\right]\right) - \rho_\infty u_\infty^2 \sin^2\theta - p_\infty \tag{8}$$

$$\rho_1 = \rho_0\left\{\frac{\rho_\infty}{\gamma\rho_0}\left[\frac{1}{4}\left(1+\frac{r_0^2}{r^2}\right)^2-\left(\frac{\psi}{\rho_\infty u_\infty r^2}\right)^2\right]+\frac{4}{(\gamma-1)M^2\sin^2\theta} + \left(\frac{\rho_\infty u_\infty r_0^2}{2\psi+\rho_\infty u_\infty r_0^2}\right)\left[\frac{4}{(\gamma-1)M^2\sin^2\theta}-\frac{\rho_\infty}{\gamma\rho_0}\right]\right\} \tag{9}$$

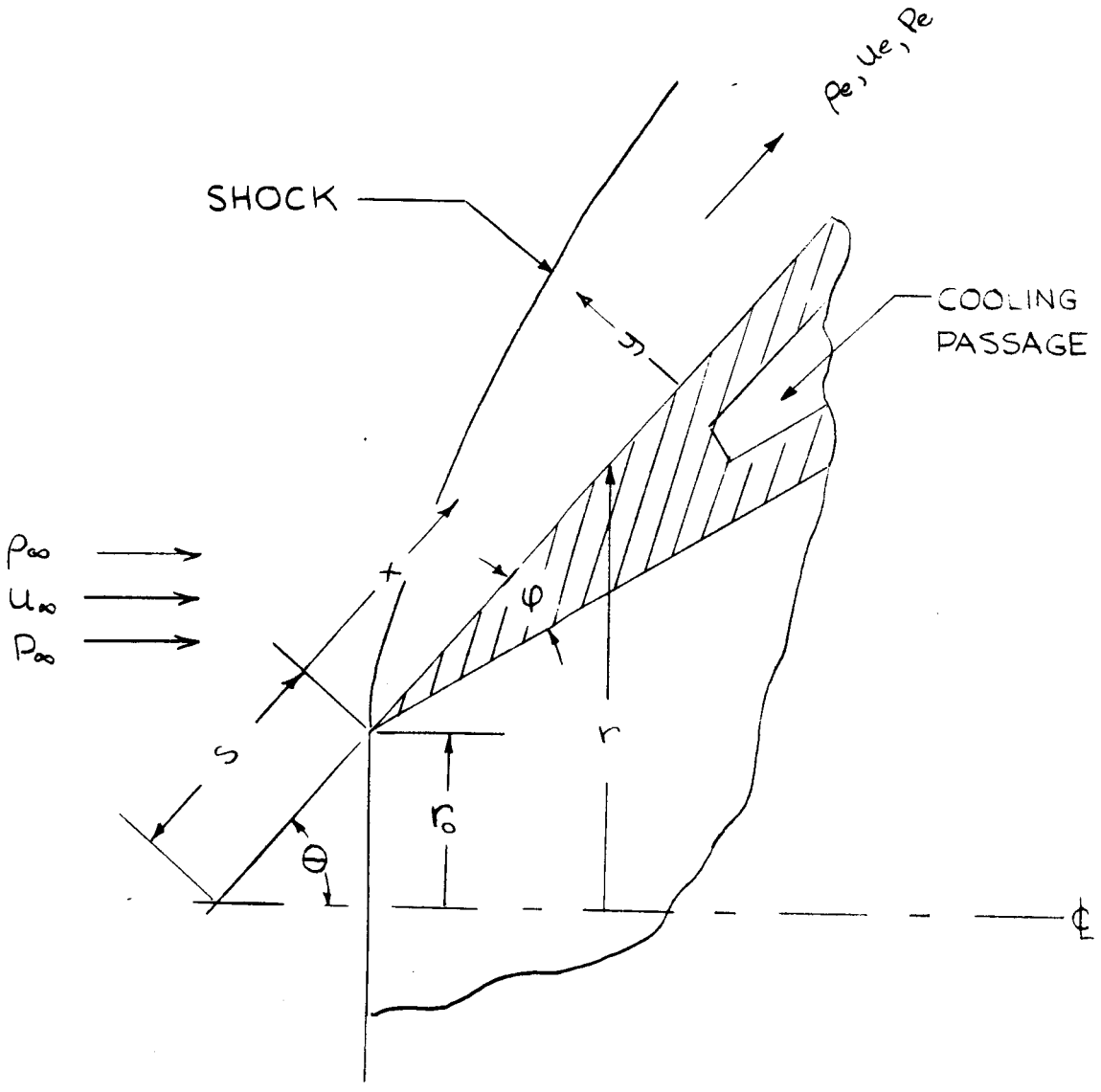

FIG. 1 EXTERNAL PROBE TIP GEOMETRY

and the stream function (Ψ) defined as

$$\Psi \equiv \left(\frac{\gamma-1}{\gamma+1}\right) \frac{\rho_\infty u_\infty r y \cos\theta}{1+\left(\frac{2}{\gamma-1}\right)\left(\frac{1}{M^2\sin^2\theta}\right)} \tag{10}$$

The pressure distribution on the surface of the body is given by:

$$p-p_\infty = \rho_\infty u_\infty^2 \sin^2\theta \left\{1+\frac{1}{4}\left(\frac{\gamma-1}{\gamma+1}\right)\left(1+\frac{2}{(\gamma-1)M^2\sin^2\theta}\right)\left(1+\frac{1}{\left(1+\frac{x\sin\theta}{r_o}\right)^2}\right)^2\right\} \tag{11}$$

These property distributions were applied in conjunction with the local similarity relationships to determine the heating distribution over the conical surface. From local similarity:

$$\dot{q}_{cw} = \frac{\dot{q}_{cw,s}}{\left\{\rho_{w_s}\mu_{w_s}\left(\frac{du_e}{dr}\right)_s\right\}^{1/2}} \frac{\rho_{w_e}\mu_{w_e}u_e r}{2\left[\int_0^x \rho_{w_e}\mu_{w_e}u_e r^2 dx\right]^{1/2}} \tag{12}$$

with the stagnation point velocity gradient given by

$$\left(\frac{du_e}{dr}\right)_s \simeq \frac{u_\infty}{R_N}\left(\frac{2\rho_\infty}{\rho_s}\right)^{1/2} \tag{13}$$

Since the velocity close to the surface, as predicted by equation 4, is not a function of distance along the surface, and if it is assumed that the surface temperature is not a function of position, then the heating distribution is simply:

$$\dot{q}_{cw} = \frac{1}{2}\frac{\dot{q}_s\sqrt{R_N}}{(2\rho_\infty/\rho_s)^{1/4}}\left(\frac{\rho_e u_e}{\rho_s u_\infty}\right)^{1/2}\left\{\frac{\rho_e r^2}{\int_0^x \rho_e r^2 dx}\right\}^{1/2} \tag{14}$$

Numerical integration of the pressure distribution for conical tips having half-angles of 30 and 40 degrees demonstrated (Figure 2) that over the Mach number range of 3.0 to 5.6 that

$$\left\{\frac{\frac{p_e}{p_a}\left(\frac{r}{r_o}\right)^2}{\int_0^x \frac{p_e}{p_a}\left(\frac{r}{r_o}\right)^2 dx}\right\}^{1/2} = 2.12\ x^{-0.375} \tag{15}$$

FIG 2 PRESSURE DISTRIBUTION

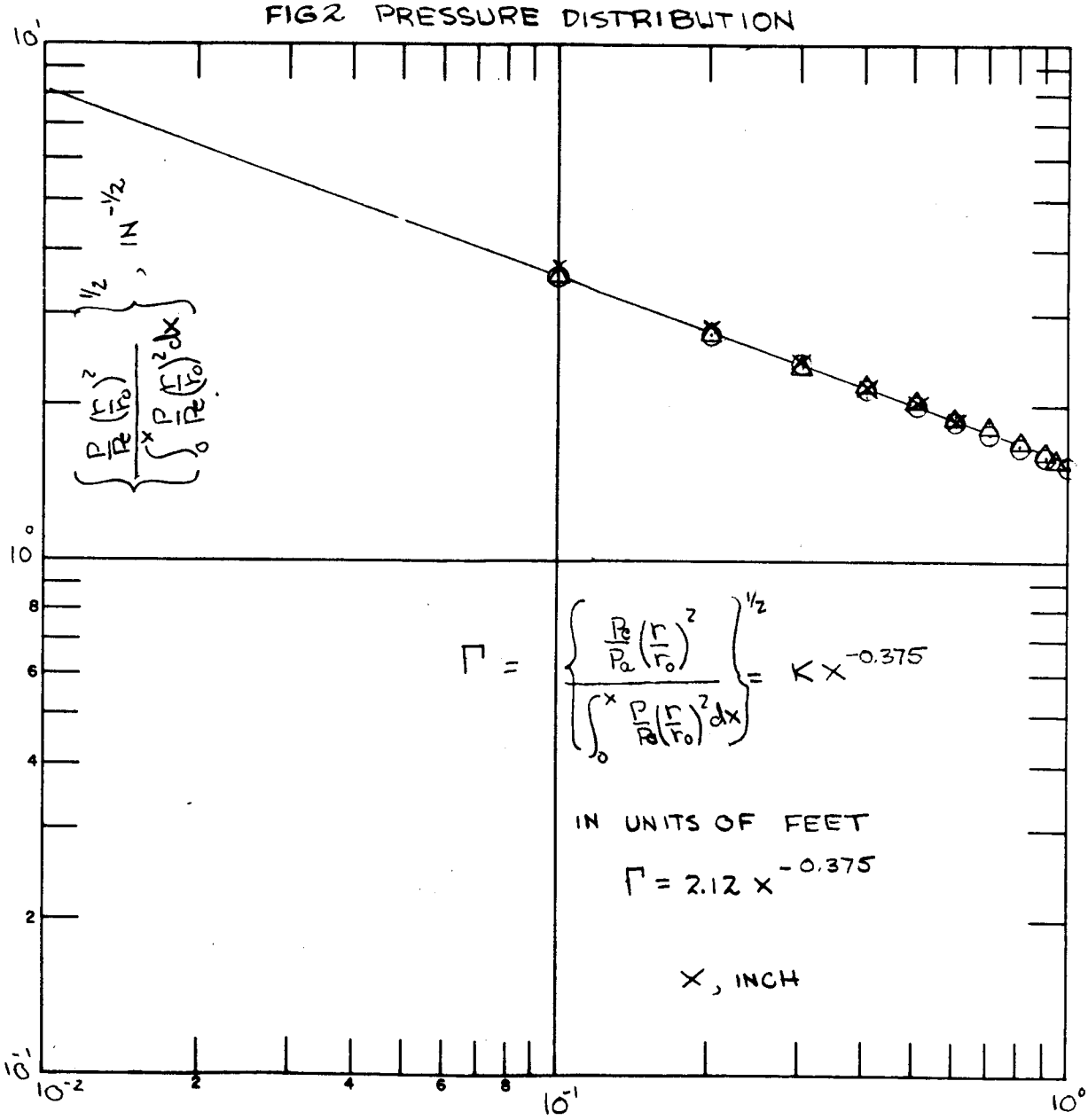

Therefore

$$\dot{q}_{cw} = 1.06 \left(\dot{q}_{cw_s} \sqrt{R_N} \right) \left(\frac{P_e u_e}{P_\infty u_\infty} \frac{P_\infty}{P_s} \right)^{1/2} \frac{x^{-0.375}}{(2 \rho_\infty / \rho_s)^{1/4}} \tag{16}$$

which upon substituting the relationships

$$\left(\frac{P_e}{P_\infty} \right)^{1/2} x^{-0.375} = K(M_\infty) x^{-0.40} \tag{17}$$

as shown in Figure 3 results in

$$\dot{q}_{cw} = \frac{1.06 \ \dot{q}_{cw} \sqrt{R_N}}{(2 \rho_\infty / \rho_s)^{1/4}} \left(\frac{P_\infty}{P_s} \frac{u_e}{u_\infty} \right)^{1/2} K(M_\infty) x^{-0.40} \tag{18}$$

If a function defined as

$$f(M_\infty) = \frac{K(M_\infty)}{(\rho_\infty / \rho_s)^{1/4}} \left(\frac{P_\infty \ u_e}{P_s \ u_\infty} \right)^{1/2} \tag{19}$$

it is found to be a function of probe tip half angle alone. Upon substitution of this relationship into equation 18 the final form of the tip heating distribution is found to be

$$\dot{q}_{cw} = 0.715 \left(\dot{q}_s \sqrt{R_N} \right) x^{-0.4} \qquad \theta = 30^\circ \tag{20}$$

$$\dot{q}_{cw} = 0.790 \left(\dot{q}_s \sqrt{R_N} \right) x^{-0.4} \qquad \theta = 40^\circ \tag{21}$$

where x is the distance along the heated surface. The heating distributions predicted by these relationships are illustrated in Figure 4 . A comparison if the heating rates calculated by equation 20 and the results of computer calculations[7] demonstrated that the two methods were in excellent agreement.

The total heat input to the probe tip is simply

$$\dot{Q} = \int_0^x \dot{q}(x) \, dA \tag{22}$$

where

$$dA = 2\pi (x+s) \sin\theta \, dx \tag{23}$$

$$\dot{q}(x) = C \ \dot{q}_s \sqrt{R_N} \ x^{-0.4} \tag{24}$$

FIG 3 PRESSURE FUNCTION

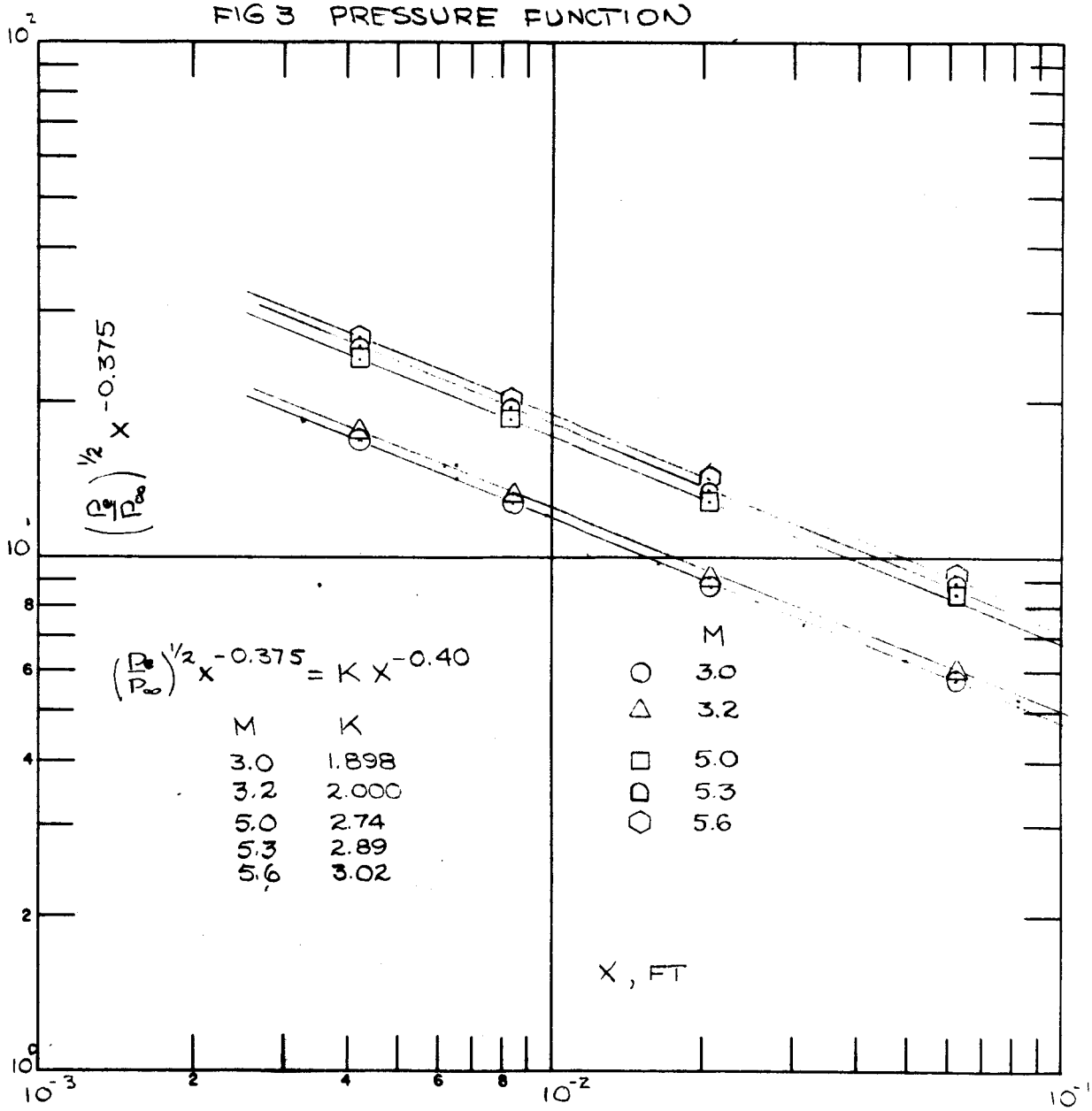

FIG 4 TIP HEATING RATES

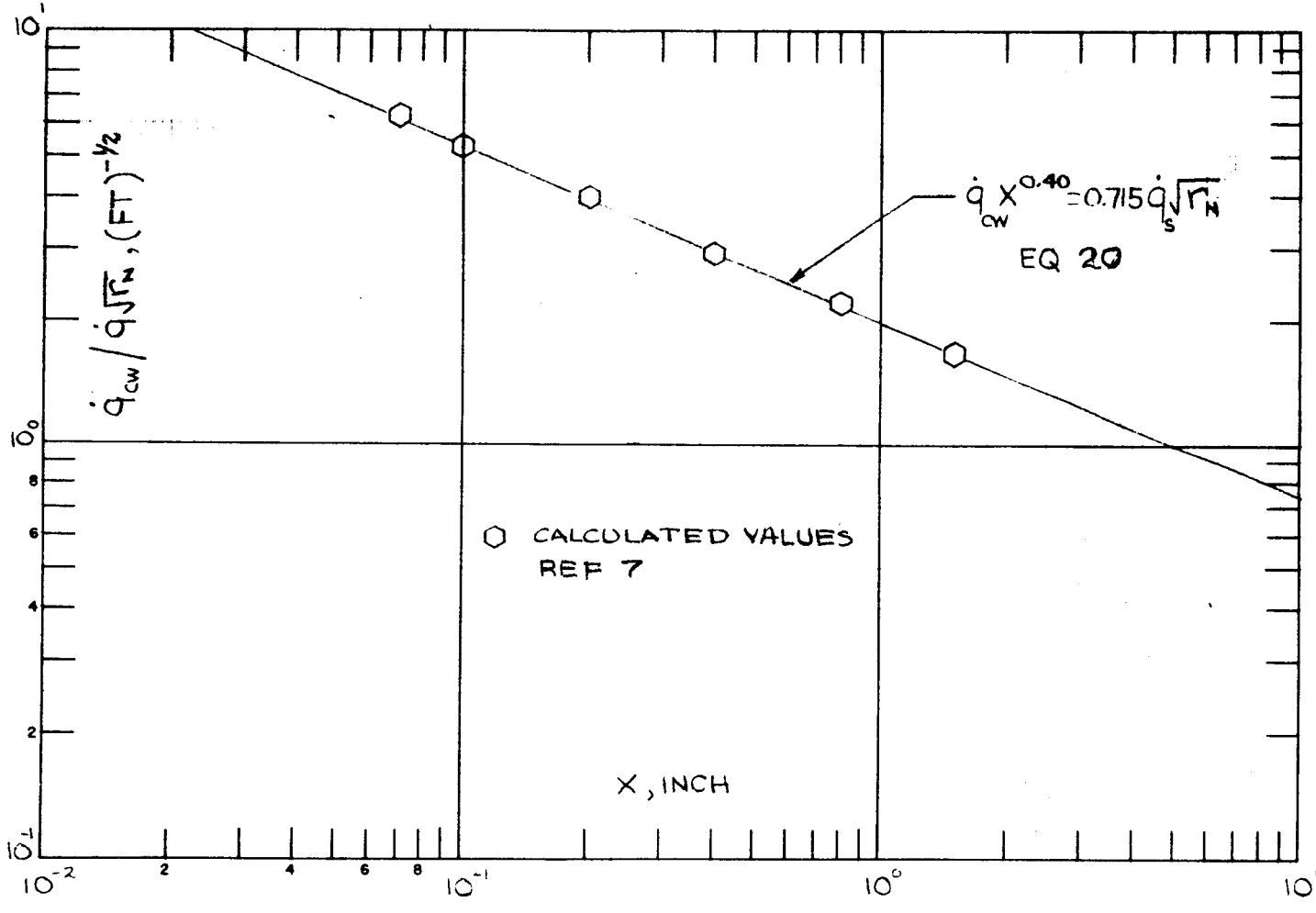

which results in

$$\dot{Q} = 2\pi S^{1.6} C \sin\theta \, \dot{q}_s \sqrt{R_N} \left(\frac{x}{S}\right)^{0.6} \left\{\frac{5}{3} + \frac{5}{8}\frac{x}{S}\right\} \tag{25}$$

where the quantity, $S^{1.6}C \sin\theta$, has values of $0.82\, r_o^{1.6}$ and $0.84 r_o^{1.6}$ for tip half angles of 40 and 30 degrees, respectively. The resulting relationship (Figure 5) indicates that for a probe tip having an internal diameter of 0.250 inch and an external diameter of 1.000 inch, the total heat input to the tip is simply

$$\dot{Q} = 0.03 \, \dot{q}_s \sqrt{R_N} \tag{26}$$

It is also of interest to consider the temperature distribution produced by the external heating within that portion of the probe tip which is forward of the internal cooling passages. The temperature distribution can be estimated from an integral energy balance with the assumption that temperature gradients normal to the heated surface are small in comparison to variations parallel to the exposed surface. With this assumption the energy balance relationship is

$$k A_w \frac{dT}{dx} + \int_o^x \dot{q}_{cw} \, dA_s = 0 \tag{27}$$

where

$$dA_s = 2\pi (S+x) \sin\theta \, dx \tag{28}$$

$$A_w = \pi S^2 \sin\theta \left\{\frac{x}{S}\tan\varphi\left[2\left(\frac{x}{S}+1\right) - \frac{x}{S}\tan\varphi\cot\theta\right]\right\} \tag{29}$$

and

$$\int_o^x \dot{q}_{cw} dA_s = 2\pi S^{1.6} \sin\theta C \, \dot{q}_s \sqrt{R_N} \left(\frac{x}{S}\right)^{0.6} \left\{\frac{5}{3} + \frac{5}{8}\frac{x}{S}\right\} \tag{30}$$

Therefore

$$\frac{dT}{dx} = \frac{1.67 C \dot{q}_s \sqrt{R_N}}{k \tan\varphi} \left\{ \frac{1 + \frac{3}{8}\frac{x}{S}}{\left(\frac{x}{S}\right)^{0.4}\left\{1 + \frac{x}{S}\left(1 - \frac{\tan\varphi\cot\theta}{2}\right)\right\}} \right\} \tag{31}$$

or

$$\frac{\tan\varphi}{1.67 C} \frac{k \Delta T}{(\dot{q}_s \sqrt{R_N}) S} = \int_0^{x/S} \frac{1 + 3/8 \, \frac{x}{S}}{1 + \frac{x}{S}\left(1 - \frac{\tan\varphi\cot\theta}{2}\right)} \frac{d(x/S)}{(x/S)^{0.4}} \tag{32}$$

FIG 5
PROBE TIP HEAT INPUT

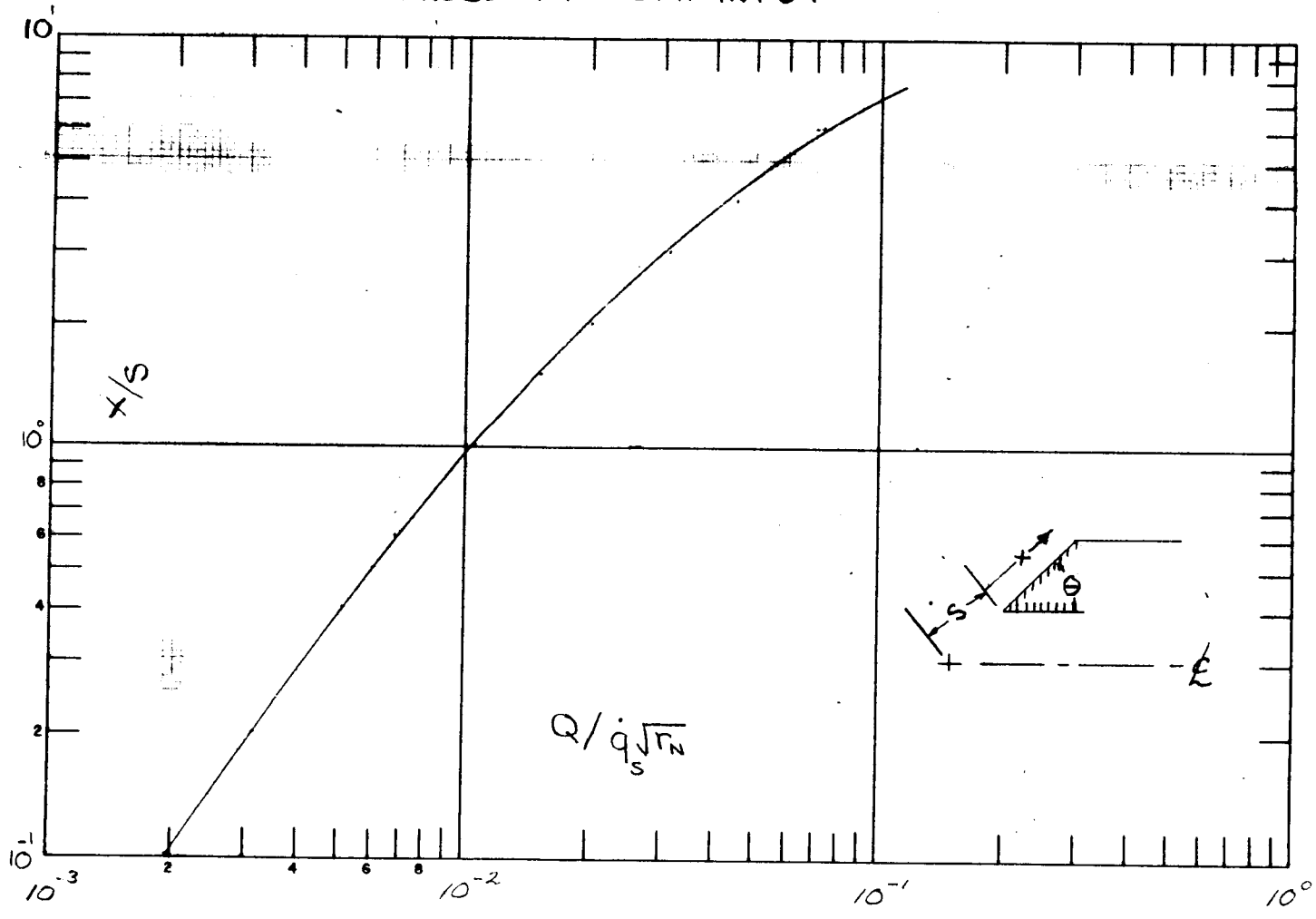

The right-hand side of this equation may be expanded in a power series and then integrated to yield

$$\frac{\tan\varphi}{1.67C}\frac{k\,\Delta T}{(\dot{q}_s\sqrt{R_N})S} = \frac{1}{0.6}\left(\frac{x}{S}\right)^{0.6} + (\alpha-\beta)\left\{\frac{1}{1.6}\left(\frac{x}{S}\right)^{1.6} - \frac{\beta}{2.6}\left(\frac{x}{S}\right)^{2.6} + \frac{\beta^2}{3.6}\left(\frac{x}{S}\right)^{3.6} - \ldots\right\} \quad (33)$$

with

$$\alpha = 0.375 \quad (34)$$

$$\beta = 1 - \frac{\tan\varphi \cot\theta}{2} \quad (35)$$

The resulting temperature distributions for tip half angles of 30 and 40 degrees are illustrated in Figure 6. It is noticed that at a stagnation point heating rate ($\dot{q}_s\sqrt{R_N}$) of 600 Btu/ft$^{3/2}$-sec a uncooled tip length of 0.20 inch that the leading edge is 1230°F and 700°F higher in temperature than the cooling passage walls with tip half angles of 30 and 40 degrees, respectively.

B. External Probe Body

In order to determine the heat transfer to the cylindrical main body of the probe, the flow along the probe tip was assumed to pass through a Prandtl-Meyer expansion having a turning angle equal to the tip half angle. The Mach number at the rear of the conical tip (M_1) was determined from the predictions of Chernyi as to the local density, pressure, and velocity, and the definition of Mach number

$$M = u/(\gamma P/\rho)^{1/2} \quad (36)$$

Therefore,

$$\frac{M_1}{M_\infty} = \frac{u_1}{u_\infty}\left(\frac{P_\infty}{P_1}\frac{\rho_1}{\rho_\infty}\right)^{1/2} \quad (37)$$

In order to simplify the heating analysis it was assumed that the pressure, velocity, and density remained constant along the entire length of the cylindrical probe body. The heat transfer rate was obtained from the standard laminar flat plate relationship[8]

$$q_{cw} = \frac{0.664}{2\,Pr^{0.4}}\left(\frac{\rho^+\mu^+}{\rho_e\mu_e}\right)^{0.5}\frac{\rho_e u_e h_s}{(Re_x)^{0.5}} \quad (38)$$

where starred quantities are evaluated at the reference enthalpy

$$\frac{h^+}{h_e} = 1 + 0.5\left(\frac{h_w}{h_e} - 1\right) + 0.22R\left(\frac{h_s}{h_e} - 1\right) \quad (39)$$

with R being the recovery factor, and the static enthalpy (he) in the external flow field given by

FIG. 6
EXTERNAL TIP TEMPERATURE DISTRIBUTION

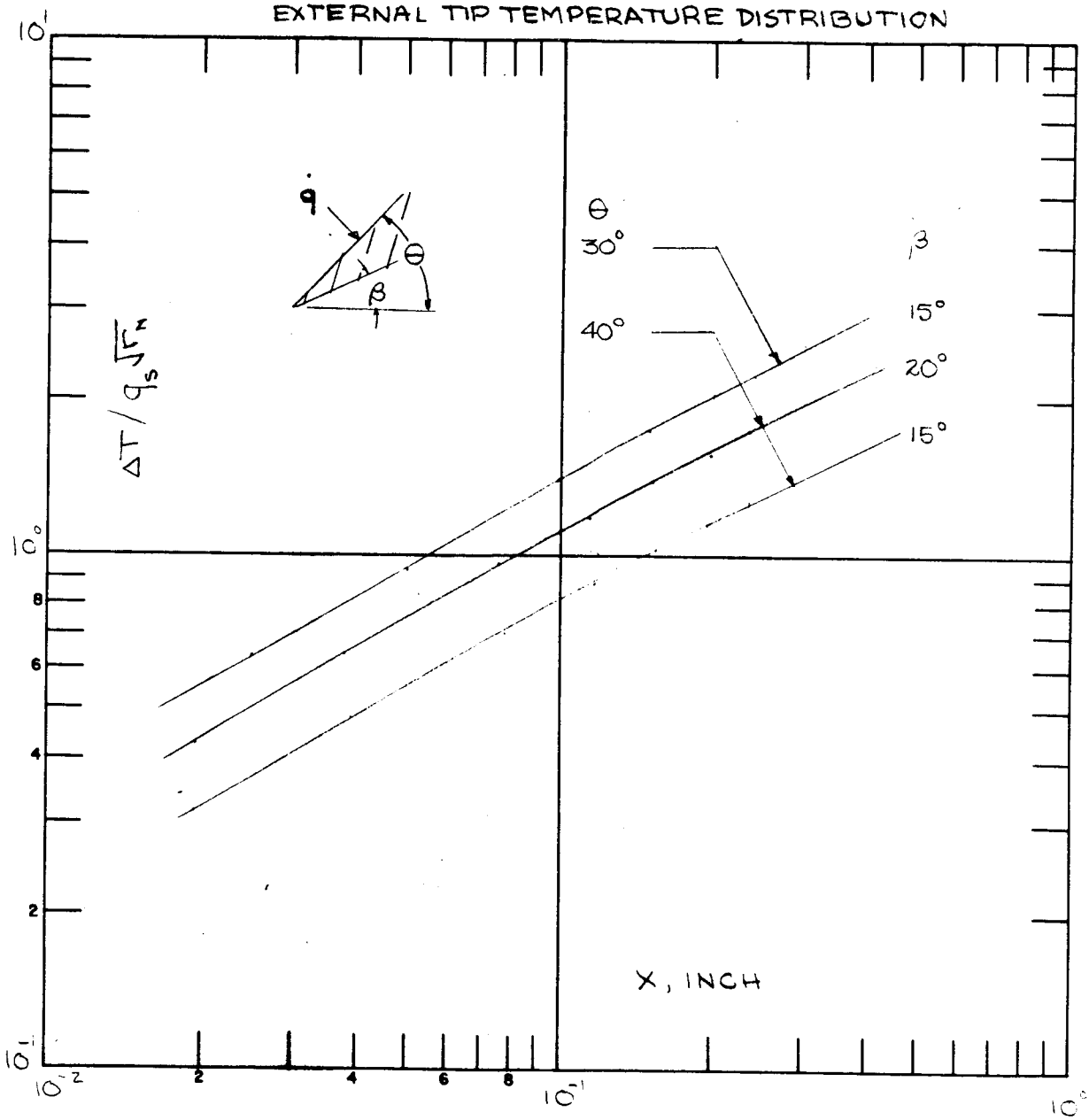

$$\frac{h_e}{RT_o} = \frac{h_s}{RT_o} - \frac{1}{2}\frac{u_e^2}{RT_o} \tag{40}$$

The resulting heating rates as a function of the stagnation point heat transfer ($\dot{q}_s\sqrt{R_N}$) are presented in Figure 7. Since there was little or no difference between the results obtained with the two tip configurations both bodies may be considered to have the same heating distribution (Figure 8).

The total heat input to the cylindrical probe body may be obtained by integrating the local heating rates over the entire surface

$$\dot{Q} = 2\pi r \int_{x_1}^{x_1+L} \dot{q}\, dx \tag{41}$$

$$= 2\pi r_m \dot{q}\sqrt{x} \int_{x_1}^{x_1+L} \frac{dx}{x^{1/2}} \tag{42}$$

with the lower limit of integration being

$$\frac{x_1}{r_o} = \left(\frac{r_m}{r_o} - 1\right)\frac{1}{\sin\theta} = \frac{3}{\sin\theta} \tag{43}$$

for a probe body having inner and outer radii of 0.125 and 0.500 inch, respectively. Hence

$$\dot{Q} = 4\pi r_m \dot{q}\sqrt{x}\left(\frac{3r_o}{\sin\theta}\right)^{1/2}\left\{\left[1 + \frac{L\sin\theta}{3r_o}\right]^{1/2} - 1\right\} \tag{44}$$

The total heat input to this portion of the probe system is depicted in Figure 9. At a stagnation point heating rate, ($\dot{q}_s\sqrt{R_N}$), of 600 Btu/ft$^{3/2}$-sec the total heat input to an 8 inch long cylindrical section would be 25 Btu/sec and 28 Btu/sec for probes having tip half angles of 30 and 40 degrees, respectively.

C. Rear Sections of Probe

The rear sections of the probe consist of a open nosed conical section which is used to securely fasten the external probe to the mounting socket on the top of the strut, and the external surfaces of the mounting socket. The open nosed conical fastener has a 30° half angle, and minimum and maximum diameters of 1.00 inch and 1.312 inch, respectively. The external diameter of the mounting socket is 1.312 inch and it has an overall length of 3.500 inches.

FIG 7 EXTERNAL PROBE BODY HEATING

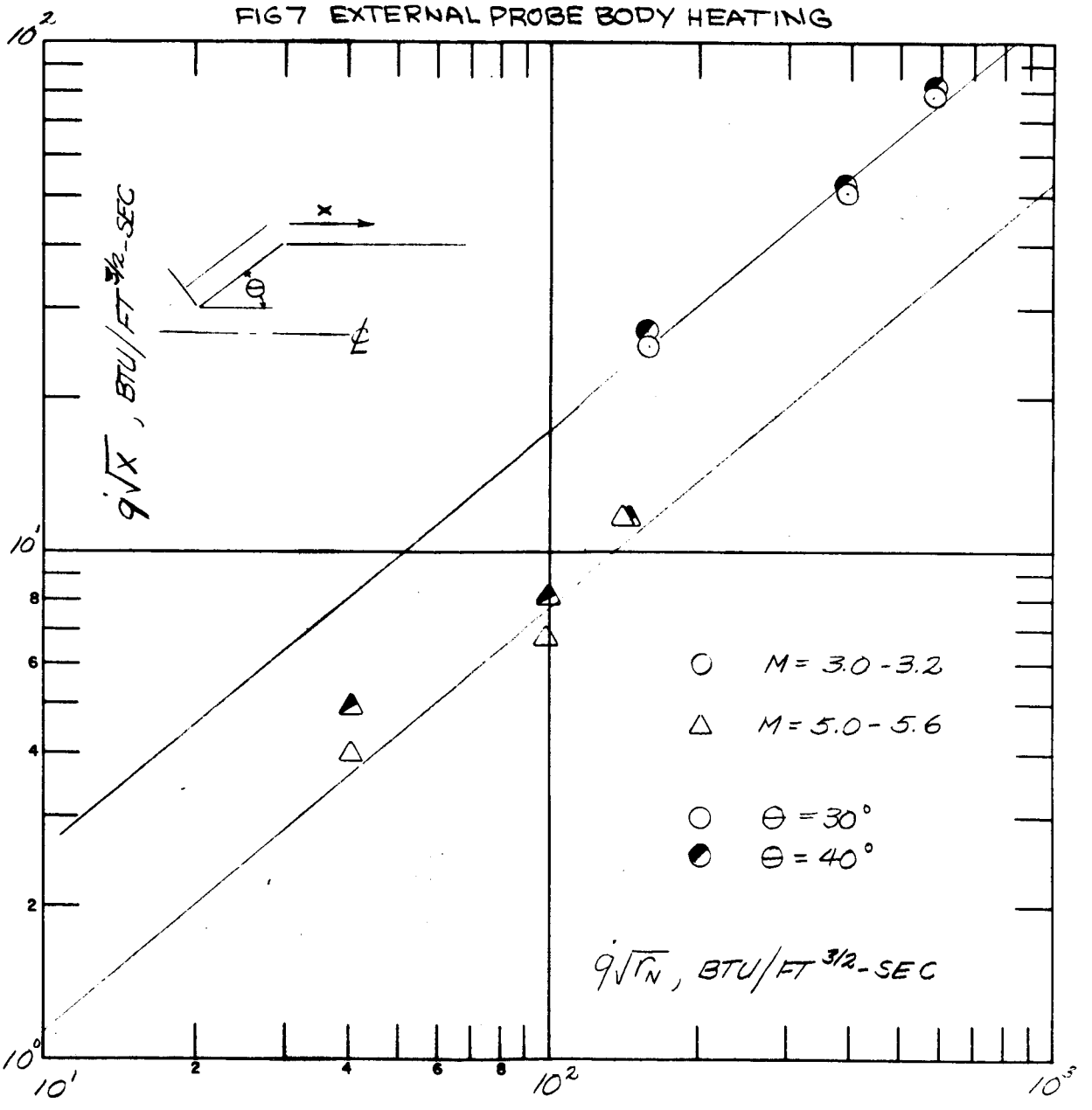

FIG. 8
EXTERNAL BODY HEATING RATES

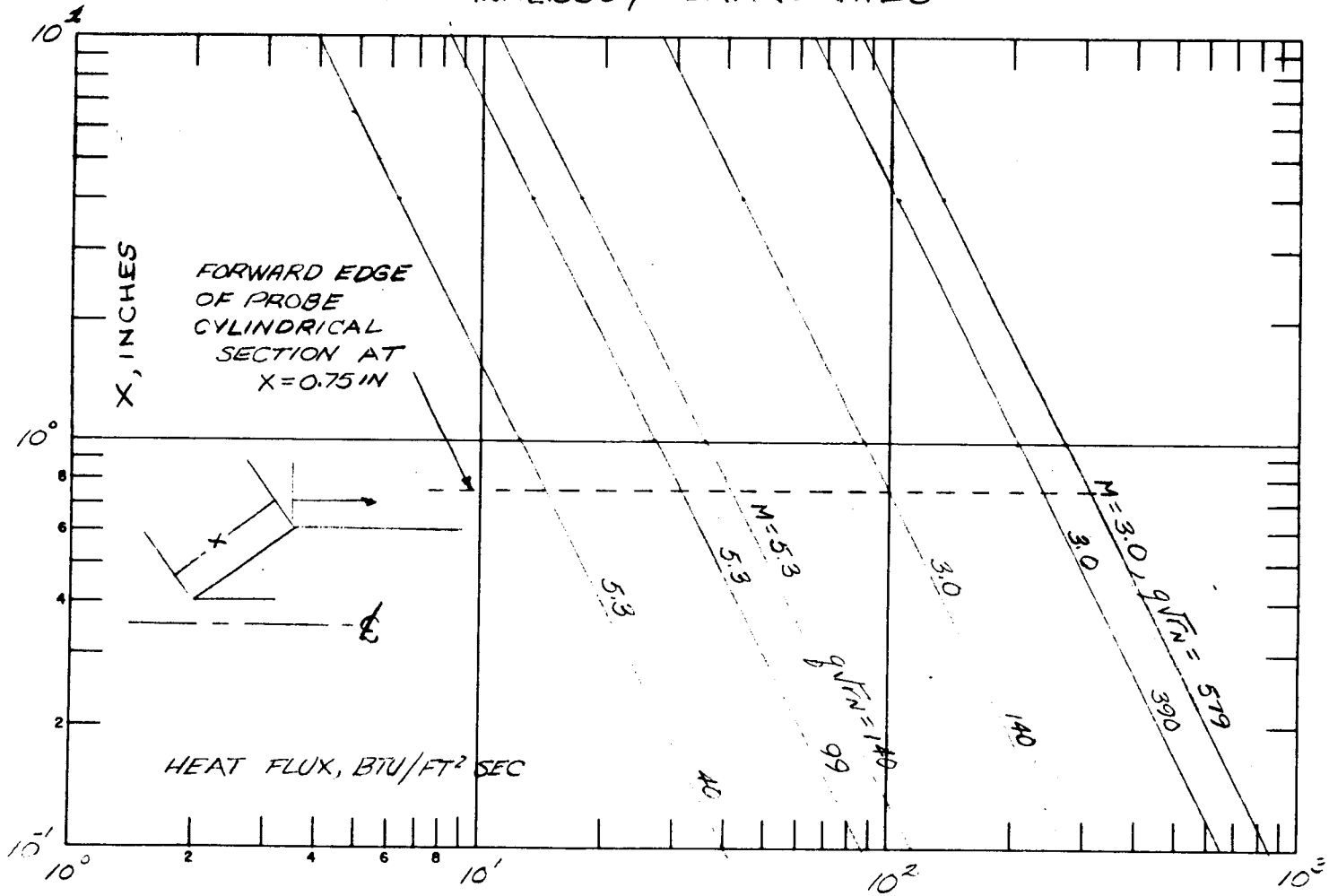

FIG. 9
HEAT INPUT TO PROBE CYLINDRICAL SECTION

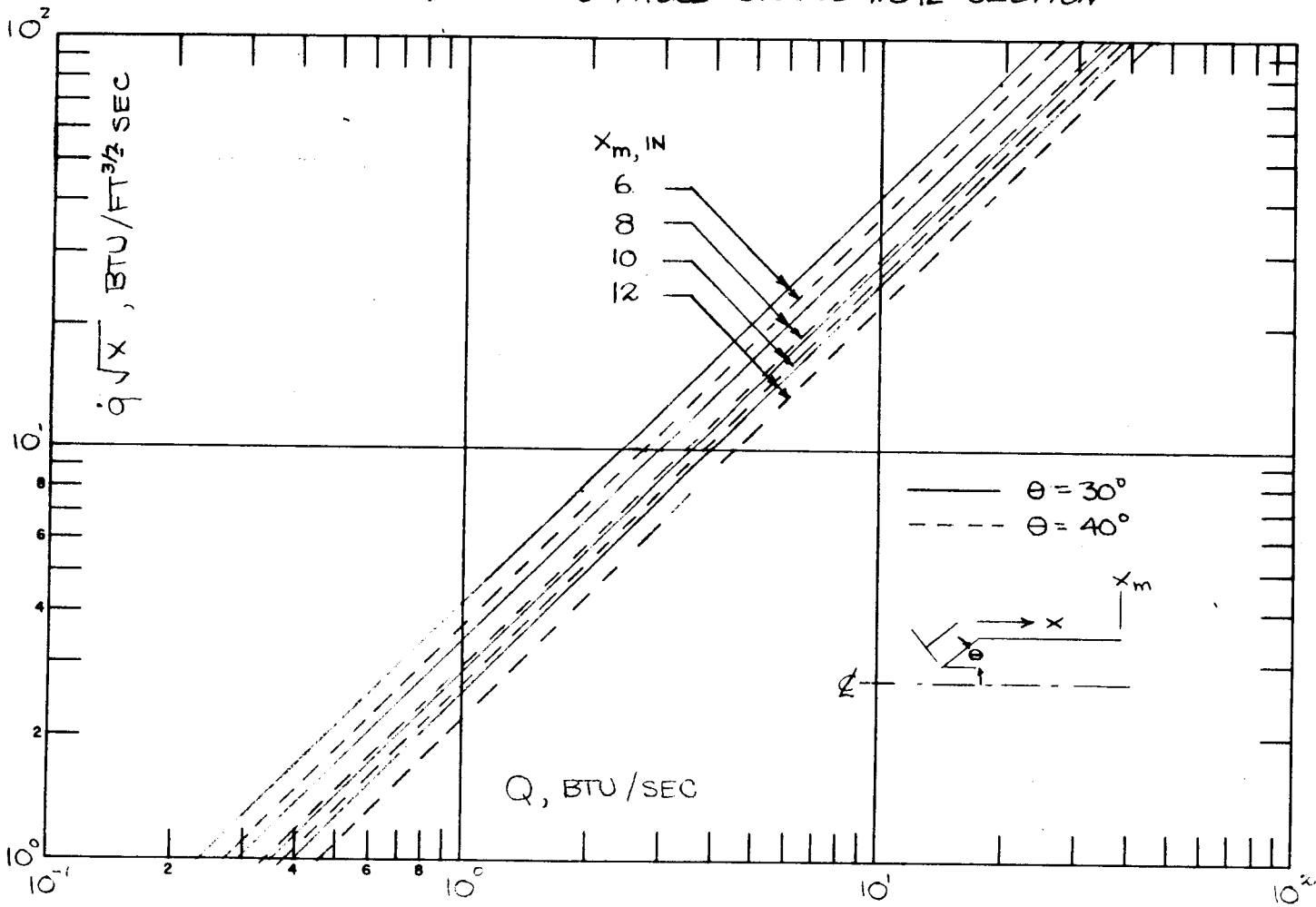

The heat transfer rates on these rear surfaces were determined in a manner similar to those discussed above. It is recognized that the presence of the boundary layer along the cylindrical portion of the probe results in velocity, density and pressure distributions on the conical surface which are considerably different from what would be predicted by Chernyi's analysis. This is demonstrated by the study of Faye-Petersen[9] on the flow field about the conical skirt of re-entry vehicles. Nevertheless, Chernyi's analysis was used to establish the flow field over this section. The flow field properties were assumed to remain constant over the remainder of the probe. This approach results in heating rates higher than what would be expected in practice since it makes no allowances for the reduction in heating downstream of the Prandtl-Meyer expansion at the rear of the conical portion. The resulting heat transfer rates at the midpoint of the two remaining probe sections are illustrated in Figure 10.

These heating rates were assumed to be representative of those experienced over the entire surface and were used to determine the total heat input to this portion of the probe from the simple equation

$$Q = \sum \dot{q}_i A_i \tag{45}$$

The total heat input to this portion of the probe is illustrated in Figure 11 .

The total heat input to all exposed surfaces of the external probe were used to determine the heat load for this portion of the system as illustrated in Figure 12 .

D. Probe Strut

The probe strut has a semi-circular leading edge with a radius of 0.375 inch and the width of the strut is 0.750 inches. The length of the external surfaces parallel to the external flow field is 31 inches and the rear of the strut is semi-circular, also.

The local heat transfer rate on the leading edge of the strut was obtained from the analysis of Hankey and Neuman( ) as shown in Figure 13 . The stagnation heating rate obtained on the strut was determined from the simple relationship

$$\sqrt{2}\left(\dot{q}_0\sqrt{R_N}\right)_{2D} = \left(\dot{q}_s\sqrt{R_N}\right)_{3D} \tag{46}$$

The local heat transfer rate on the parallel sides of the strut was evaluated from the standard laminar flat plate heating relationship

$$\dot{q} = \frac{0.664}{2\,Pr^{0.4}}\left(\frac{\rho^*\mu^*}{\rho_e\mu_e}\right)^{0.5}\frac{\rho_e u_e h_s}{(Re_x)^{1/2}} \tag{47}$$

Flow properties over this portion of the external surface were evaluated assuming that the flow passed through a Prandtl-Meyer expansion from the stagnation point with a total turning angle of 90 degrees. The local heating rates obtained

FIG 10
EXTERNAL PROBE HEATING RATES

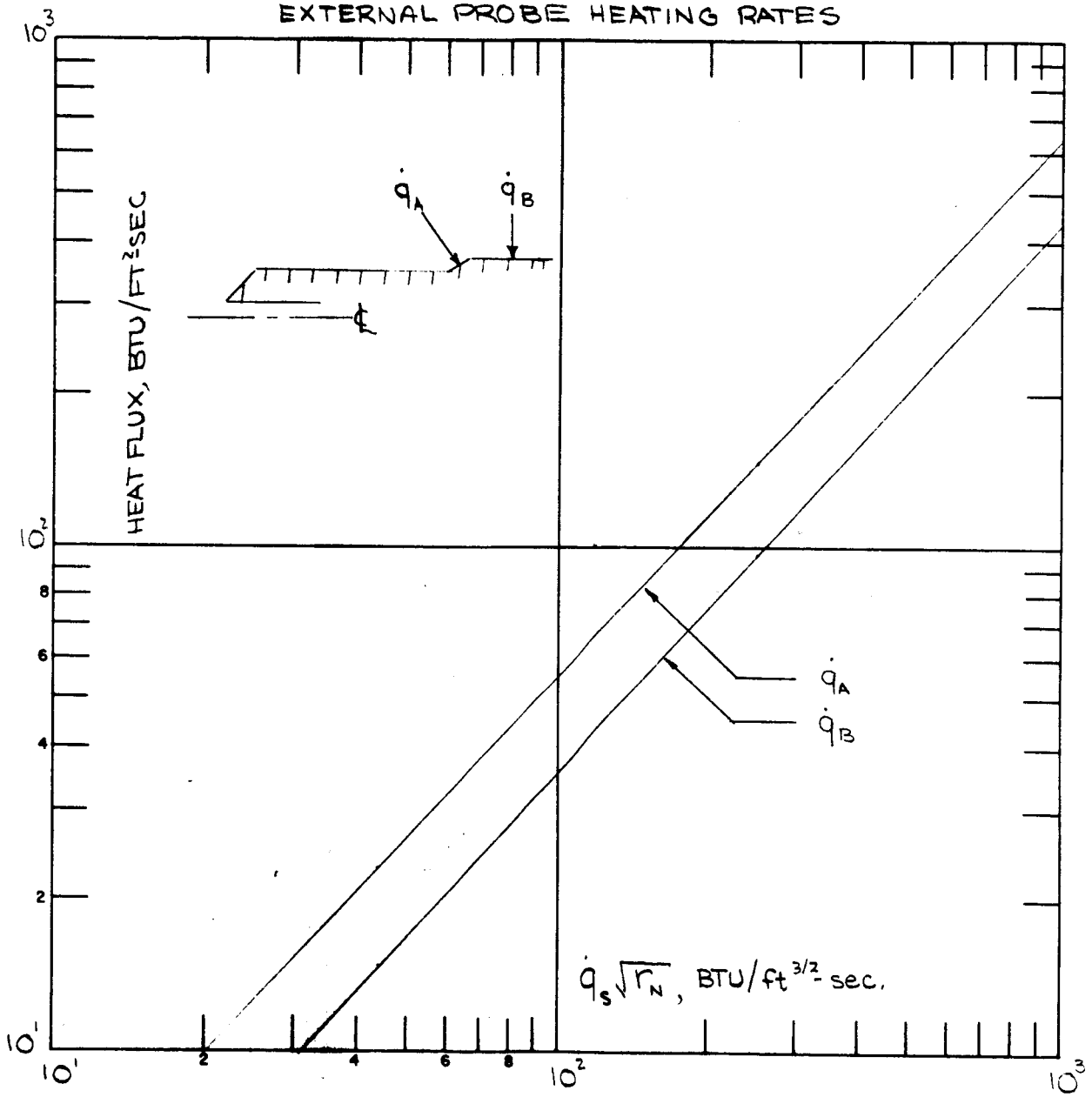

FIG 11
HEAT INPUT TO PROBE REAR SECTIONS

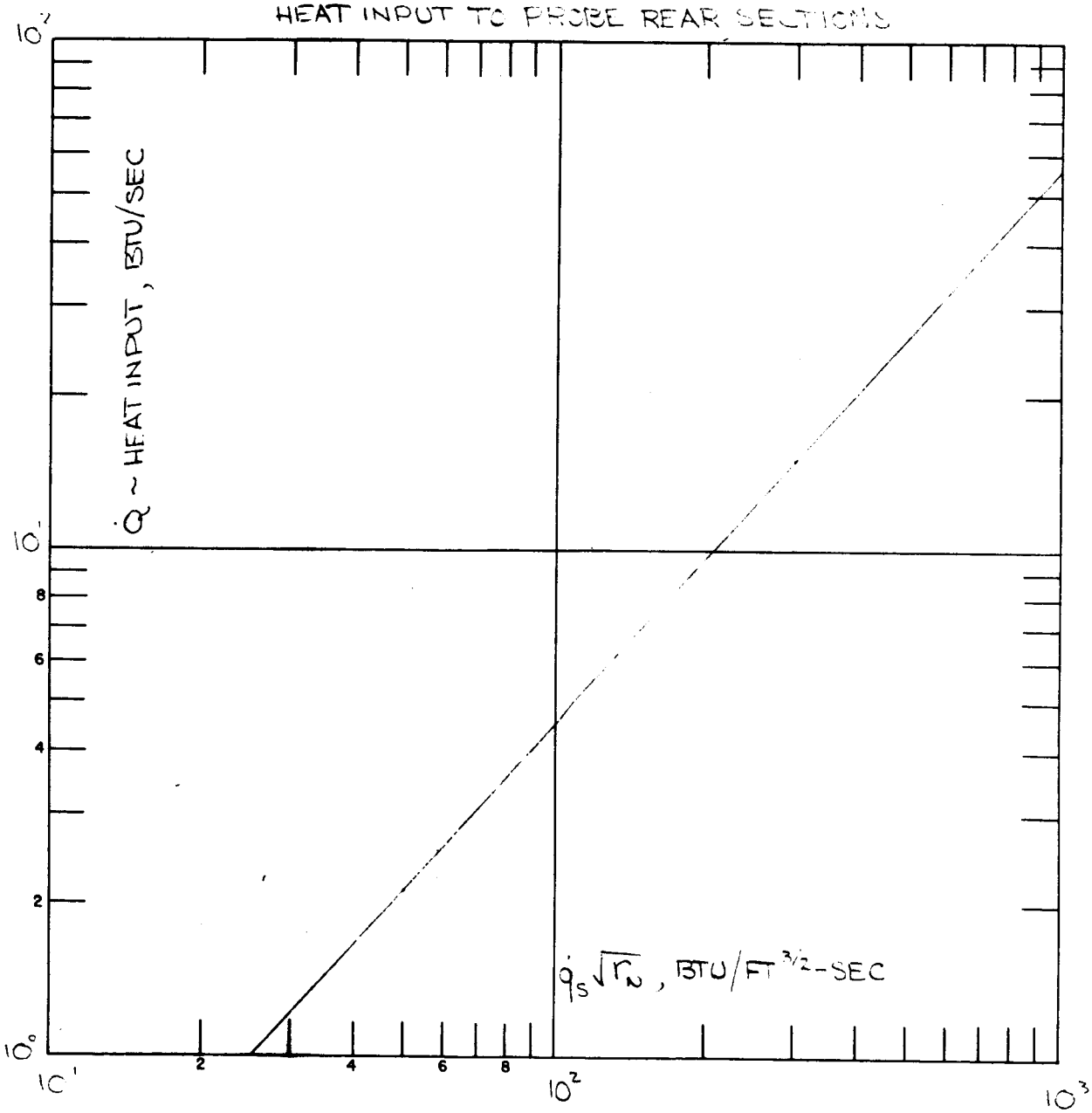

FIG 12
TOTAL HEAT INPUT TO EXTERNAL PROBE

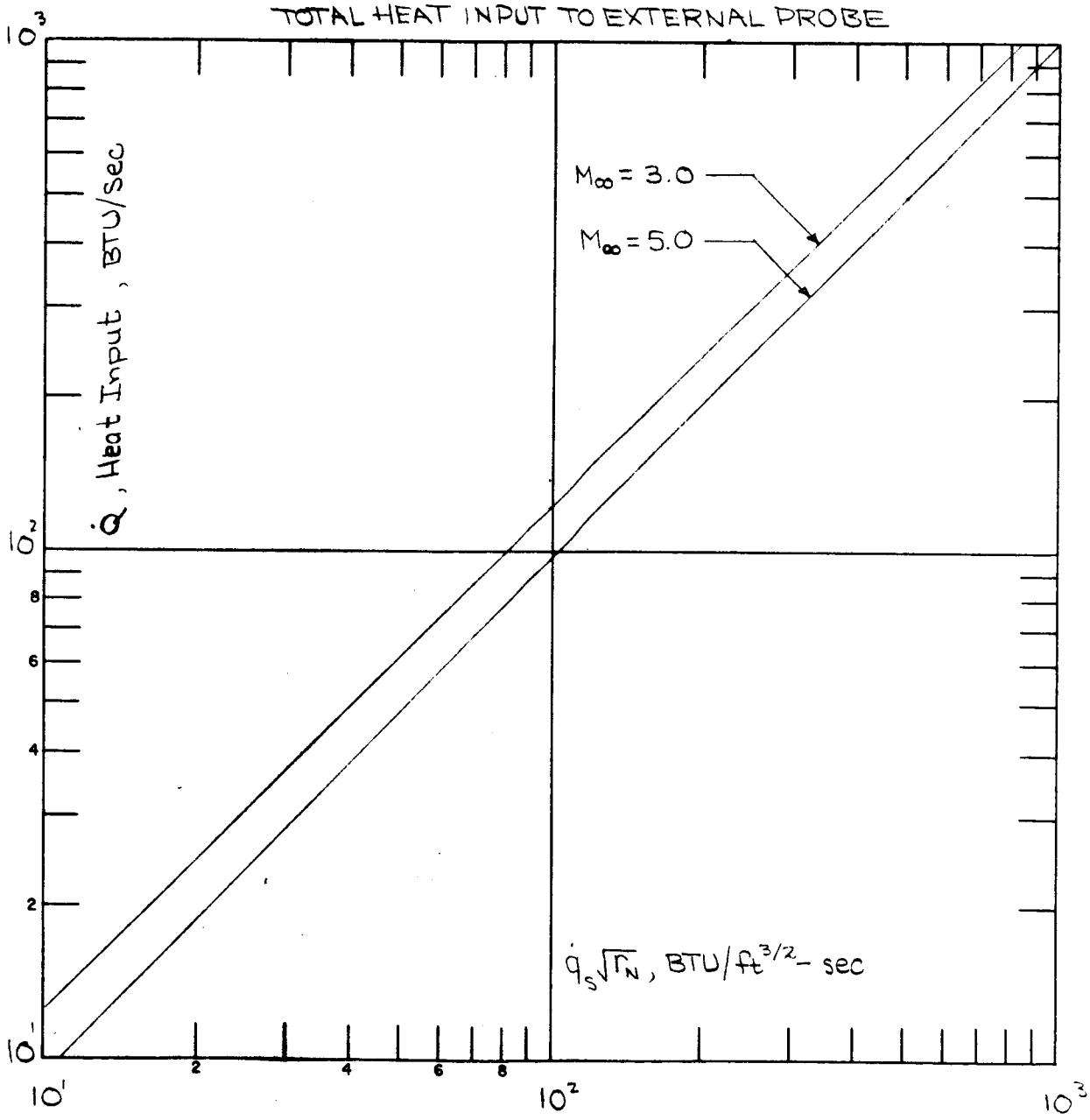

FIG 13
HEATING DISTRIBUTION ON PROBE STRUT

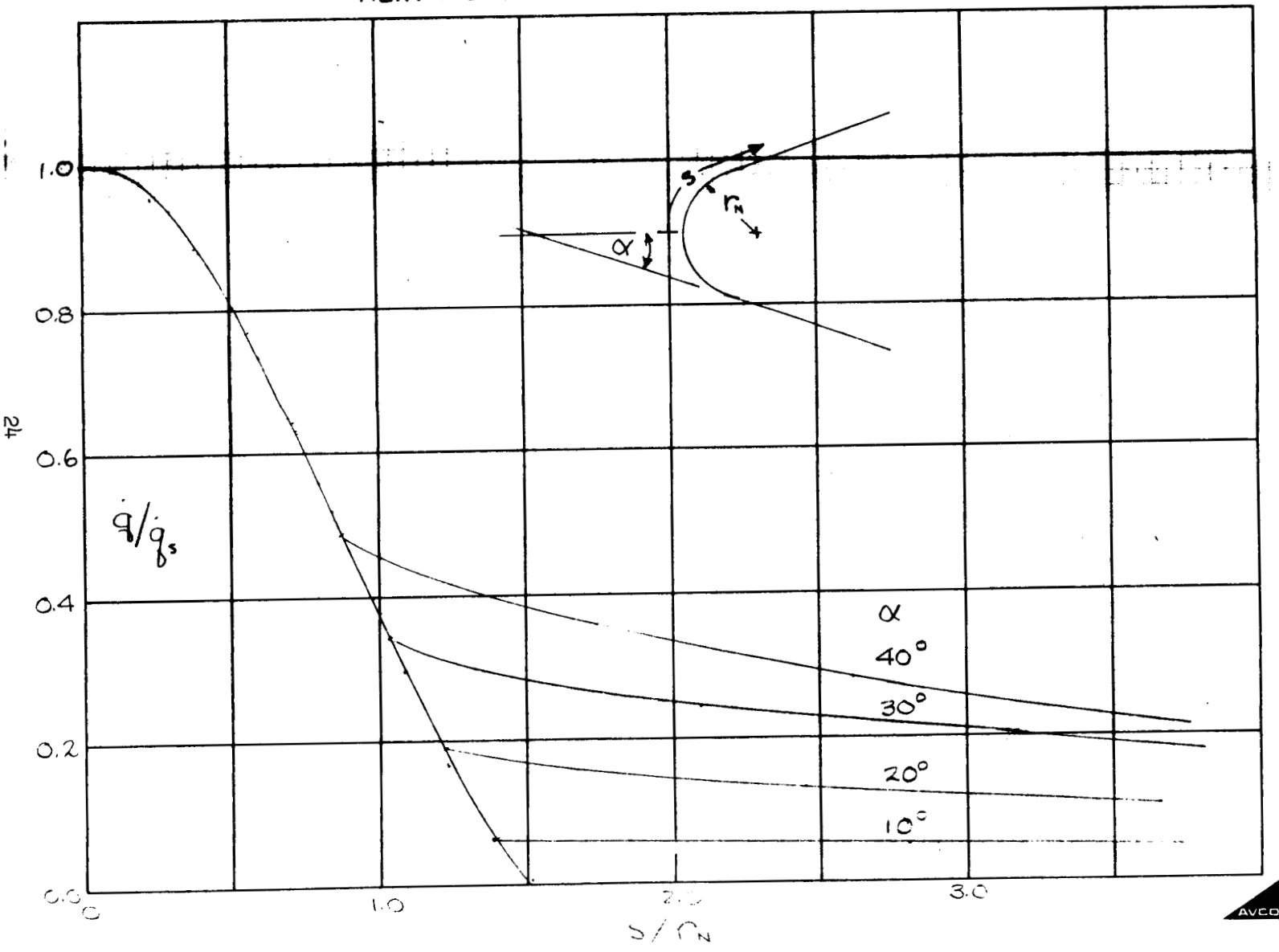

in this manner are illustrated in Figure 14.

The local heat transfer rates on all the exposed strut surfaces were integrated to obtain the total heat input to this portion of the system as a function of free stream conditions and the width of the flow field. For the purposes of this analysis it was assumed that the ARMSEF exhaust stream was uniform and that it was possible to expose a length of strut which was equal to the nozzle exit diameter. The resulting total heat input to the strut is illustrated in Figure 15.

INTERNAL FLOW FIELD

A. Probe Tip

The proper functioning of the probe system as a mass flux ($\rho_\infty u_\infty$) device is governed primarily on the ability of the sampling system to pass the flow without choking due to friction. If the combined length-to-diameter ratio of the sampling train were too large, the flow at the rear end of the train would be sonic and the mass flow which could be aspirated through the system would be limited and would be independent of free stream mass flux. It has been Avco's experience that in probes of this type, the gas flow through the system would depend solely on the impact pressure of the stream. It is also required that the portion of the sample lines within the internal calorimetric probe be of sufficient length to cool the aspirated gas sample to a temperature level which can be measured with a thermocouple.

The primary concern in insuring the survivability of the internal probe in a high enthalpy gas stream is centered about the heat transfer rates and temperature distributions near the leading edge of the probe. For the purposes of determining the heating rates within the sampling tube it was assumed that the mass flow through the probe was equal to the free stream mass flux and that the flow was free of shocks. The local heating rate may be determined from

$$\dot{q} = \frac{0.664}{2 P_r^{0.4}} \left(\frac{\rho^* u^*}{\rho_e u_e} \right)^{0.5} \frac{\rho_e u_e h_s}{(Re_x)^{1/2}} \qquad (48)$$

where starred quantities are evaluated at the reference enthalpy defined by equation 39. The local heat transfer rate at a distance of one diameter down the tube is presented in Figure 16 for several ARMSEF operating conditions. As a first approximation it is seen the

$$\dot{q}_o = \dot{q}(D_o) = \dot{q}_s \sqrt{R_N} \qquad (49)$$

As shown in Figure 17, the leading edge of the internal probe is uncooled for a considerable length and as was the case with the external probe it is of interest to determine the temperature distribution within this portion of the probe. An integral energy balance for the uncooled tip is simply

$$-k A_w \frac{dT}{dx} = \int_0^s 2\pi r \dot{q}(s)\, ds \qquad (50)$$

FIG 14
STRUT HEATING DISTRIBUTION, LAMINAR

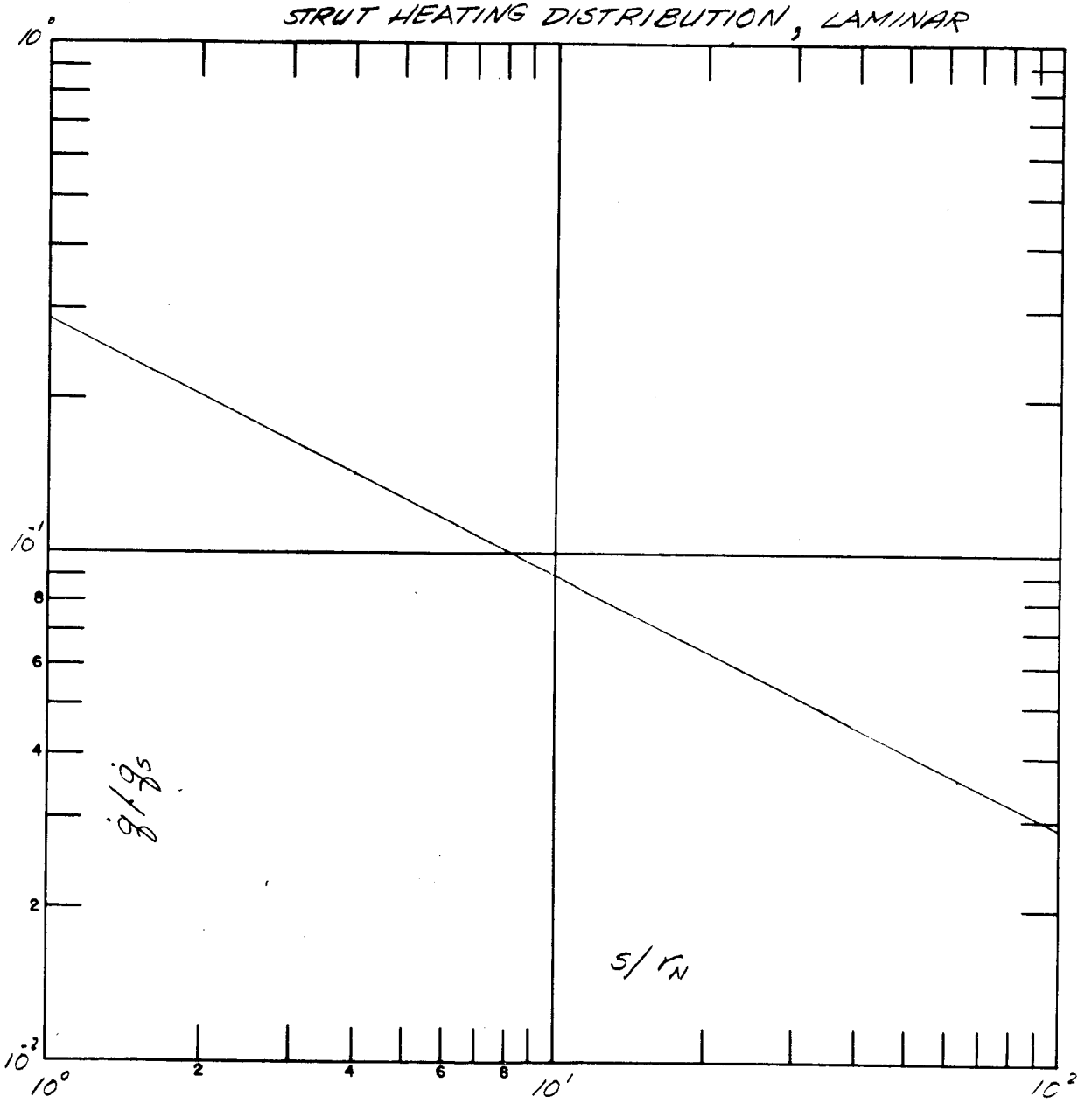

FIG 15
INTEGRATED STRUT HEATING

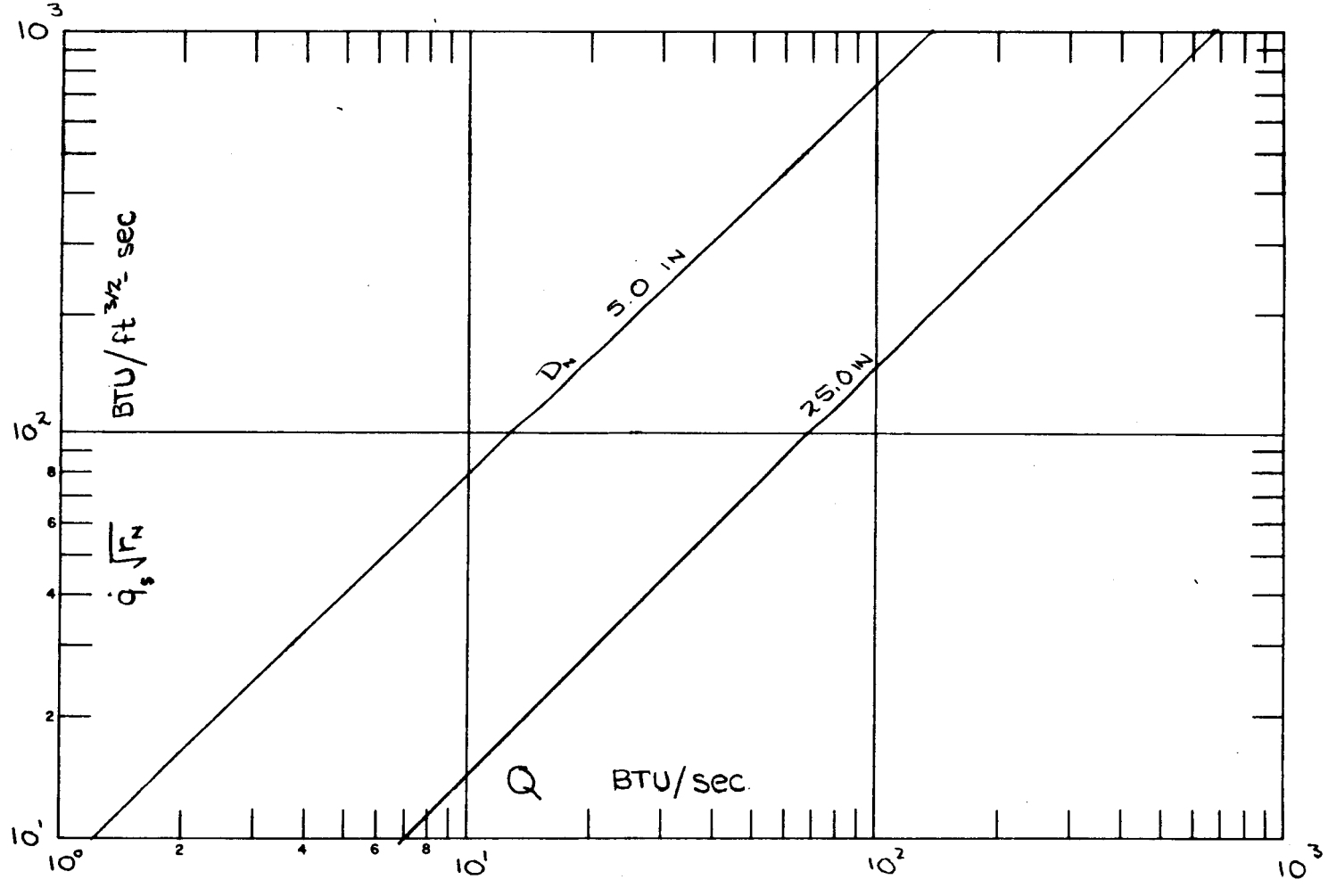

FIG 16
INTERNAL HEATING, SAMPLING TUBE

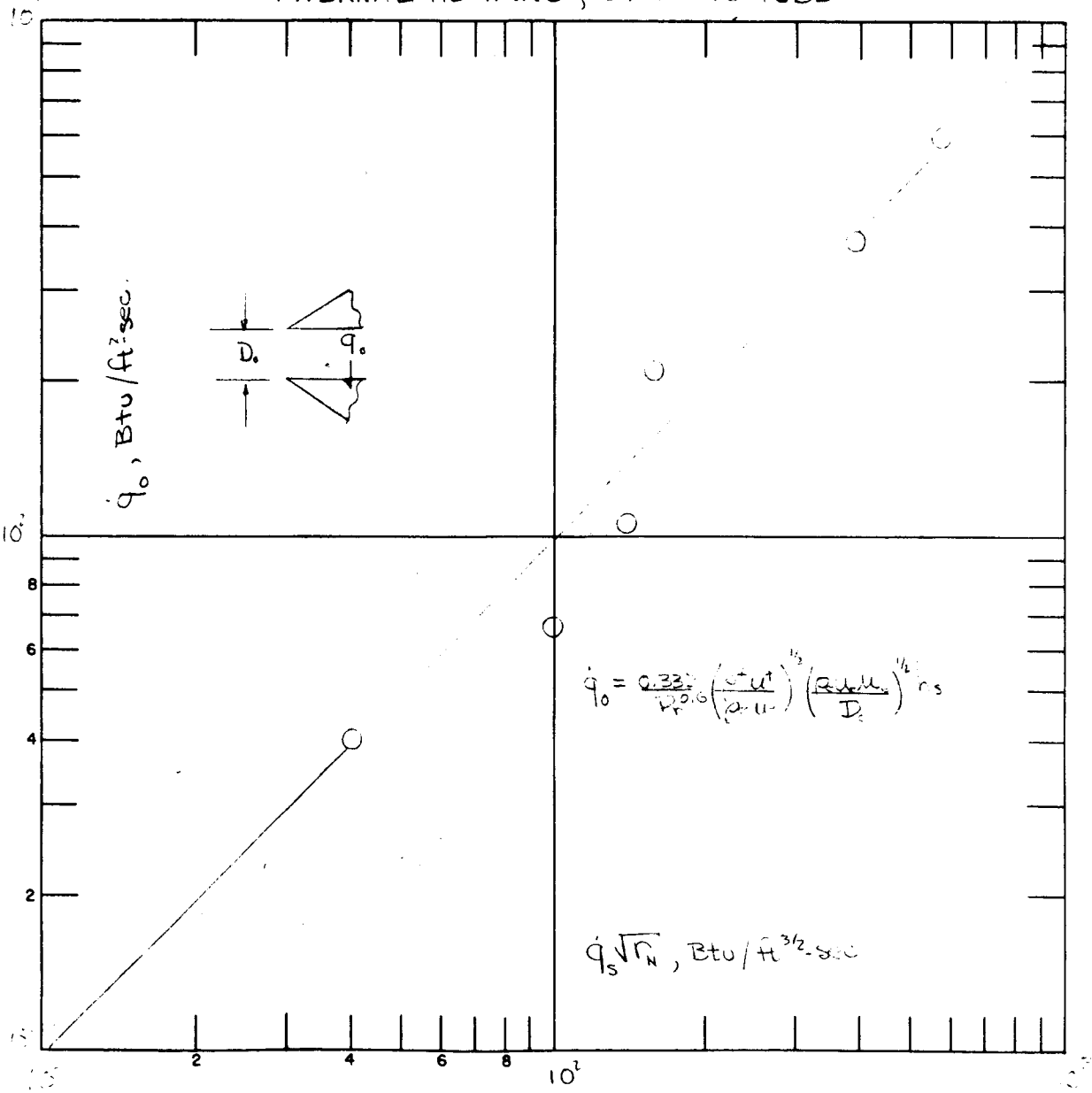

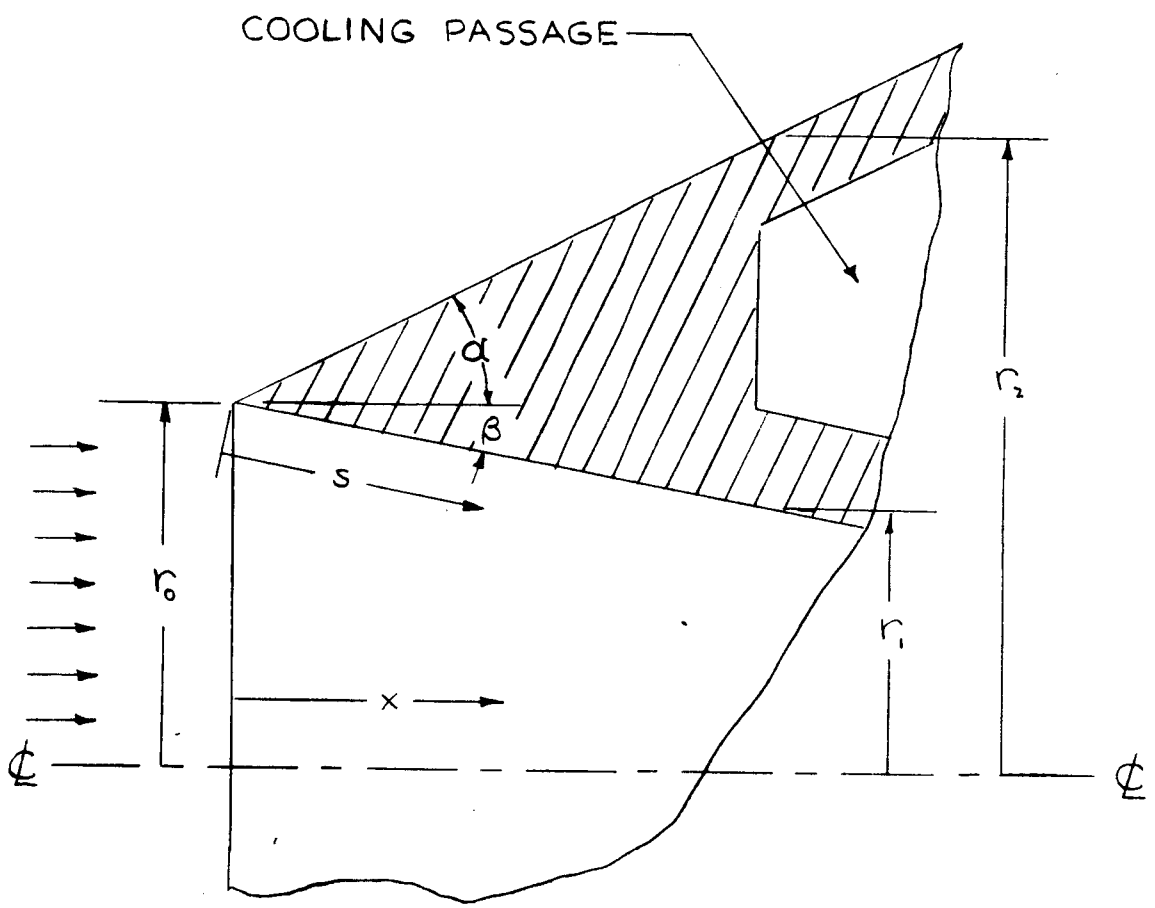

FIG 17 INTERNAL PROBE TIP GEOMETRY

where temperature gradients normal to the tube axis have been neglected. If we define a heat transfer rate (q_o) as that obtained in a straight tube at a distance of one tube diameter back from the probe tip then the local heating rate is simply

$$\dot{q}_s = \dot{q}_o \left(\frac{D_o}{s}\right)^{1/2} \left(\frac{\rho u}{\rho_o u_o}\right)^{1/2} \tag{51}$$

or since the mass flow through the tube is constant at any axial station

$$\dot{q}_s = \dot{q}_o \left(\frac{r_o}{r_i}\right)\left(\frac{D_o}{s}\right)^{1/2} \tag{52}$$

with

$$r_i = r_o - s \sin\beta \tag{53}$$

Therefore after integrating equation

$$k A_w \frac{dT}{dx} = -4\pi \dot{q}_o r_o (D_o s)^{1/2} \tag{54}$$

$$= -4\pi \dot{q}_o r_o \left(\frac{D_o x}{\cos\beta}\right)^{1/2} \tag{55}$$

The area of the wall available for heat conduction is

$$A_w = \pi \left(r_2^2 - r_i^2\right) \tag{56}$$

with

$$r_2 = r_o + x \tan\alpha \tag{57}$$

$$r_i = r_o - x \tan\beta \tag{58}$$

which results in

$$A_w = \pi \left(\tan\alpha + \tan\beta\right) D_o^2 \left\{1 + \frac{x}{D_o}\left(\tan\alpha - \tan\beta\right)\right\}\left(\frac{x}{D_o}\right) \tag{59}$$

After substitution of this expression into equation 54 and rearranging terms it is found that

$$\frac{dT}{d(x/D_o)} = \frac{-2 D_o \dot{q}_o}{k(\cos\beta)^{1/2}} \frac{1}{(\tan\alpha + \tan\beta)} \left\{\frac{1}{(x/D_o)^{1/2}\left[1 + \frac{x}{D_o}(\tan\alpha - \tan\beta)\right]}\right\} \tag{60}$$

which may be integrated directly to give

$$T_o - T_{x/D} = \frac{2\dot{q}_o D_o}{k(\cos\beta)^{1/2}} \frac{1}{(\tan\alpha+\tan\beta)} \left\{ \frac{2\tan^{-1}\left[\frac{x}{D_o}(\tan\alpha-\tan\beta)\right]^{1/2}}{(\tan\alpha-\tan\beta)^{1/2}} \right\} \tag{61}$$

For small values of α (and β)

$$\tan^{-1}\left[\frac{x}{D_o}(\tan\alpha-\tan\beta)\right]^{1/2} = \tan^{-1}\left[\frac{x}{D_o}(\alpha-\beta)\right]^{1/2} = \left[(\alpha-\beta)\frac{x}{D_o}\right]^{1/2} \tag{62}$$

Therefore allowing equation 61 to be simplified considerably to the following

$$T_o - T_{x/D} = \frac{4\dot{q}_o (xD_o)^{1/2}}{k(\cos\beta)^{1/2}(\tan\alpha+\tan\beta)} \tag{63}$$

$$T_o - T_{x/D} = \frac{4\dot{q}_o (xD_o)^{1/2}}{k(\alpha+\beta)(\cos\beta)^{1/2}} \tag{64}$$

If the further restriction is placed that the angle β shall not exceed 10 degrees

$$T_o - T_{x/D} = 4\dot{q}_o \frac{(xD_o)^{1/2}}{k(\alpha+\beta)} \tag{65}$$

At a heat flux of 580 Btu/ft^2-sec and a total tip half angle 20 degrees, a temperature drop of 1600°F (Figure 18) is obtained when x and D_o are assigned values of 0.126 inch and 0.250 inch, respectively.

It is also required to obtain some estimate as to the final temperature of the gas stream leaving the sampling tube or conversely what length of sampling tube is necessary to decrease the gas temperature to approximately 2000°F. For the purpose of this estimate it is assumed that the aspirated flow passes through a normal shock immediately after entering the sampling tube. An energy balance on the gas stream is simply

$$\frac{1}{(h_s - h_w)} \frac{dh_s}{d(x/D)} = -4 \frac{Nu}{Re\, Pr} \tag{66}$$

Where the Nusselt number[10] is given by

FIG 18
INTERNAL TIP TEMPERATURE DROP

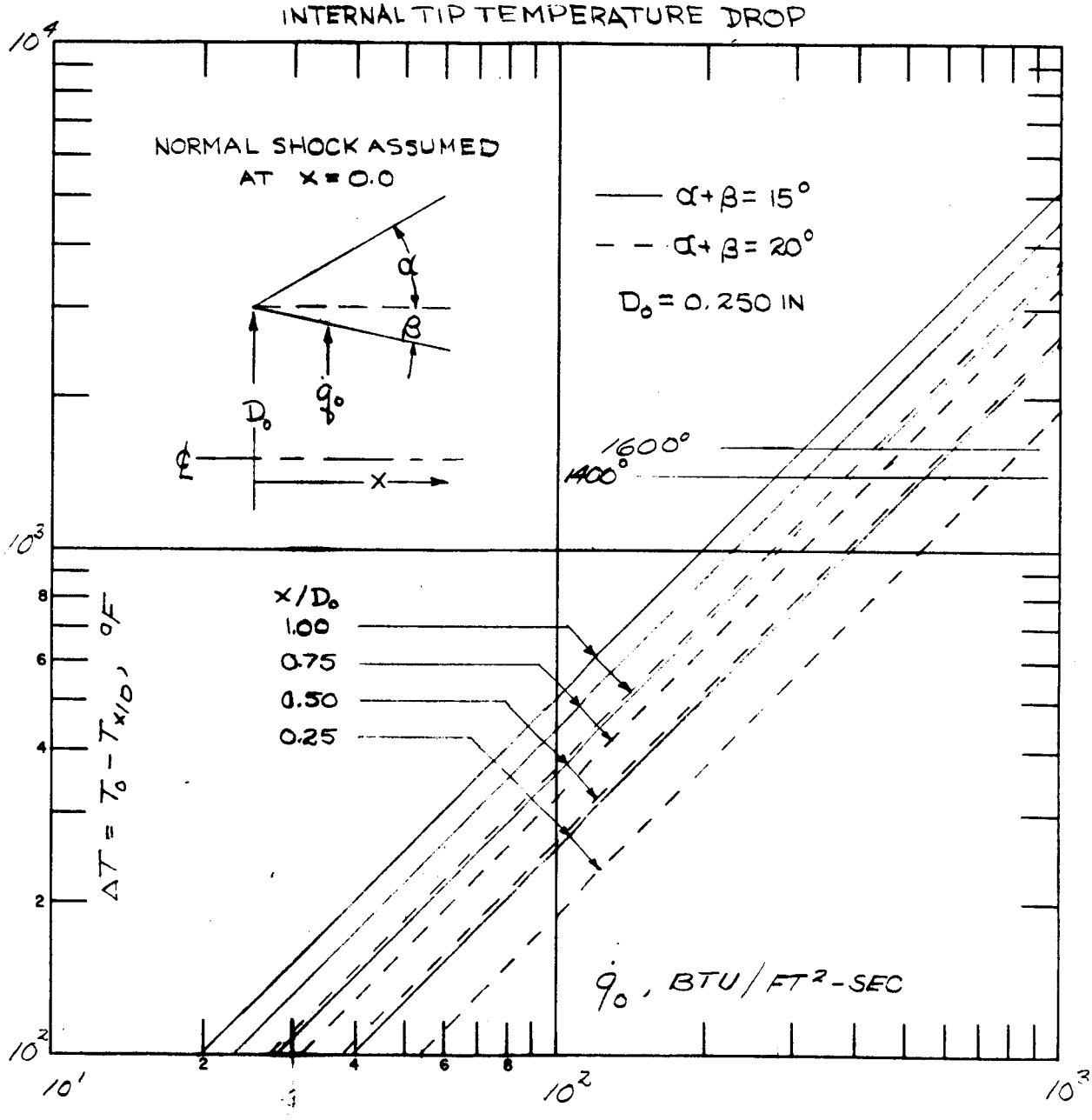

$$Nu = Nu_\infty + \frac{K_1 Re_D Pr (D/x)}{1 + K_2 [Re_D Pr\ D/x]^n} \tag{67}$$

with the constants being

$$Nu_\infty = 3.66$$

Region	K_1	K_2	n
Entrance	0.104	0.016	0.8
Fully Developed	0.0668	0.04	2.3

The maximum length of tube would be obtained in the case where

$$Nu = Nu_\infty = 3.66 \tag{68}$$

Since the variation in Re_D is a direct result of changes in viscosity with temperature, equation 66 may be rewritten as

$$\frac{1}{(h_s - h_w)}\left(\frac{\mu_o}{\mu}\right)\frac{dh_s}{d(x/D)} = \frac{-4Nu_\infty}{(Re_D)_o\ Pr} \tag{69}$$

or, since[11]

$$\mu_o/\mu = (h_o/h)^{1/3} \tag{70}$$

$$\frac{(h_o/h)^{1/3}}{(h_s - h_w)}\frac{dh_s}{d(x/D)} = \frac{-4Nu_\infty}{(Re_D)_o\ Pr} \tag{71}$$

Defining

$$\eta \equiv (h/h_o)^{1/3} \tag{72}$$

$$\eta_w \equiv (h_w/h_o)^{1/3} \tag{73}$$

The energy balance may be written as

$$\frac{\eta\, d\eta}{\eta^3 - \eta_w^3} = \frac{-4Nu_\infty}{(Re_D)_o\ Pr}\, d\left(\frac{x}{D}\right) \tag{74}$$

which can be integrated to give

$$\frac{1}{3\eta_w}\left\{\frac{1}{2}\ln\left(\frac{1+3\eta_w}{(1-\eta_w)^2}\right)-3^{1/2}\tan^{-1}\left(\frac{1+2/\eta_w}{\sqrt{3}}\right)\right.$$

$$\left.-\frac{1}{2}\ln\left(\frac{1+3N}{(N-1)^2}\right)+3^{1/2}\tan^{-1}\left(\frac{2N+1}{\sqrt{3}}\right)\right\}=-\frac{4Nu_\infty}{(Re_D)_o Pr}\left(\frac{x}{D}\right) \qquad (75)$$

and

$$N \equiv \eta_f/\eta_w = (h_f/h_w)^{1/3} \qquad (76)$$

with subscripts w and f referring to properties evaluated at the wall, and final gas temperatures, respectively. Equation 75 may be rewritten as

$$-\frac{1}{3\eta_w}\left[f\left(\frac{h_f}{h_w}\right)-f\left(\frac{h_w}{h_o}\right)\right]=-\frac{4\,Nu_\infty}{(Re_D)_o Pr}\left(\frac{x}{D}\right) \qquad (77)$$

The two enthalpy functions indicated in the above expression were evaluated and are illustrated in Figures 19 and 20. Equation 77 was employed to evaluate the exit gas temperature as a function of free stream enthalpy, tube length and initial Reynolds number as shown in Figures 21 and 22. This analysis indicates that for all conditions listed in Table I with the exception of condition 1 the exit gas stream has a temperature of less than 1500 R if the sample tube (0.250 inch diameter) is 8.0 inches in length. However, the same exit temperature for condition 1 can be achieved only if the sampling tube is 56 inches in length.

PROBE COOLING REQUIREMENTS

The amount of forced convection cooling necessary to protect the external surfaces of the probe from the environment was established from an evaluation of coolant pressure drop, coolant convective heat transfer coefficients, and the total coolant temperature rise. For this analysis the probe system is considered to have two coolant supplies one of which is employed in cooling the external probe surfaces and the second which is used exclusively in the calorimetric probe. Each of these streams is considered separately in the following sections of this report.

A. Pressure Drop

The coolant pressure drop in each section of the external probe cooling passages may be determined from

$$P_1+\frac{\rho u_1^2}{2}=P_2+\frac{\rho u_2^2}{2}+4f\left(\frac{L}{D}\right)\frac{u^2}{2}+F_c+F_{exp}+F+\rho\left(Z_2-Z_1\right) \qquad (78)$$

TABLE I

ARMSEF OPERATING CONDITIONS

Condition No.	1	2	3	4	5	6
Mass Flow Rate, lb/sec	1.00	1.00	0.04	0.04	0.10	0.10
Plenum Pressure, atm	7.83	7.83	2.64	2.64	1.65	1.65
Enthalpy, h/RT_o	118	118	766	766	766	766
Throat Diameter, in	1.50	1.50	0.75	0.75	1.50	1.50
Nozzle Diameter, in	5.0	25.0	5.0	25.0	5.0	25.0
Impact Pressure, atm	1.30	0.072	0.14	0.008	0.29	0.016
Mach No.	3.2	5.3	3.0	5.6	3.2	5.0
Heating Rate ($\dot{q}\sqrt{r_N}$), $Btu/ft^{3/2}$-sec	157	40	390	99	575	140

FIG 19 ENTHALPY FUNCTION

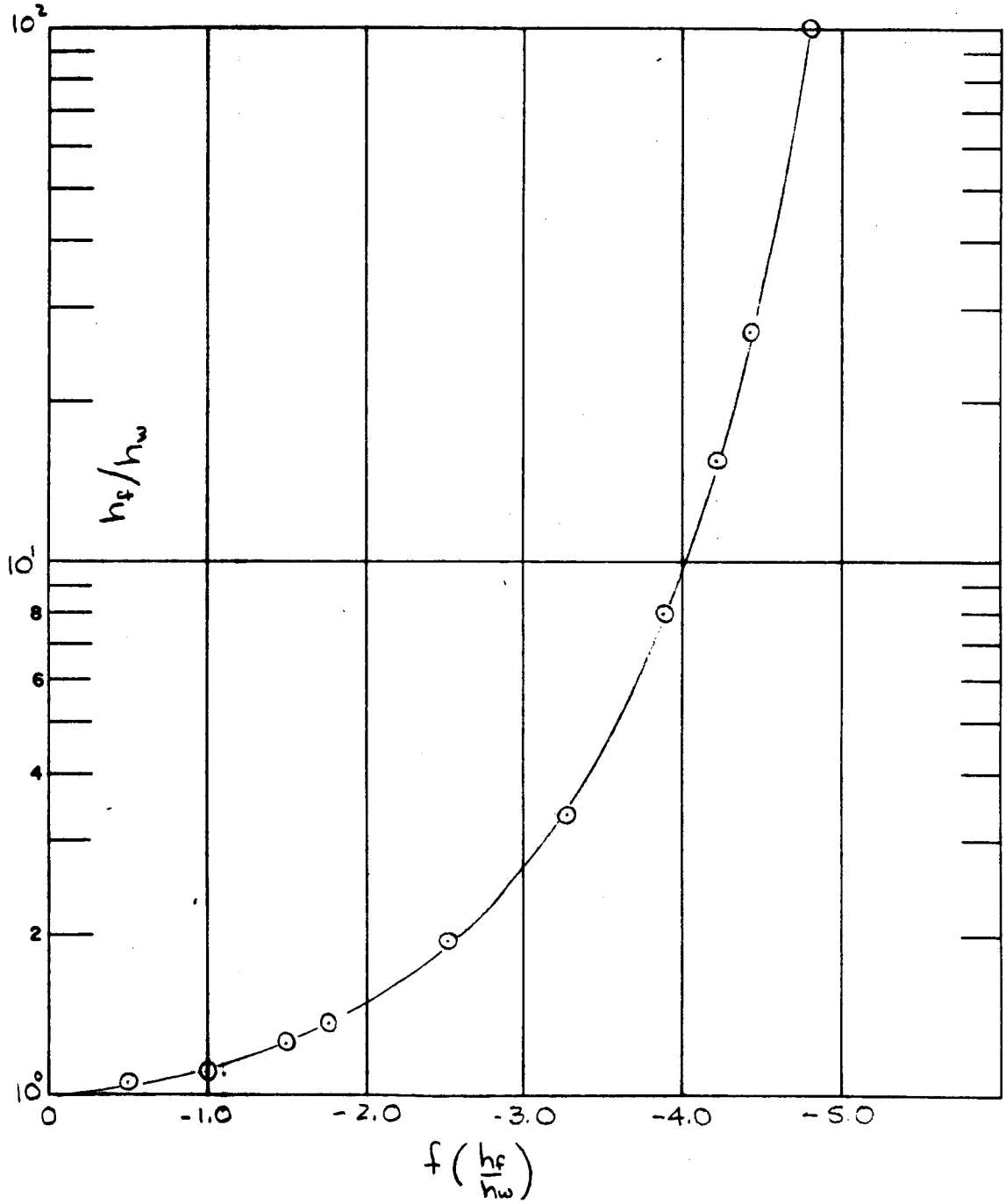

FIG 20 ENTHALPY FUNCTION

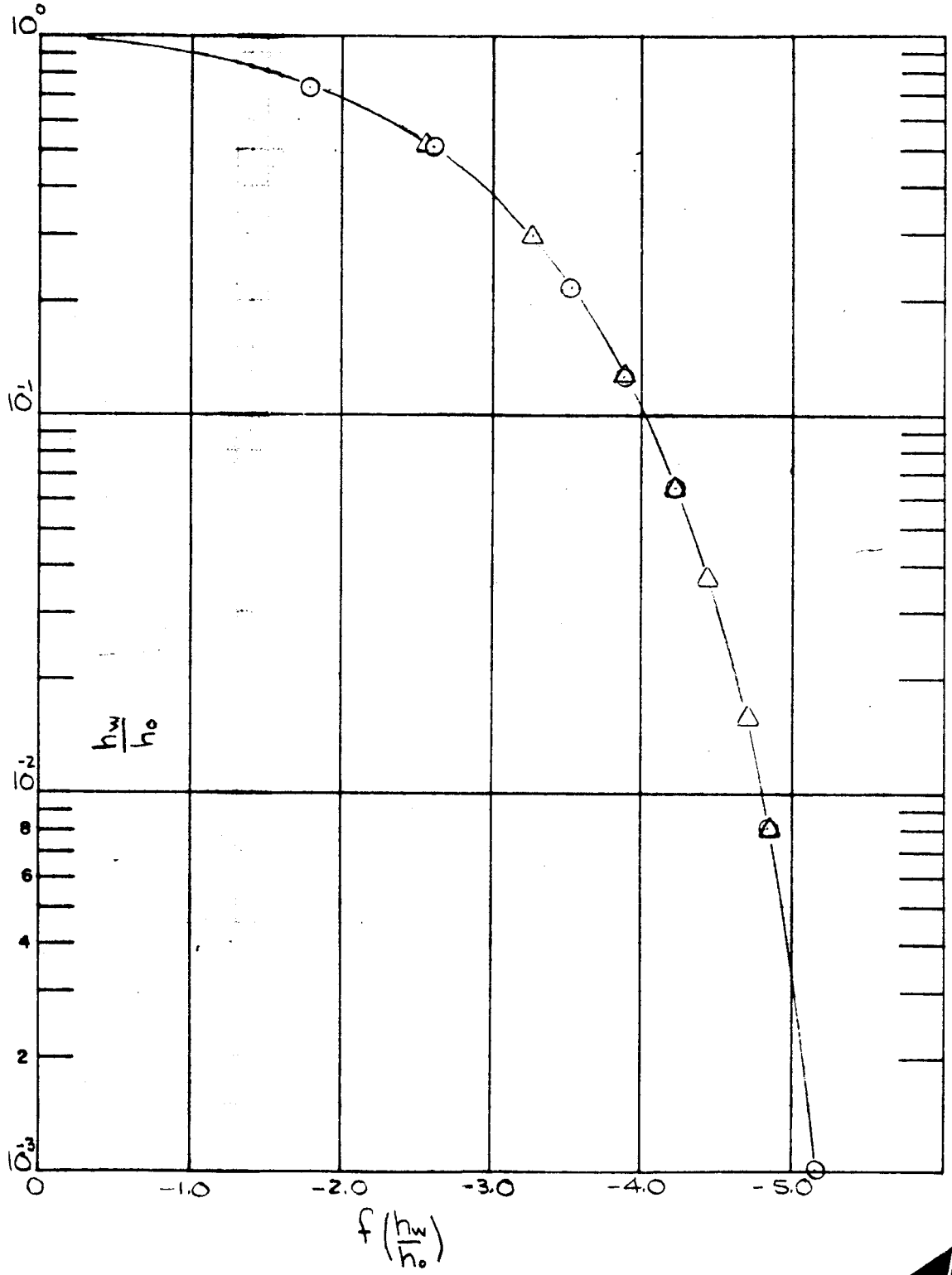

FIG 21

EXIT GAS TEMPERATURES VS. REYNOLDS NO.

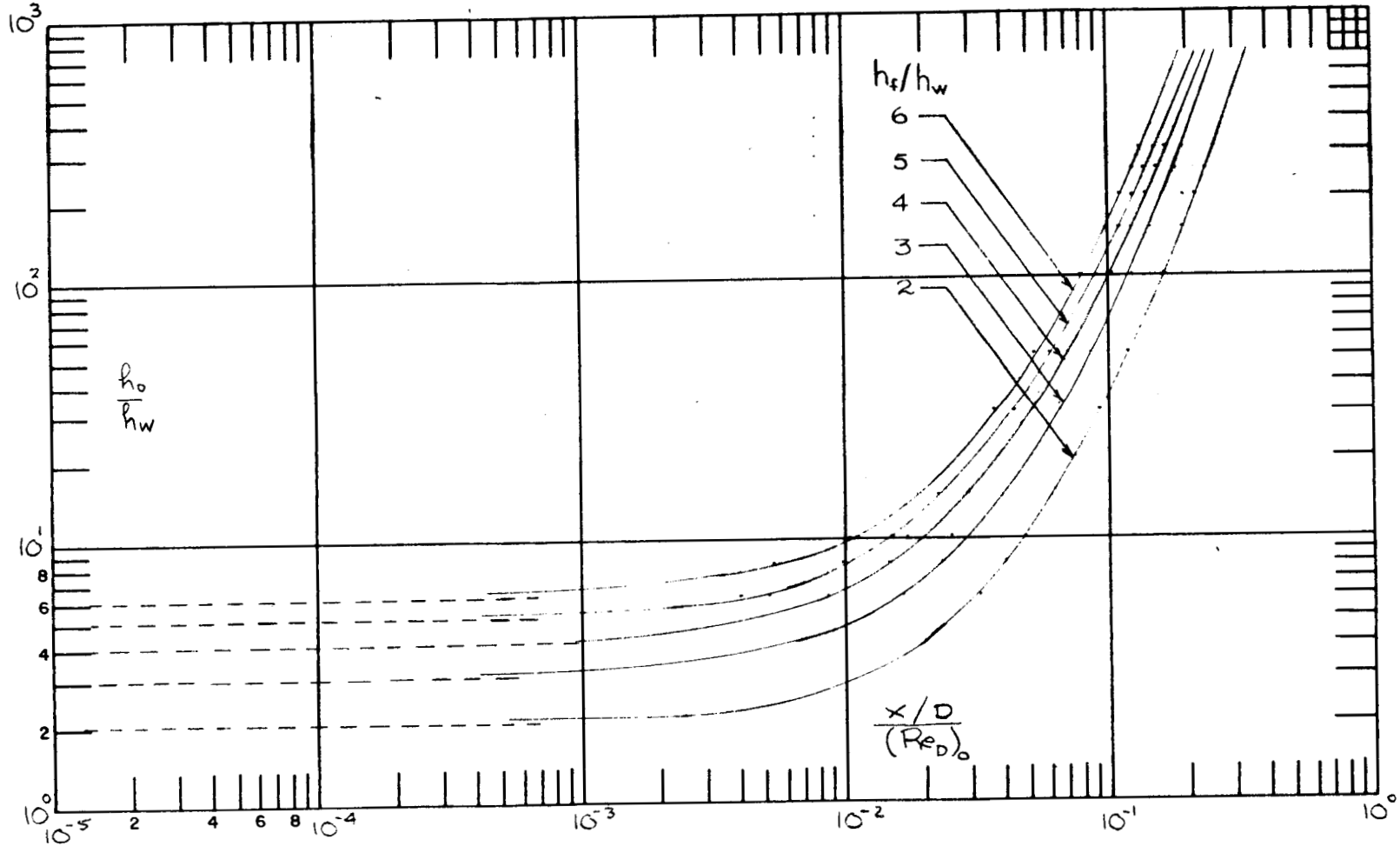

FIG 22
EXIT GAS TEMPERATURES

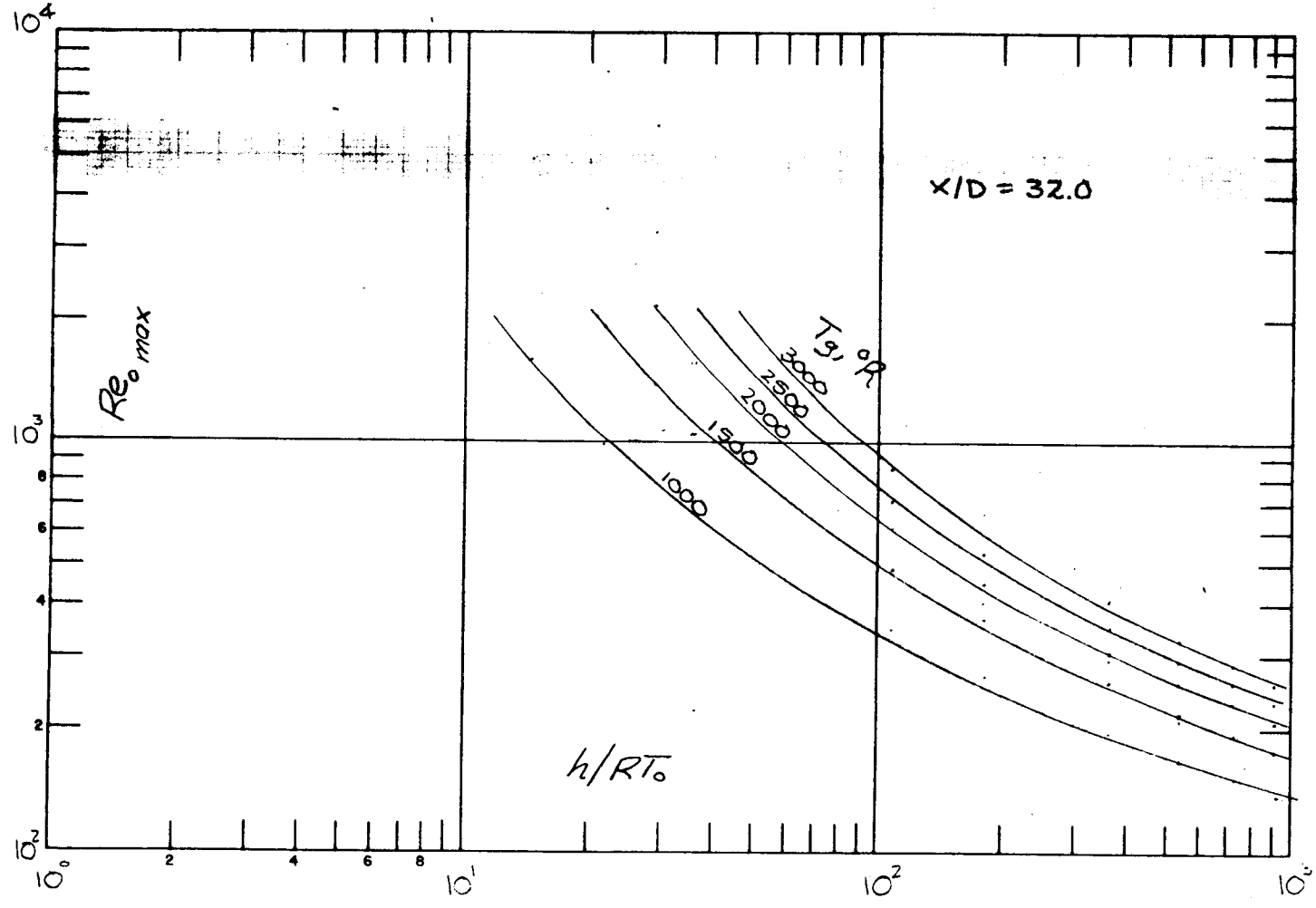

where subscripts 1 and 2 refer to the inlet and outlet to a particular portion of the probe system. The quantities F, F_c, and F_{exp} contain the pressure drop experienced by the fluid in changing direction (e.g. elbows), and changes in cross sectional area of the flow. In particular, the pressure losses, over and above those directly attributable to changes in velocity, which are incurred in an expansion are[12]

$$F_{exp} = \left(1 - \frac{A_1}{A_2}\right) \frac{\rho u_1^2}{2} \tag{79}$$

where subscripts 1 and 2 refer to the smaller and larger cross sections, respectively. Similarly in a contraction, the additional pressure drop is given by[13]

$$F_c = K_c \frac{\rho u_1^2}{2} \tag{80}$$

where

$$K_c = 0.40\ (1.25 - A_1/A_2) \quad A_1/A_2 < 0.715 \tag{81}$$

$$K_c = 0.75\ (1 - A_1/A_2) \quad A_1/A_2 > 0.715 \tag{82}$$

with subscript 1 referring to the smaller passage.

In its path through the probe the coolant was assumed to flow through the following channels.

a) a 0.250 inch diameter circular tube 31.0 inches in length

b) a 1.250 inch wide by 0.250 inch high rectangular channel

c) a total of 19 parallel circular passages 0.078 inch diameter 1.875 inches long

d) a 0.078 inch by 1.00 inch slot

e) a total of 36 parallel circular holes 0.032 inch diameter

f) a 6.75 inch long annular channel, 0.650 inch ID by 0.750 inch OD

g) a total of 45 parallel circular holes, 0.032 inch diameter

h) a rectangular slot 0.032 inch by 0.500 inch

i) a total of 45 parallel circular holes, 0.032 inch diameter

j) a 6.75 inch long annular channel, 0.800 inch ID by 0.900 inch OD

k) flow through 4 0.250 inch diameter holes

l) flow through 2 slots, 0.062 inch by 0.312 inch

m) flow through a 0.250 inch diameter hole

n) flow through a 0.250 inch diameter tube 31.0 inches in length

It was also assuming that during this process, the flow passed through a total of 10 ninetry degree elbows.

The resulting pressure drop is illustrated in Figure 22. The coolant pressure at the probe tip is also included in Figure 23.

A similar procedure was followed in determining the pressure drop experienced by the calorimetric probe cooling water at various flow rates. In this instance the coolant was assumed to flow through the following sequence of passages:

a) a 0.250 inch diameter tube 31.0 inches in length

b) two parallel rectangular passages 0.318 inch by 0.063 inch

c) a total of 16 parallel 0.063 inch diameter holes

d) an annular space 0.546 inch OD by 0.400 inch ID

e) an annular channel 0.460 inch OD by 0.400 inch ID which has a length of 6.80 inches

f) a 180 degree turn at the probe tip

g) an annular channel 0.300 inch ID by 0.360 inch OD which has a length of 7.50 inch

h) flow through two 0.250 inch diameter holes

i) flow through a rectangular channel 0.312 inch by 0.046 inch

j) flow through a single 0.250 inch diameter hole

k) flow through a 0.250 inch by 0.050 inch rectangular channel

l) flow through a 0.250 inch diameter tube 31.0 inches in length

The resulting pressure drop as a function of coolant flow rate is illustrated in Figure 24. Also included in Figure 24 is the coolant pressure at the probe tip.

In a similar fashion, the pressure drop at various coolant flow rates which would be obtained in flow through the probe strut were calculated (Figure 25).

B. Heat Transfer

In addition to these considerations, the local convective cooling heat transfer coefficients at critical locations within the probe were evaluated in order to establish the maximum survivability limits of the probe system. The local heat transfer coefficient is given by[14]

$$\frac{hD_e}{k} = 0.023 \left(\frac{\rho u D_e}{\mu}\right)^{0.8} \left(\frac{C_p \mu}{k}\right)^{0.4} \qquad (83)$$

FIG 23 EXTERNAL PROBE PRESSURE DROP

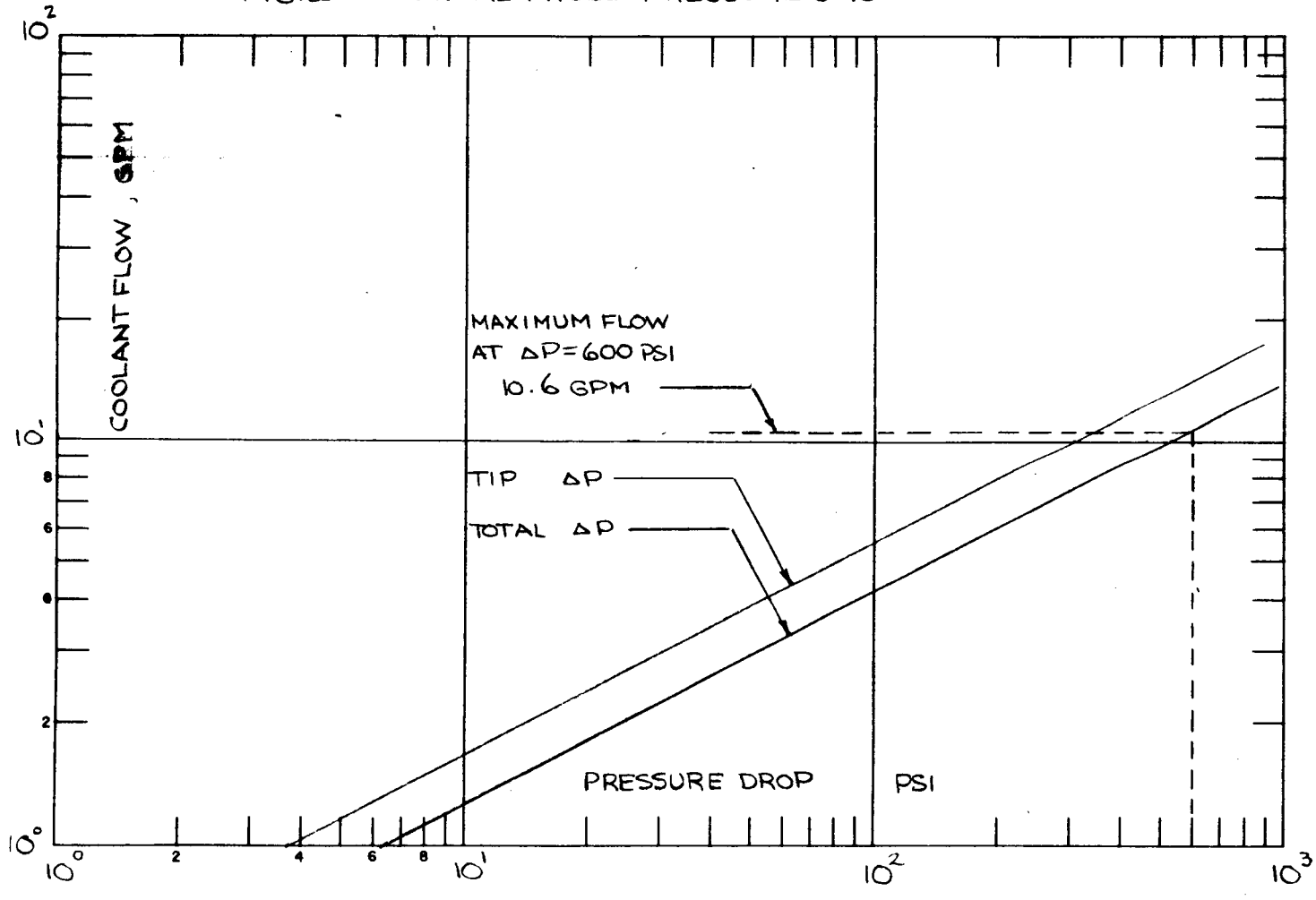

FIG 2.4
INTERNAL PROBE PRESSURE DROP

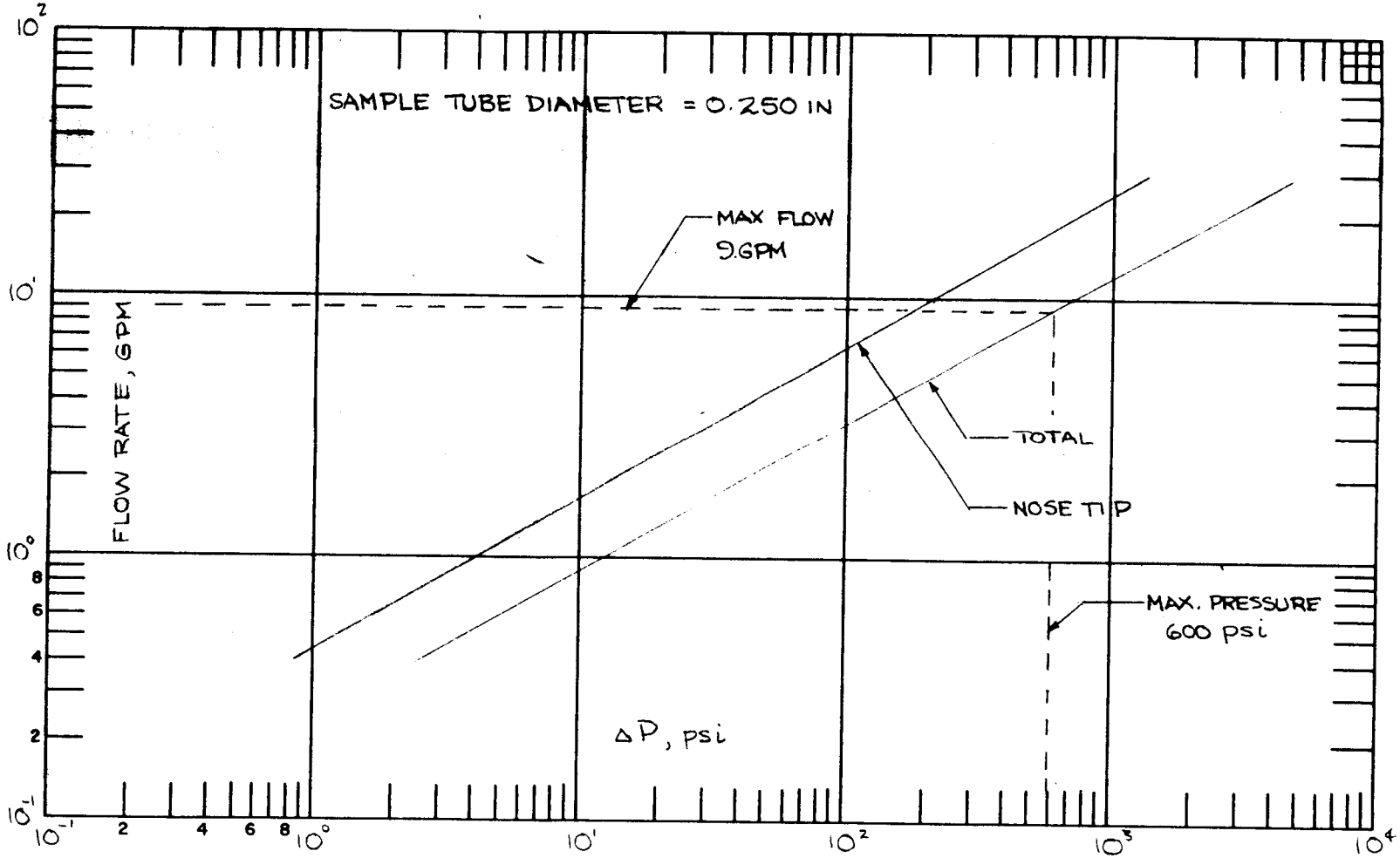

FIG 25
STRUT PRESSURE DROP

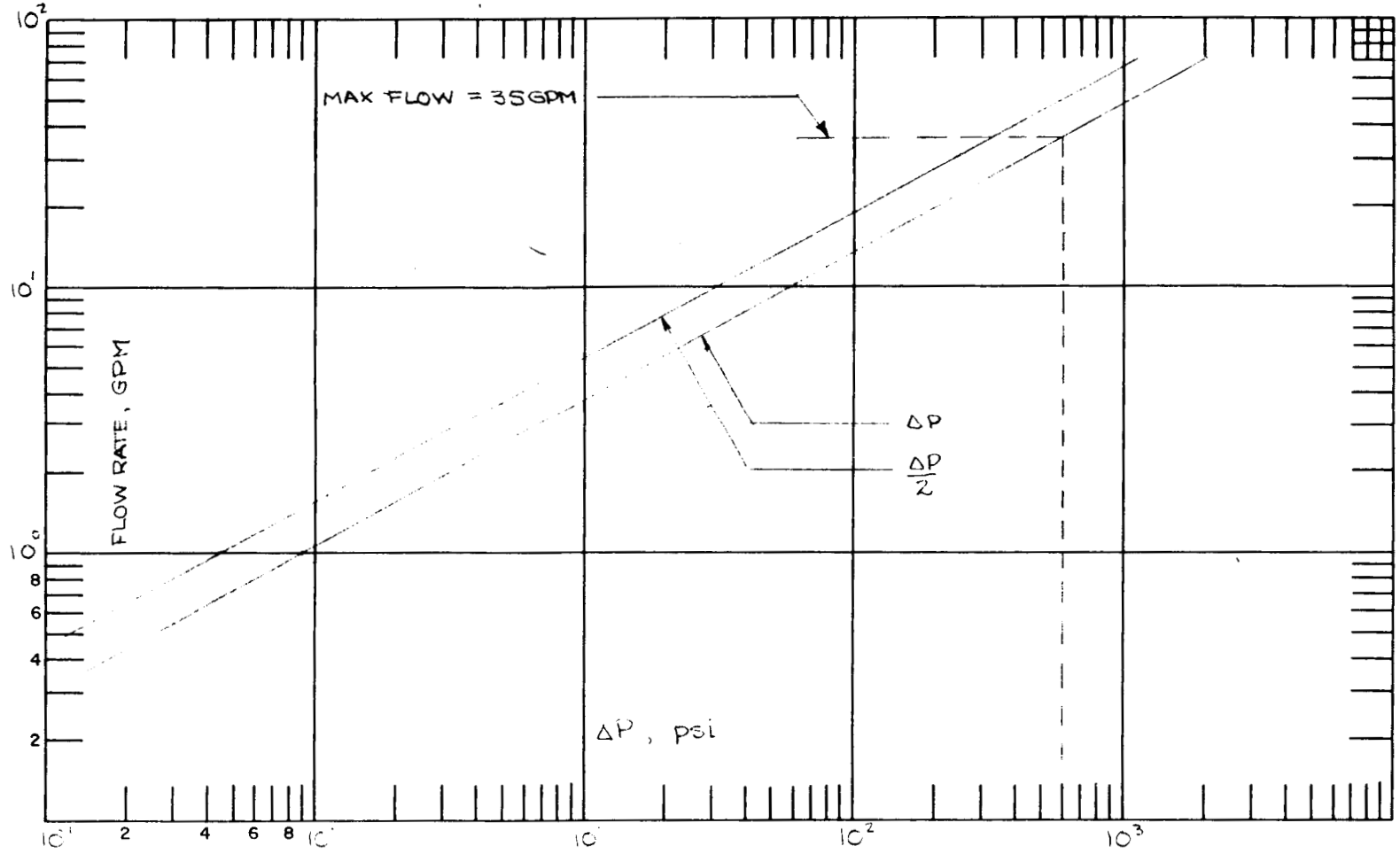

for Reynolds numbers in excess of 10,000. At lower Reynolds numbers, the heat transfer correlation[15] shown in Figure 26 was utilized. Regions of the probe which were of primary concern in this portion of the design included the forward edge of the internal probe, the forward edge of the external probe, and the leading edge of the strut.

1. Internal Probe

The cooling water channels at the forward portion of the internal probe flows through an annular channel having a width of 0.020 inch. The equivalent diameter (D_e) of an annular channel is given by

$$D_e = 4A/P = D_o - D_i \tag{84}$$

where A is the cross sectional area of the channel and P is the wetted perimeter. Using the properties of water at an assumed temperature of 100°F, the local convective heat transfer coefficient was found to vary with water flow rate in the manner shown in Figure 27. The internal wall temperature as a function of flow rate and heat transfer rate is given by

$$\dot{q} = h\,(T_w - T_\ell) \tag{85}$$

and are illustrated in Figure 28 for heat transfer rates in the range of 100 to 600 Btu/ft^2-sec. Also included in Figure 28 are the cooling water saturation temperature as a function of coolant flow rate and inlet water pressure which may be obtained from the computed cooling water pressure drop and the vapor pressure curve for water. It is obvious in those situations where the wall temperature as calculated from equation 85 exceeds the saturation temperature that boiling will occur.

In these situations, the heat transfer rate[16] is given by

$$\dot{q}_{TOTAL} = \dot{q}_{CONVECTION} + \dot{q}_{BOILING} \tag{86}$$

where the convection heat transfer is obtained in the manner described above and the heat transfer in the boiling process[17] is

$$\frac{C_{p_\ell}(T_w - T_{sat})}{\Delta H_{vap}} = 0.013 \left\{ \frac{\dot{q}_{BOIL.}}{\mu_\ell \Delta H_{vap}} \sqrt{\frac{g_e \sigma}{g(\rho_\ell - \rho_v)}} \right\}^{1/3} Pr_\ell^{1.7} \tag{87}$$

Since all the fluid properties are a function of saturation pressure

$$\dot{q}_{BOILING} = K(P)\ (T_w - T_{sat})^3 \tag{88}$$

where K(P) is a function of saturation pressure as shown in Figure 29. Hence,

$$\dot{q}_{TOTAL} = h\,(T_w - T_\ell) + K(P)\,(T_w - T_{sat})^3 \tag{89}$$

The total heat transfer rate due to both convection and boiling is illustrated

FIG 26

FIG HEAT TRANSFER COEFFICIENTS AT LOW REYNOLDS NUMBERS

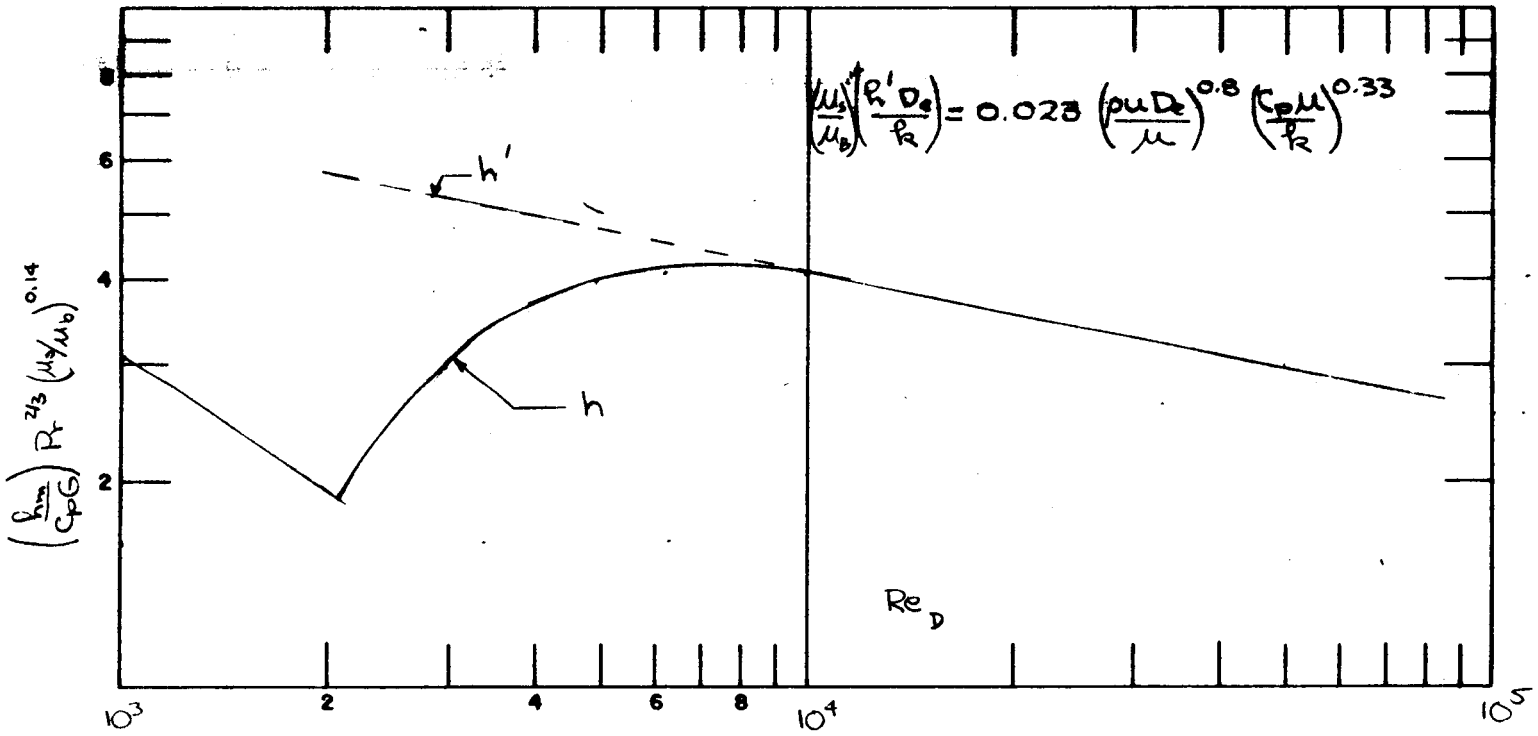

FIG 27
INTERNAL PROBE HEAT TRANSFER COEFFICIENT

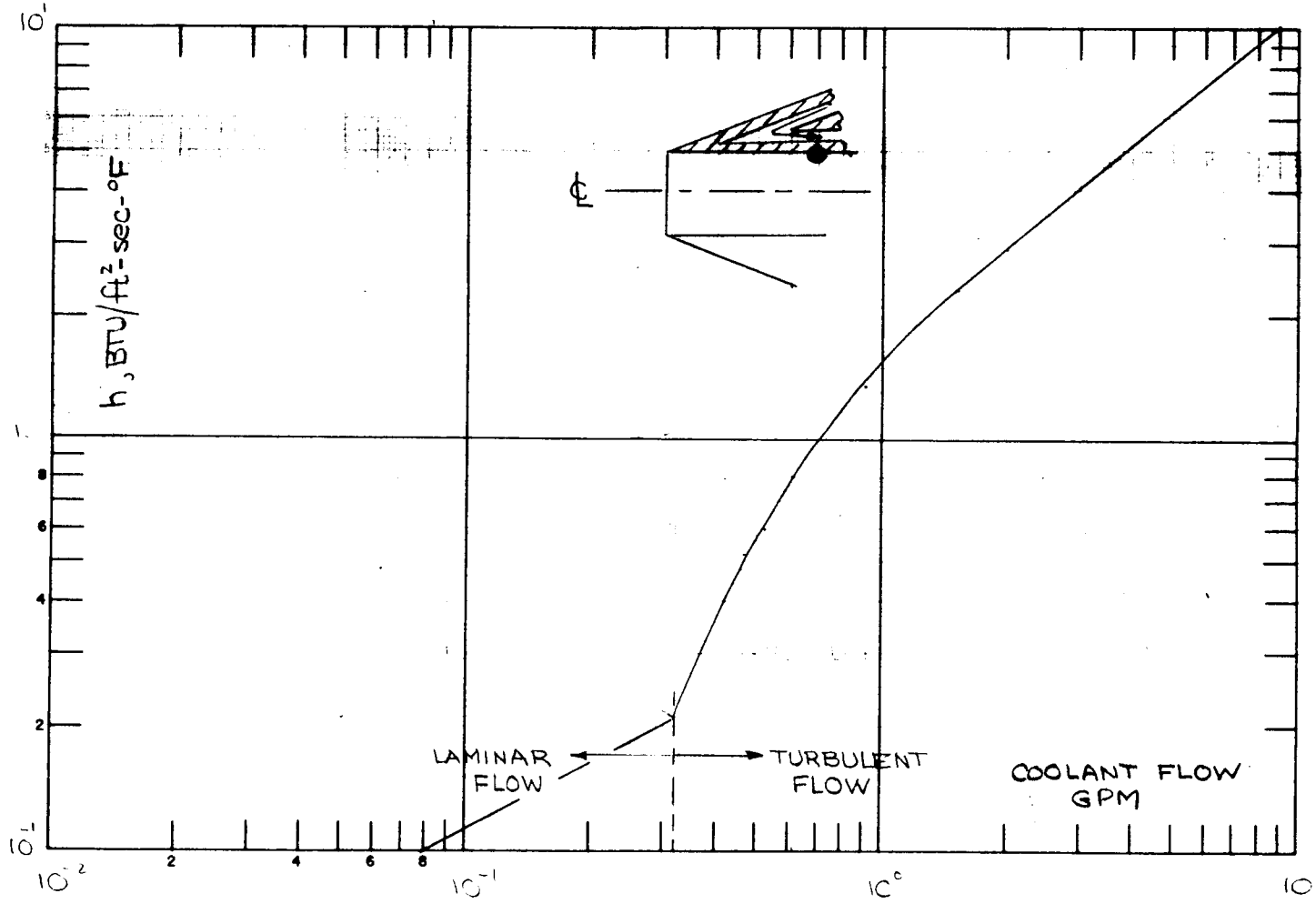

FIG 28
INTERNAL PROBE WALL TEMPERATURES

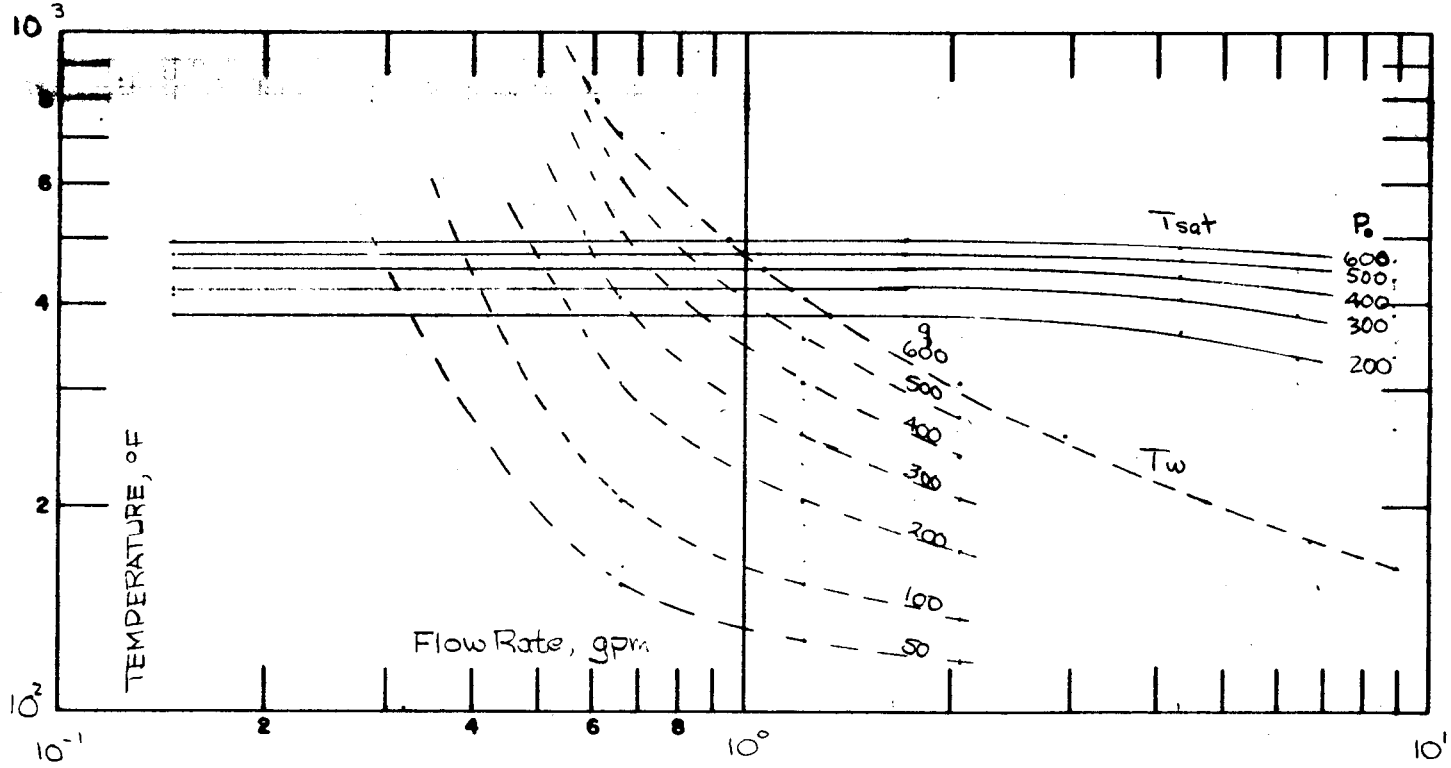

FIG 29
BOILING HEAT TRANSFER CORRELATION

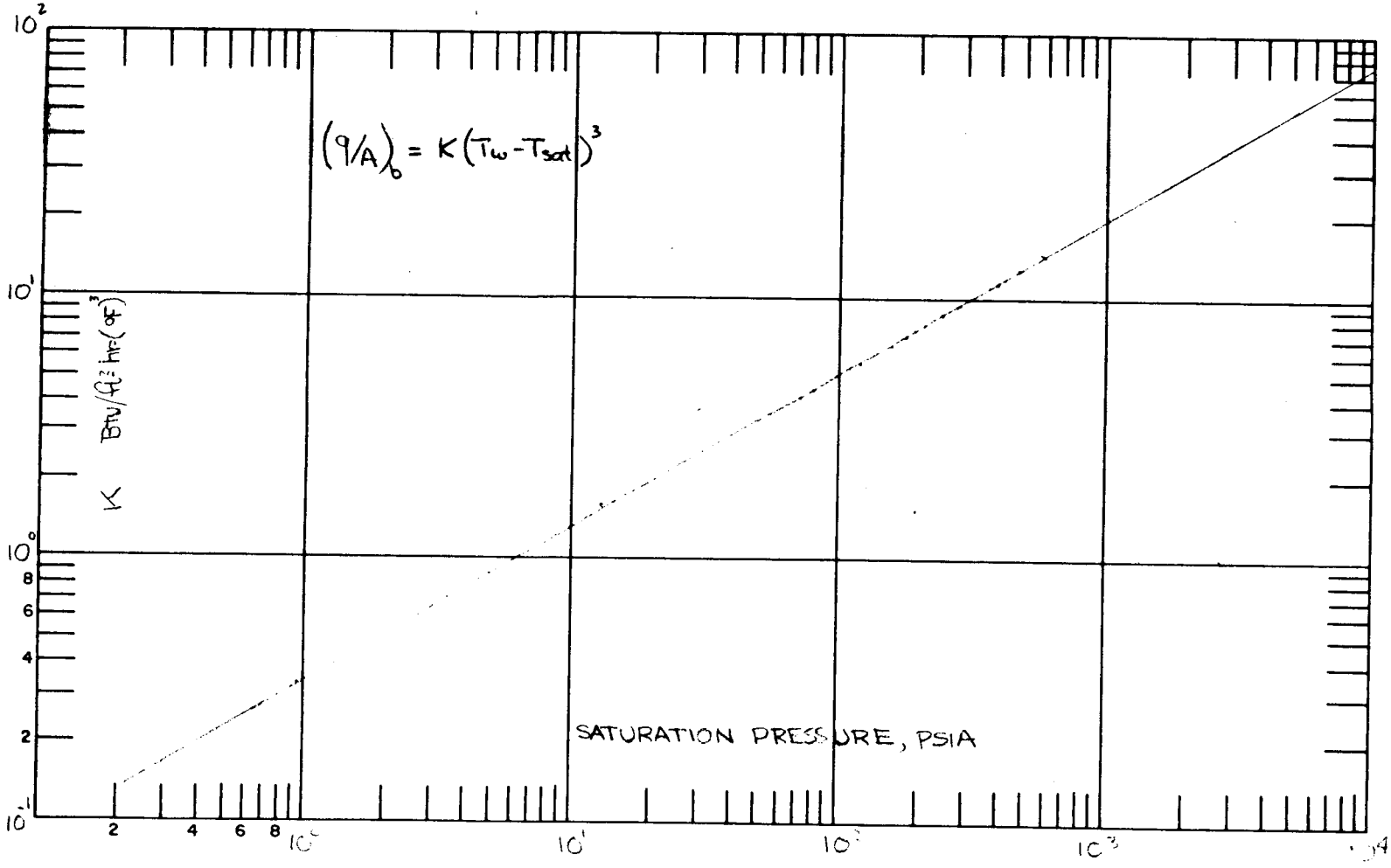

in Figure 30. The calculations show that at a heating rate of 1500 Btu/ft^2-sec that cooling water having an inlet pressure of 300 psia flowing at a rate of 1.5 gpm is sufficient to maintain the internal wall temperature at a temperature of 480°F. The temperature drop across the 0.025 inch wall of the copper sampling tube is simply

$$\dot{q} = k\,\Delta T/\Delta x \tag{90}$$

or 51 degrees at 1500 Btu/ft^2-sec making the temperature of the heated surface 531°F.

Since the energy absorbed by this coolant stream is used directly in the determination of gas enthalpy by means of an energy balance:

$$\dot{m}_g h_g = \dot{m}_{H_2O} C_{p_{H_2O}} \Delta T + \dot{m}_g C_{p_g} (T_g - T_o) \tag{91}$$

it is readily apparent that the magnitude of the cooling water temperature rise must be such that the accuracy of the measurement does not suffer. The cooling water temperature rise was estimated by assuming that the gas leaving the probe was at an enthalpy of 266 Btu/lb (8 RT_o). The coolant water temperature rise is then

$$\Delta T = \left(\frac{D_p}{D_N}\right)^2 \frac{\dot{m}_f (h_o - 266)}{\dot{m}_{H_2O} C_{p_{H_2O}}} \tag{92}$$

which results in the temperature rise curves shown in Figure 31 for nozzle diameters (D_N) of 5.0 and 25.0 inches and a probe sampling tube diameter of 0.250 inch. Also included in Figure 31 are the minimum cooling water flow rates required to prevent boiling within the cooling channels as a function the stagnation point heating rate (Figure 32) since it is desirable to eliminate boiling whenever possible. Typical examples of the use of this figure are given below for the following free stream conditions:

Condition	3	4
h_e, Btu/lb	26000	26000
$\dot{m}_f$, lb/sec	0.04	0.04
D_N, in.	5.0	25.0
$q\sqrt{r_N}$, Btu/ft$^{3/2}$-sec	390	99
$\dot{m}_f h_o$, Btu/sec	1040	1040

For condition 3, the minimum flow rate to prevent boiling at a 400 psia inlet pressure is 0.69 gpm. At this flow and for a total free stream energy flux of 1040 Btu/sec the coolant temperature rise is found to be 26°F. For condition 4 however, the same procedure results in a coolant temperature rise of 1.4°F which

FIG 30 PROBE HEATING RATES

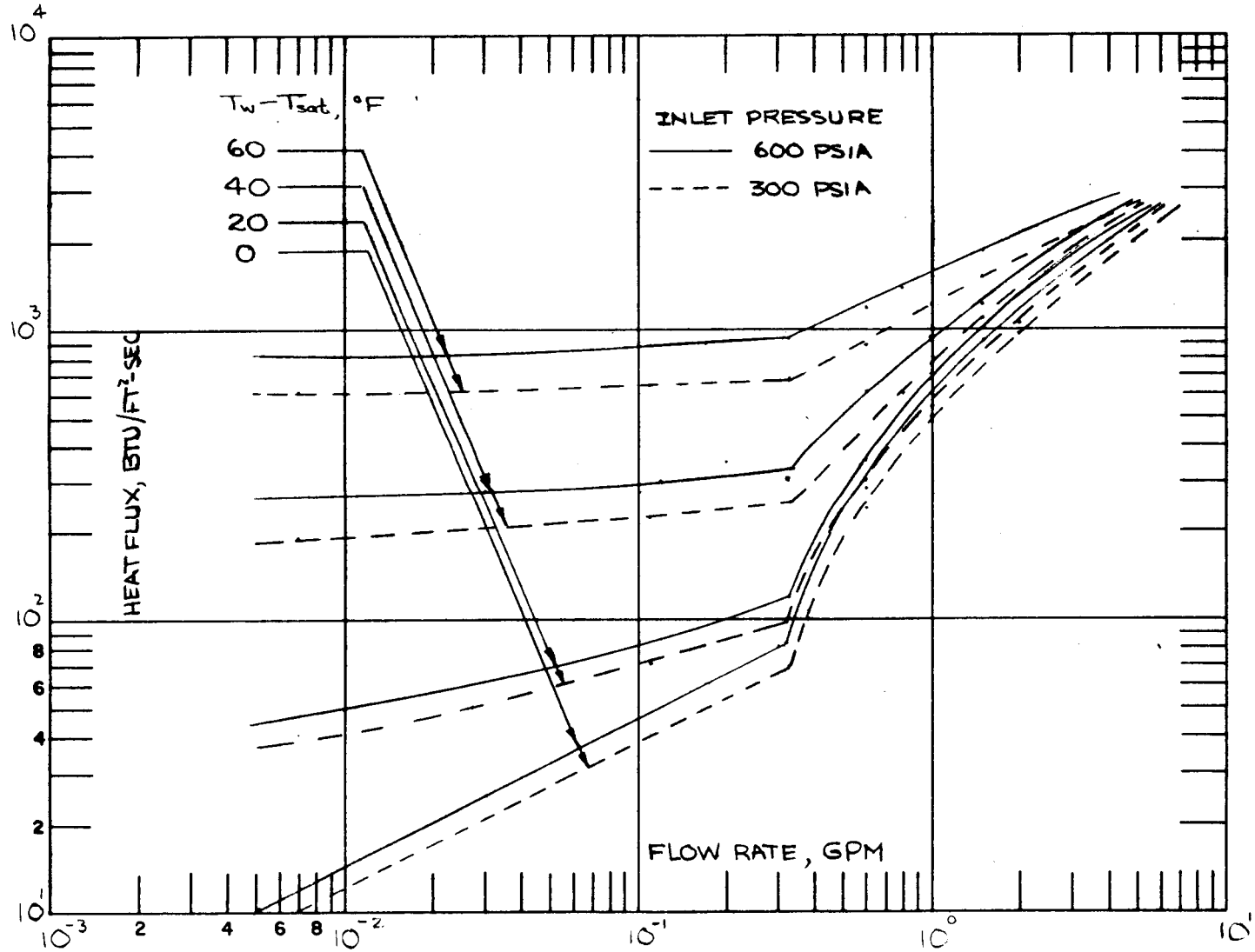

FIG 31 COOLANT TEMPERATURE RISE

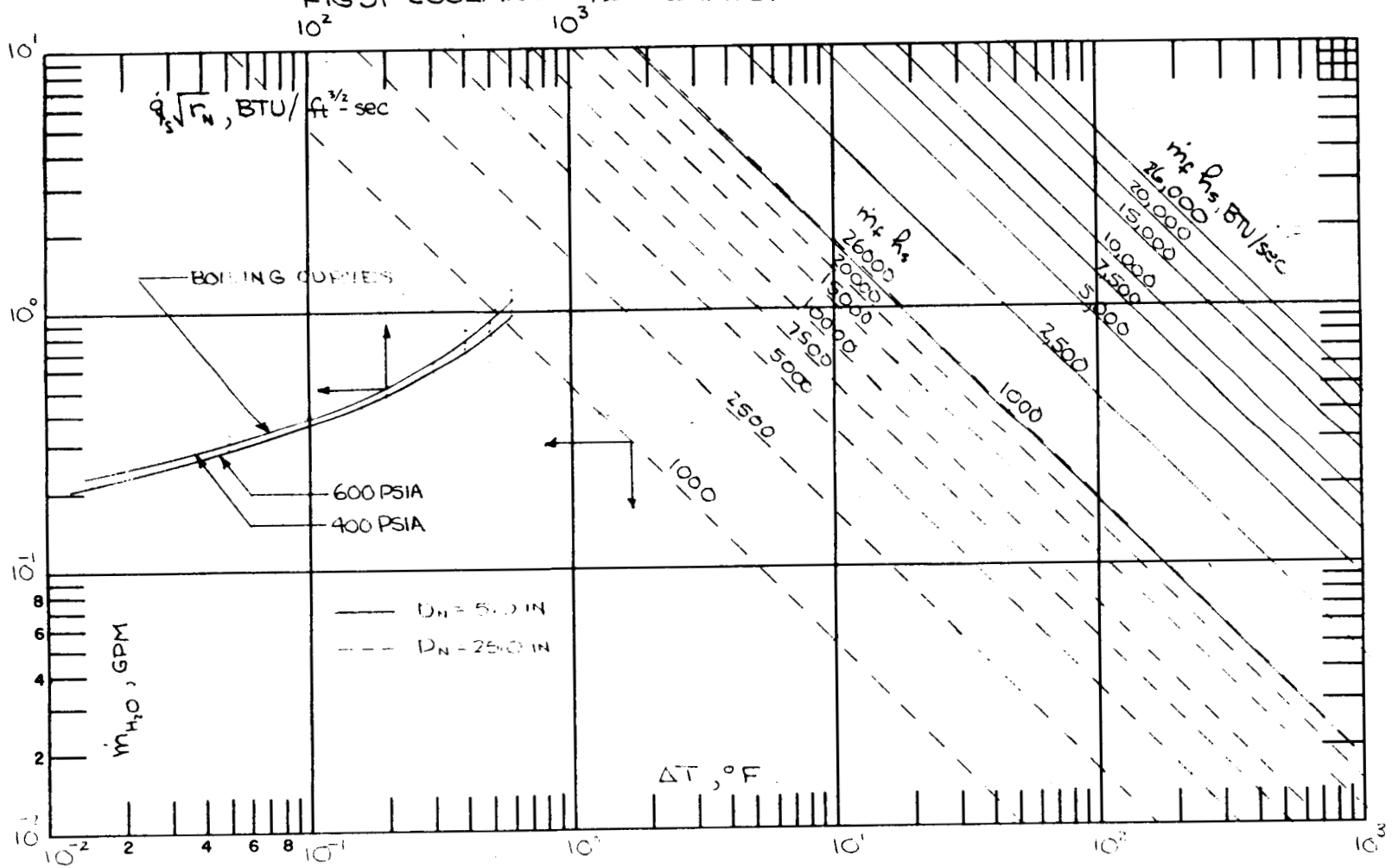

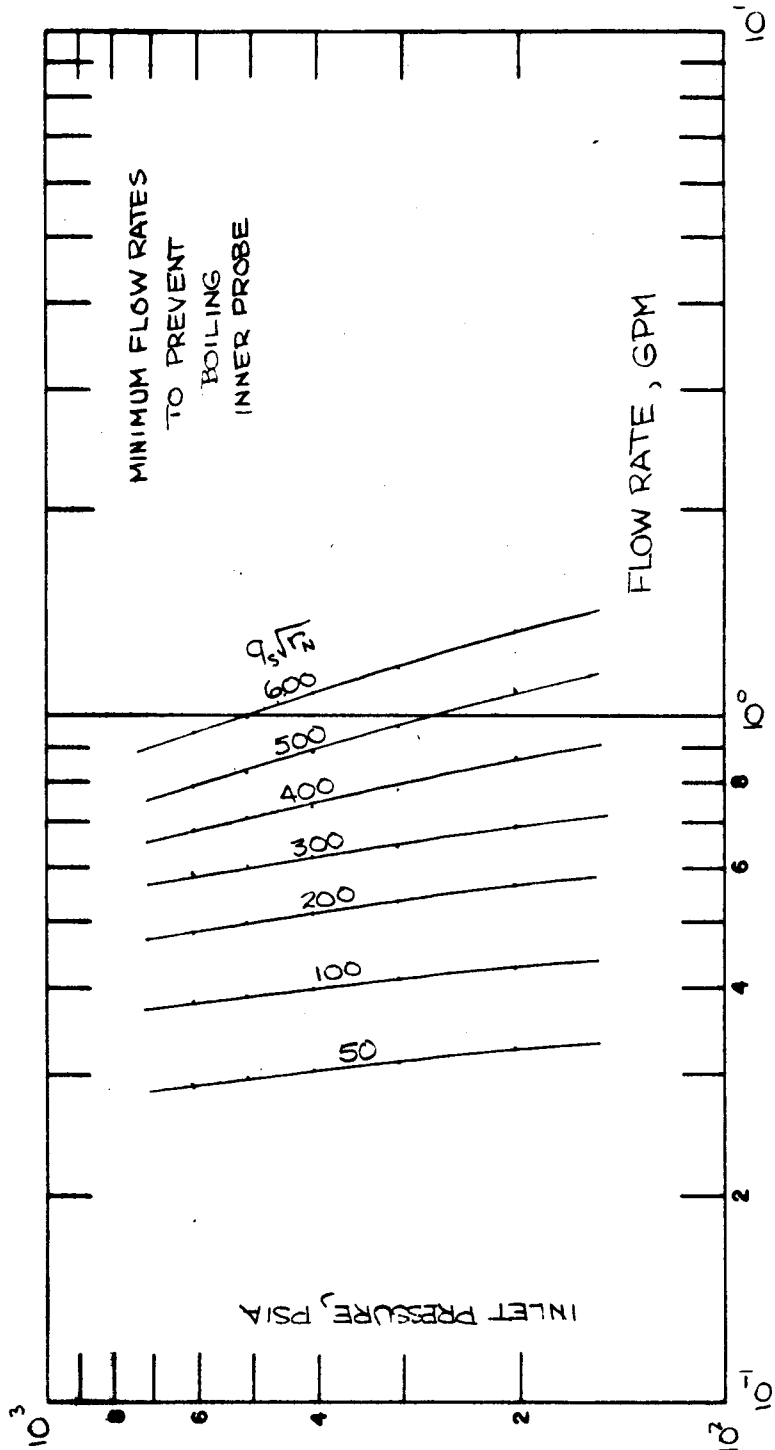

FIG 32 BOILING HEAT TRANSFER REGIMES

is clearly not sufficient to insure reasonable accuracy for the system. Reducing the flow rate to a value which would produce a 10°F temperature rise implies a coolant flow of 0.044 gpm. Referring to Figure 30, it is found that, at this flow rate, boiling would occur and the wall temperature would be approximately 30°F above the saturation temperature.

It is noted that the above discussion has considered the convective heat transfer coefficient to be equal to that which would be obtained in fully developed flow in smooth passages. In reality however the coolant flow is in the process of negotiating a 165 degree change in flow direction. By analogy with the pressure drop experienced by fluids flowing through such a bend[18] it is expected that the local heat transfer coefficient would be increased by a factor of 60 over that obtained in smooth channels. At any particular heat flux it is expected that the difference between the wall and fluid temperatures would by less than those shown in Figure 28 would be reduced by the same factor. If it is assumed that the heat transfer coefficient is increased by a factor of 10 over that illustrated in Figure 27, boiling does not occur at any of the ARMSEF conditions listed in Table I even when the coolant flow is adjusted to produce a temperature rise of 10°F.

2. External Probe Tip

Local heat transfer coefficients in the cooling channels behind the conical tip of the external probe were determined in a similar manner and are illustrated in Figure 33. Included in this illustration are convective cooling coefficients at various other positions along the external probe cooling passages. The external probe tip convective cooling coefficients were used to calcuate the wall temperature on the surface of the cooling passage in the manner discussed above. By comparing these temperatures with the saturation temperature of the cooling water (Figure 34) it was determined that it was possible to cool the external probe tip without boiling occurring at all the ARMSEF conditions listed in Table I.

3. Strut

The critical area of concern in the heat transfer analysis of the probe strut is the leading edge of this portion of the system. Local heat transfer coefficients were computed from the turbulent flow relationship

$$\frac{h}{\rho u C_p} Pr^{2/3} \left(\frac{\mu_w}{\mu_b}\right)^{0.14} = 0.023 Re^{-0.2} \qquad (93)$$

and are illustrated in Figure 35 for various wall temperature with the coolant assumed to be at 100°F. Wall temperatures at various heating rates are shown in Figure 36. A comparison of the wall temperatures and the saturation temperature of the cooling water as a function of flow rate demonstrates that boiling will not occur if the local heating rate is below 1700 Btu/ft^2-sec. This corresponds to a stagnation line heat transfer rate ($\dot{q}_s \sqrt{r_{N_{3D}}}$) of 425 Btu/ft$^{3/2}$-sec. However since there is considerable lateral conduction within the external shell of the strut, the amount of coolant available would be sufficient to cool the strut at a considerably higher heat flux level. For example, if lateral conduction could be considered to produce a uniform temperature on the rear surface strut leading edge, then coolant flow available is sufficient to coolt the device at an average leading edge heating rate of 1700 Btu/ft^2-sec. This average flux level is equivalent to a stagnation point heating rate ($\dot{q}_s \sqrt{r_{N_{3D}}}$) of 475 Btu/ft$^{3/2}$-sec.

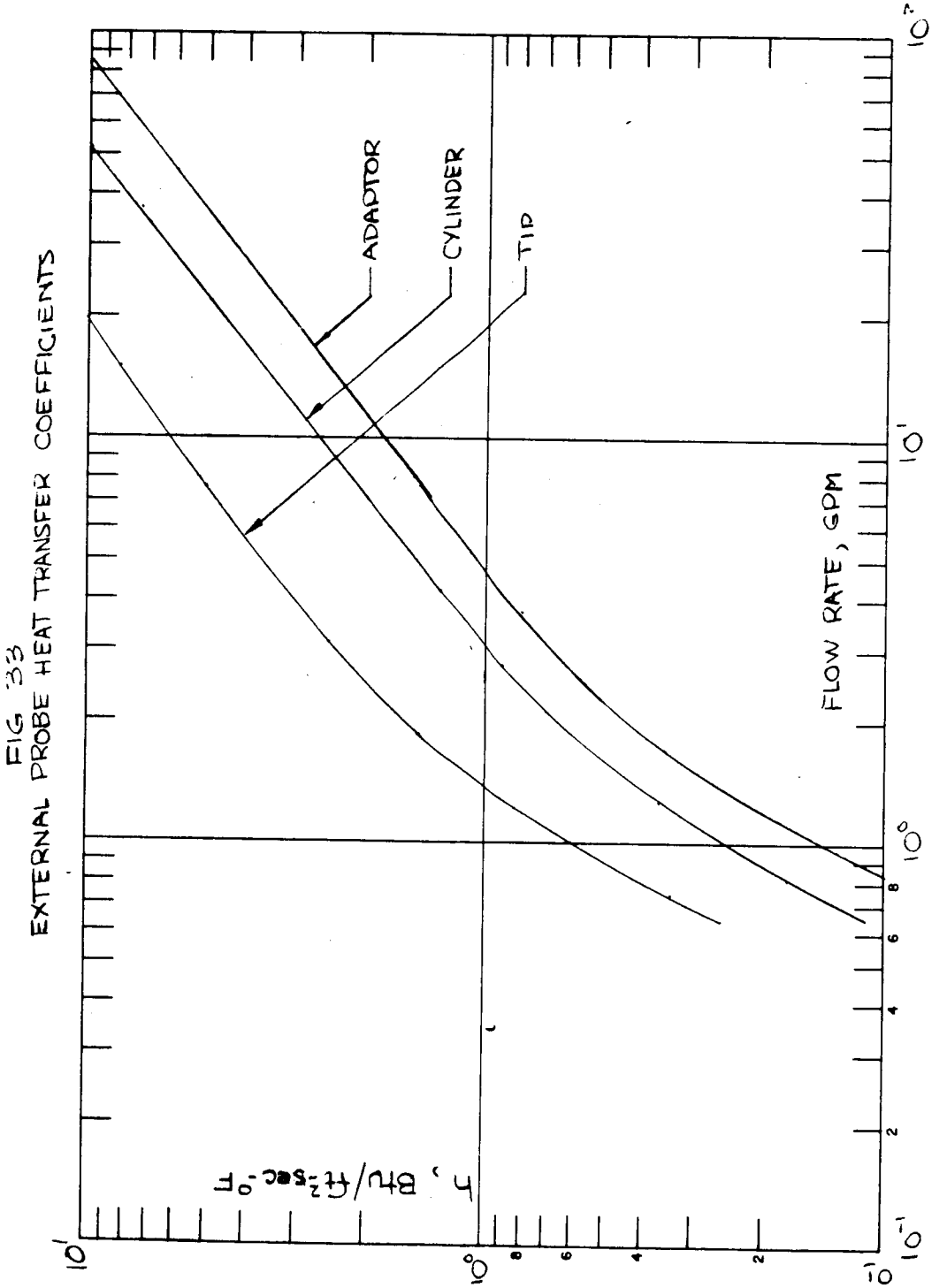

FIG 33
EXTERNAL PROBE HEAT TRANSFER COEFFICIENTS

FIG 34
OUTER PROBE COOLING REQUIREMENTS

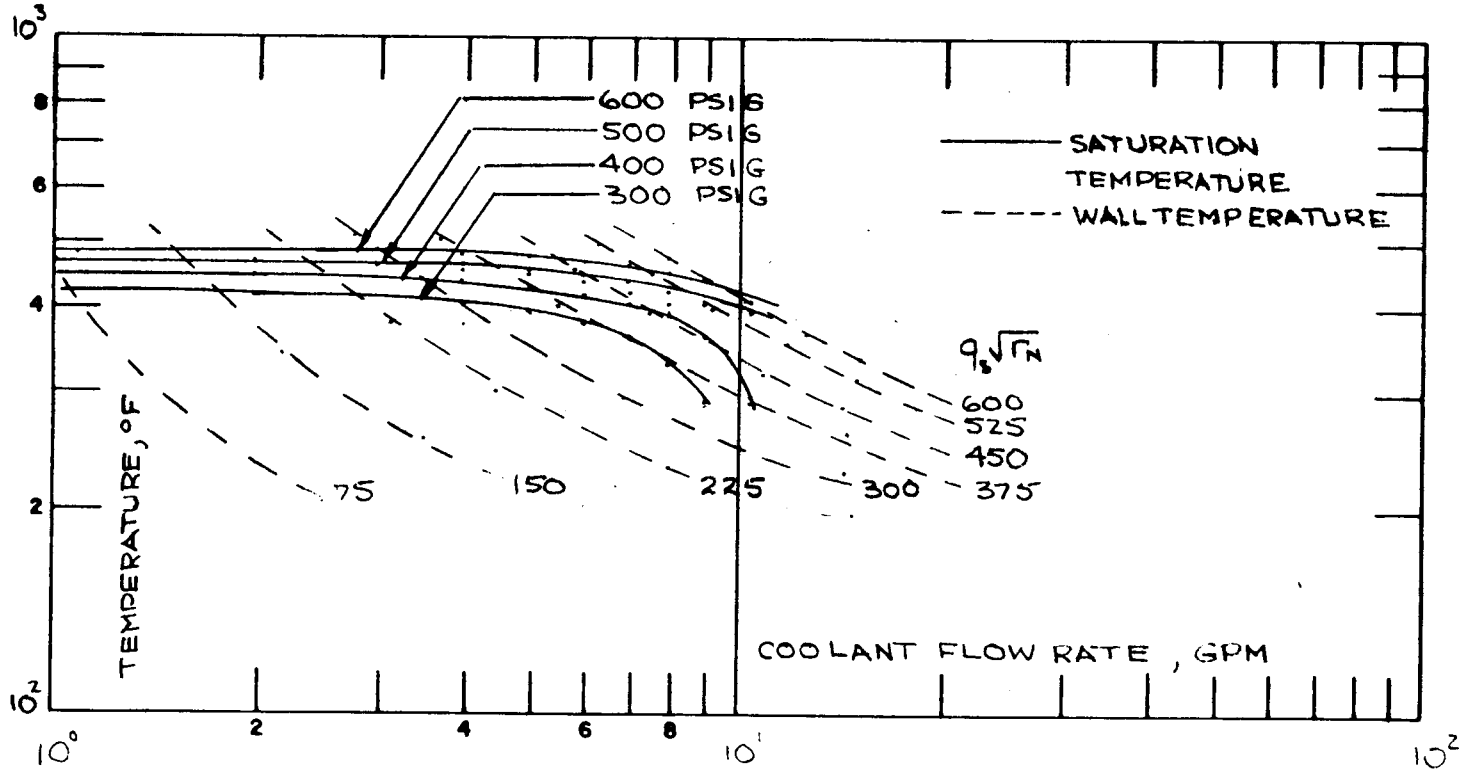

FIG 35
STRUT HEAT TRANSFER COEFFICIENTS

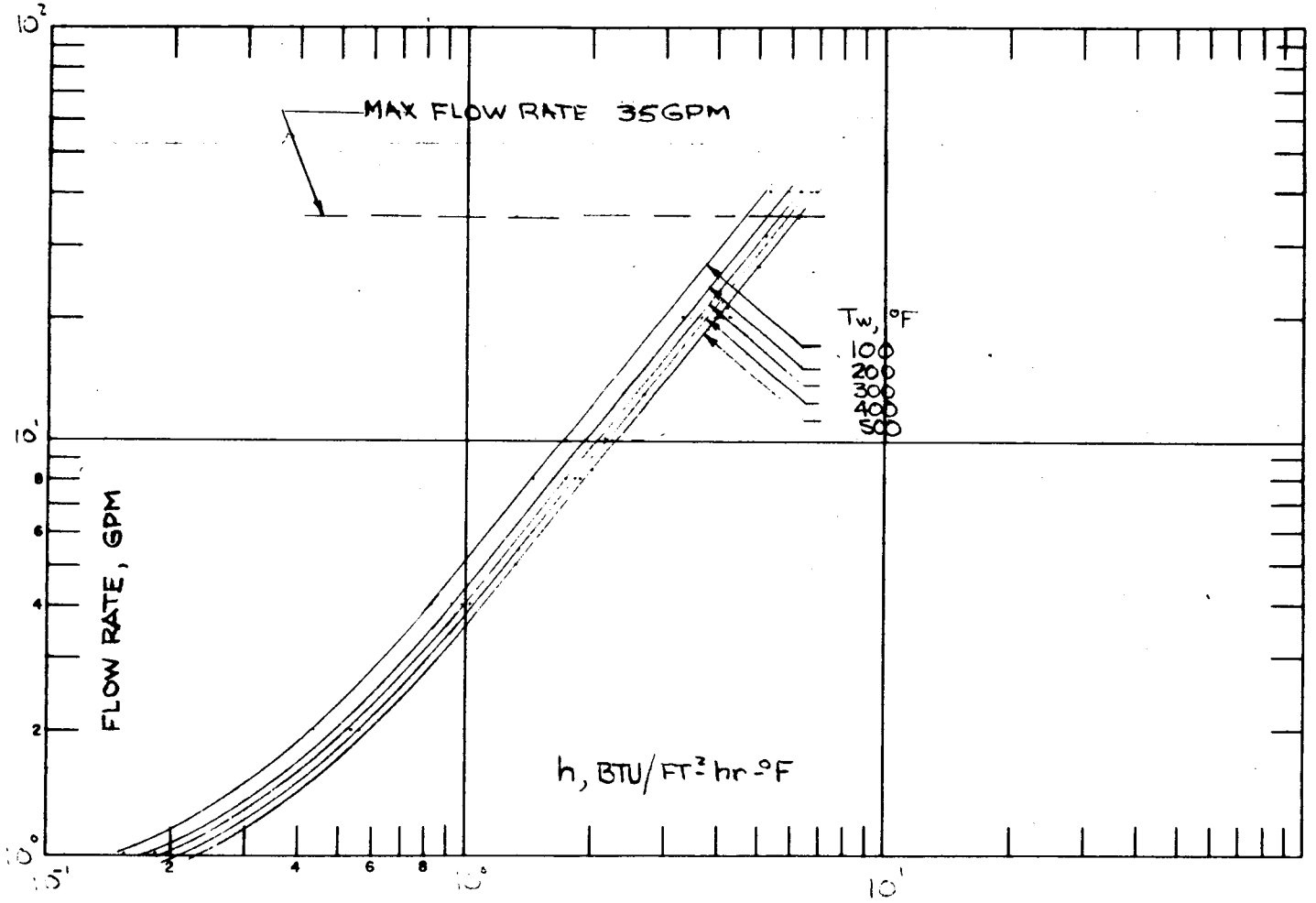

FIG 36
STRUT WALL TEMPERATURES

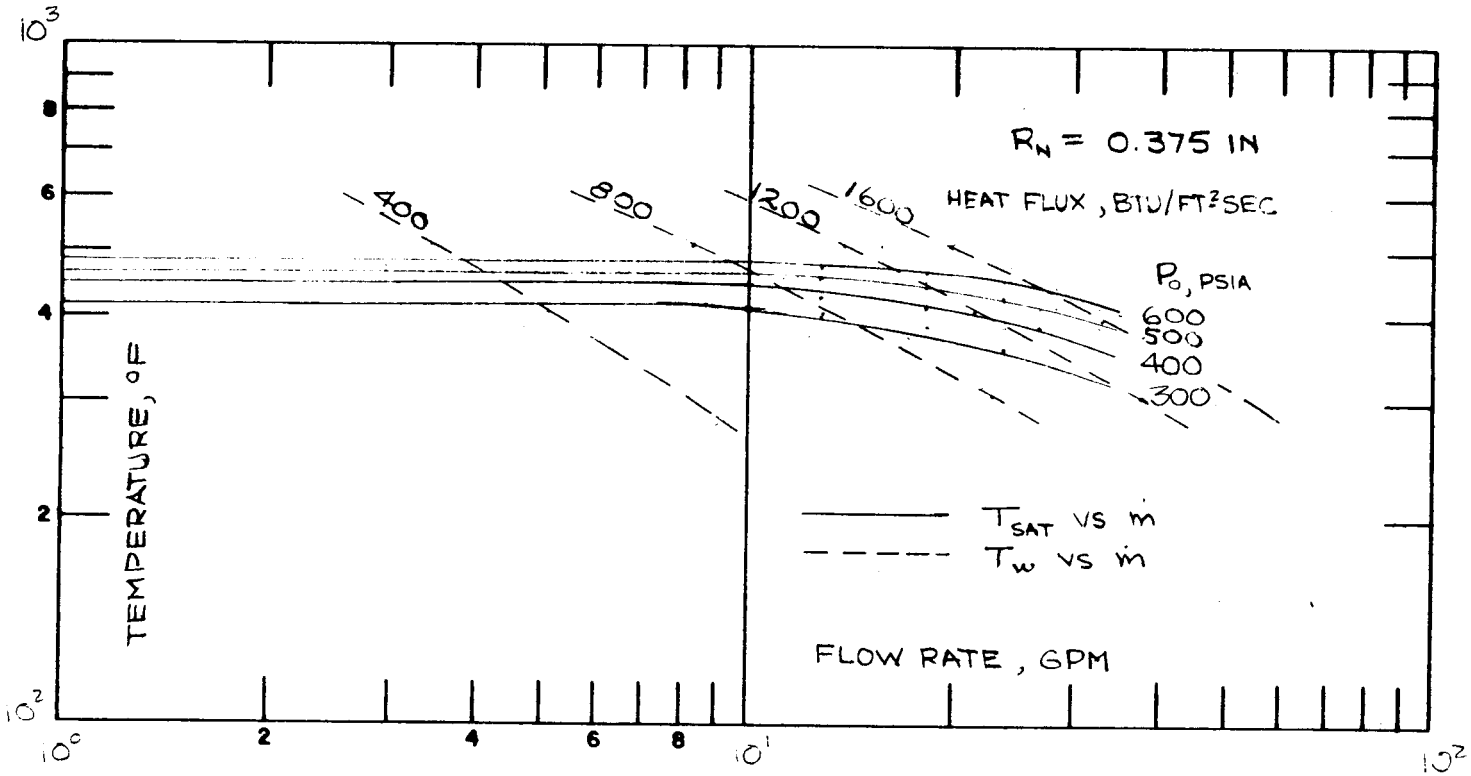

In actuality however, the real convective heat transfer limit will be somewhere between the two values cited above (the average of these two values is $\dot{q}\sqrt{r_N} = 585$ Btu/ft$^{3/2}$-sec). Hence it is expected that the cooling water available will be sufficient to provide the necessary protection of the strut from its environment even at the most severe conditions produced by the ARMSEF with, at most, a minimum amount of boiling at the maximum heating condition.

There is however a small region along the stagnation line of the strut where interaction of the probe bow shock with the shock on the strut leading edge results in augmentation of the local heat transfer rate by an approximate factor of two. This shock interaction region is confined to a region having a width of approximately 0.3 strut leading edge diameters (0.225 inch). As shown by Comfort[9] in his integral analysis of lateral heat conduction within the interaction region, the external surface temperature on the strut leading edge can easily be maintained at less than 800°F.

STRESS ANALYSIS

The stresses in critical areas of the probe were examined to insure that the various tubes, etc. used to fabricate the instrument have sufficient strength to withstand the maximum loading expected during operation of the device. The areas examined included the outer and inner shells of both the exterior and inner probes, and the outer shell of the water cooled strut. In regions where there is no heat transfer, the stresses in the structure are due to pressure loading alone, however in regions where there are temperature gradients thermal stresses must be considered, also.

The outer shell of the exterior probe consists of a copper tube having inner and outer diameters of 1.000 inch and 0.900 inch, respectively. At a internal pressure of 600 psia, the stress in this portion of the probe caused by pressure loading is simply

$$S_p = \frac{P}{2}\left(\frac{D_o + D_i}{D_o - D_i}\right) = 5700 \text{ psi} \tag{94}$$

Since there is heat transferred through this wall, thermal stresses must be considered, also. The thermal stresses on the outer and inner surface of a tube may be determined from[20]

$$S_{T_o} = \frac{\alpha_T E \Delta T}{2(1-m)}\left[\frac{2(r_o/r_i)^2}{(r_o/r_i)^2 - 1} - \frac{1}{\ln(r_o/r_i)}\right] \tag{95}$$

$$S_{T_i} = \frac{\alpha_T E \Delta T}{2(1-m)}\left[\frac{2}{(r_o/r_i)^2 - 1} - \frac{1}{\ln(r_o/r_i)}\right] \tag{96}$$

where the temperature difference across the wall is given by

$$\Delta T = \frac{\dot{q} r_i}{k} \left(\frac{r_o}{r_i} - 1 \right) \qquad (97)$$

For the case where the heat transfer occurs on the external surface of tube, the thermal stresses result in a compressive loading on the exterior and a tensile stress on the interior wall. At a heat transfer rate of 320 Btu/ft^2-sec it was found that with the following properties of copper

$k = 220$ Btu/ft-hr-$^\circ$F

$\alpha_T = 9.8 \times 10^{-6}$ $(^\circ F)^{-1}$

$E = 15.6 \times 10^6$ psi

$m = 0.355$

The thermal stress on the inner tube wall was calculated to be 2900 psi (tension) and -2780 psi (compression) on the inner wall. Hence the combined stresses are 8600 psi and 2920 psi on the inner and outer surfaces. The maximum stress is well below the yield point of deoxidized copper: 12000 to 14000 psi.

A similar procedure was followed in determining the stresses in the external walls of the strut. Since pressure loading produces the maximum stress when the width of the strut is a maximum, stresses were calculated for the sides of this member which are parallel to the flow field. At a pressure of 600 psia, the stress due to pressure loading for a strut width of 0.750 inch and a wall thickness of 0.0625 inch is 3300 psi (tension). The stress produced by a temperature gradient in the wall of the strut is given by

$$S_T = \frac{\alpha_T E \Delta T}{(1-m)} = \frac{\alpha_T E}{(1-m)} \left(\frac{\dot{q} \Delta x}{k} \right) \qquad (98)$$

which results in a tensile stress of 3400 psi at a heat flux of 170 Btu/ft^2-sec. Hence the maximum stress on the strut wall is 6700 psi.

IV. SAMPLING SYSTEM DESIGN

The measurement of the local gas enthalpy within the exhaust jet by energy balance techniques with an enthalpy probe requires accurate knowledge of the mass flow of the aspirated gas. If more information concerning the properties (density and velocity) of the flow field is required it is also necessary that the aspirated gas sample flow rate be identical to that in the free stream. To satisfy this condition, there is a maximum pressure drop which can be experienced by the gas sample and yet allow the probe to operate correctly. While operating in this manner, the probe has "swallowed the bow shock" and operates as a mass flux measuring device. If the pressure drop in the sampling system is allowed to exceed the maximum allowable value, the flow through the sampling train adjusts to some value less than that in the free stream and there is a bow shock off the leading edge of the probe tip. The design of the sampling train therefore is of critical concern if the instrument is desired to be capable of measuring local free stream mass flux in the ARMSEF. The primary concern in this portion of the probe design is in the pressure drop experienced by the flow in passing through the sample system.

Probe and Strut Pressure Drop

The pressure drop experienced by the aspirated gas sample in flowing through the 0.250 inch I.D. sampling lines contained within this portion of the system was determined with the following assumptions. It was assumed that the flow passes through a normal shock immediately after entering the gas sampling tube and that due to the low Reynolds number of the flow cooling of the gas to a low temperature ($\sim 1000^{\circ}R$) takes place within a short distance of the probe tip. The change in pressure accompanying the cooling process was assumed to be negligibly small. With these assumptions, the pressure at the tip of the probe is equal to that immediately downstream of a normal shock and the Mach number of the flow is given by

$$M = \frac{\dot{m}_\infty}{A_p P}\left(\frac{RT_1}{g\gamma}\right)^{1/2} \tag{99}$$

where T_1 is assumed to be $1000^{\circ}R$. The pressure drop resulting from flow down the sampling tube can be obtained from the compressible flow analysis of Shapiro[21]. Shapiro shows that for any given initial Mach number there is a maximum length of tubing, defined as the length required to produce sonic flow at the downstream end, which is given by

$$4\bar{f}\left(\frac{L}{D}\right)_{max} = \frac{1-M^2}{\gamma M^2} + \frac{\gamma+1}{2\gamma}\ln\left\{\frac{(\gamma+1)M^2}{2\left(1+\frac{\gamma-1}{2}M^2\right)}\right\} \tag{100}$$

where $\bar{f}$ is the mean friction coefficient defined as

$$\bar{f} = \frac{1}{L_{max}}\int_0^{L_{max}} f\,dx \tag{101}$$

and

$$f = f(Re_D) \tag{102}$$

Shapiro further demonstrates that the length of duct required for the flow to pass from a given initial Mach number, M_1, to a final Mach number, M_2 is given by

$$4\bar{f}\left(\frac{L}{D}\right) = 4\bar{f}\left(\frac{L}{D}\right)_{max,M_1} - 4\bar{f}\left(\frac{L}{D}\right)_{max,M_2} \tag{103}$$

In addition, the change in pressure resulting in flowing from M_1 to sonic flow at (L/D)max is simply

$$p/p^* = \frac{1}{M_1}\left\{\frac{\gamma+1}{2\left(1+\frac{\gamma-1}{2}M_1^2\right)}\right\}^{1/2} \tag{104}$$

where p^* being the pressure at (L/D)max (i.e., M = 1.0). The change in pressure accompanying the flow from the initial Mach number (M_1) to its final value (M_2) can in turn be obtained simply from

$$p_2/p_1 = \frac{(p_2/p^*)}{(p_1/p^*)} \tag{105}$$

Equations 100 and 104 are illustrated in Figures 37 and 38, respectively.

A typical sample of the method employed in evaluating the pressure drop is as follows. The sampling line within the probe and strut is assumed to be 41 inches in length and to contain two 90 degree bends which for a 0.250 inch diameter line results in a total equivalent length of 225 tube diameters. For a flow which has an initial Mach number of 2.3×10^{-2} and a Reynolds number of 15.3

$$f = 16/Re_D \tag{106}$$

$$4fL/D = 945 \tag{107}$$

and

$$\left(4f\frac{L}{D}\right)_{max} = 1350 \tag{108}$$

The Mach number of the flow at the end of this portion of the sampling line corresponds to that at which

$$\left(4f\frac{L}{D}\right)_{max,M_2} = 1350 - 945 = 305 \tag{109}$$

FIG 37

MAXIMUM LENGTH OF SAMPLING TUBE

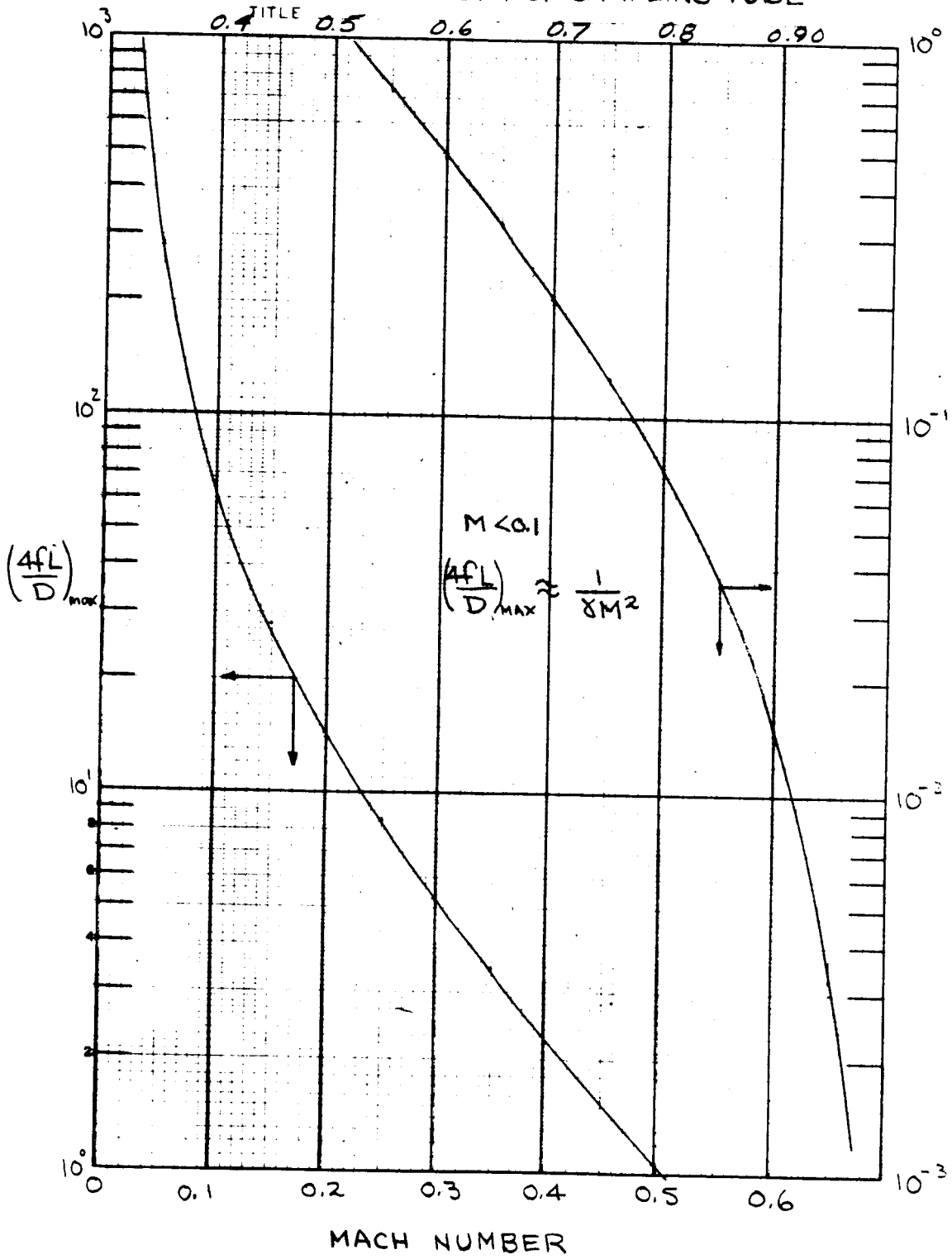

FIG 38

SAMPLE TUBE PRESSURE DISTRIBUTION

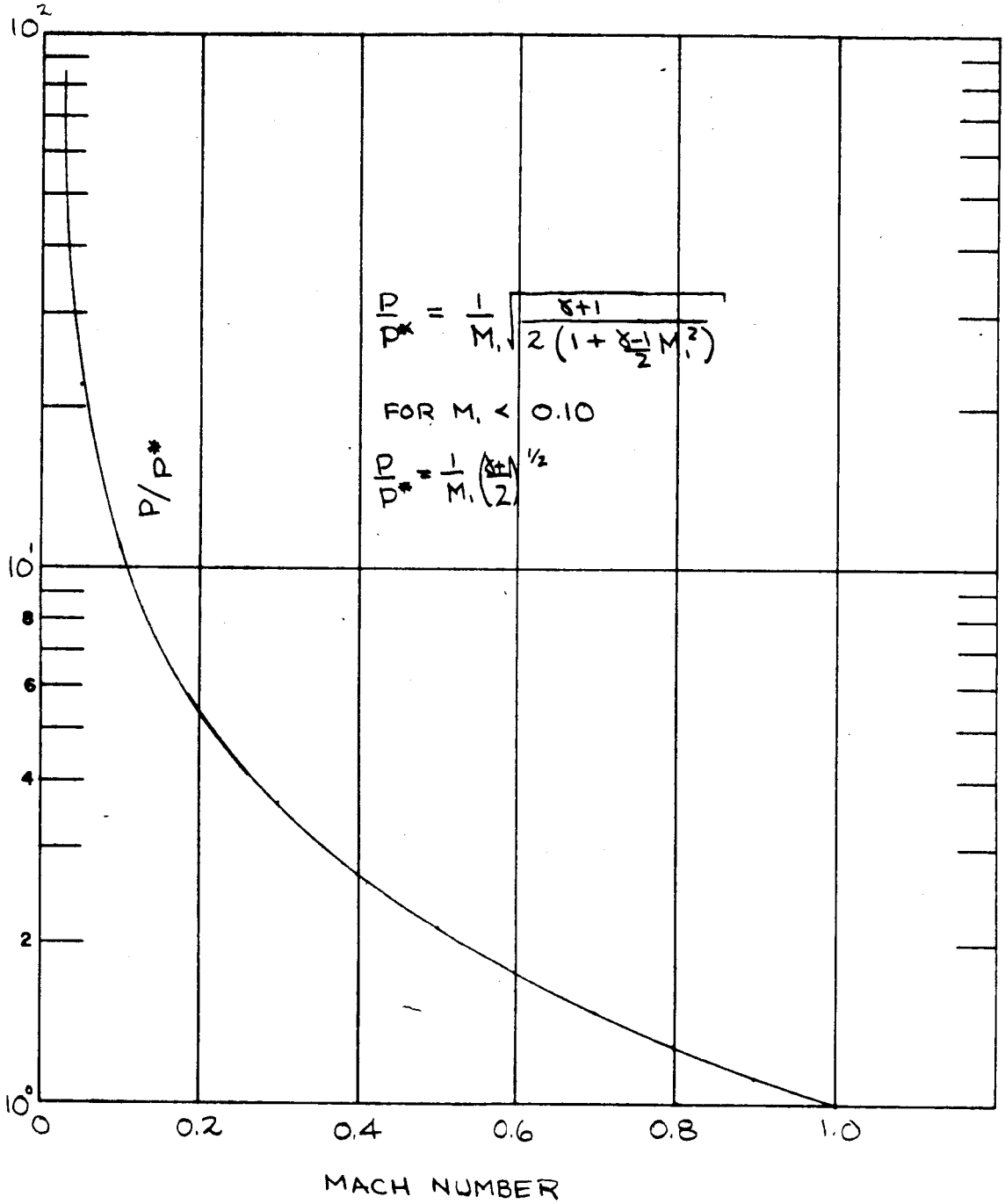

Referring to Figure 37, it is found that the Mach number of the flow has increased to 4.8×10^{-2}. From the initial and final Mach numbers, it is found that the pressures at the inlet and outlet are given by

$$P_1/P_2 = M_2/M_1 = 2.08 \tag{110}$$

Initial and final conditions for other typical ARMSEF operating points are listed in Table 2.

Pumping Requirements

The size of the vacuum pump necessary to insure that the sampling system is capable of aspirating the required mass flow rates at the pressures expected can be determined by comparing pumping speed curves (volumetric flow rate as a function of inlet pressure) with the expected flow properties. A typical example is shown in Figure 39, included in this illustration are expected pressures at various mass flow conditions at ARMSEF. The inlet pressure to the pump as obtained from the pumping curve must be lower than the line pressure in order to have a feasible system. Alternately for a mass flow rate of 2.5×10^{-4} lb/sec at a calculated pressure of 186 mm Hg the inlet pressure to the pump is given by the interesection of the pumping curve, and the constant mass flow line shown in Figure 39 as 14 mm Hg. Hence the particular pump illustrated would satisfy the pumping requirements of the probe system.

A comparison of the pump inlet pressures required for aspirating flow rates typical of those expected in ARMSEF and the calculated pressures in the probe sampling lines (Figure 40) makes it possible to consider measurement of the aspirated flow with either orifice plates or Venturi flow meters. Orifice plates have the advantage that the output of the meter can be made a maximum value at any combination of flow rate and pressure; however, they do offer a high resistance to the flow. On the other hand Venturi flow meters provide the least resistance to the flow due to the low pressure drop.

The maximum output signal which could be obtained with an orifice plate would result if the orifice diameter were made small enough to insure sonic flow through the flow meter. In this case, the flow rate is directly proportional to the pressure immediately upstream of the orifice and is given by

$$\dot{m} = PA \left\{ \frac{g\gamma}{RT} \left(\frac{2}{\gamma+1} \right)^{\frac{\gamma+1}{\gamma-1}} \right\}^{1/2} \tag{111}$$

which for air may be written simply as:

$$\dot{m} = 0.533 \frac{PA}{\sqrt{T}} \tag{112}$$

A direct comparison of the flow rate at various pressures and orifice diameter and the actual line conditions expected in ARMSEF is given in Figure 40. It is seen that it may be possible to use a 0.100 inch diameter orifice to measure all the flows expected at ARMSEF.

TABLE II

SUMMARY OF CONDITIONS WITHIN SAMPLING LINES

Condition	1	2	3	4	5	6
Facility mass flow, lb/sec	1.00	1.00	0.04	0.04	0.10	0.10
Gas enthalpy, h/RT_o	118	118	766	766	766	766
Plenum pressure, atm	7.83	7.83	2.64	2.64	1.65	1.65
Mach number	3.2	5.3	3.0	5.6	3.2	5.0
Probe Variables						
$\dot{m}_p$, lb/sec	2.5×10^{-3}	1.0×10^{-4}	1.0×10^{-4}	4.0×10^{-6}	2.5×10^{-4}	1.0×10^{-5}
M_1	0.105	0.074	0.039	0.023	0.048	0.033
Re ($1000^{\circ}R$)	9000	370	370	15.3	900	37
f	0.0082	0.043	0.043	1.04	0.017	0.432
$4f(L/D)$	8.3	38.8	38.8	945	15.3	388
M_2	0.115	0.091	0.043	0.048	0.051	0.053
p_1, atm	1.18	0.067	0.126	0.0074	0.260	0.015
p_2, atm	1.08	0.055	0.114	0.0038	0.244	0.00935
p_2, mm	820	420	87	2.90	186	7.10
P_{pump}, mm	270	11.0	11.0	0.47	26.5	1.18
$4f(L/D)_{max}$	45	74	400	300	250	250

FIG 39 PUMP SELECTION CRITERIA

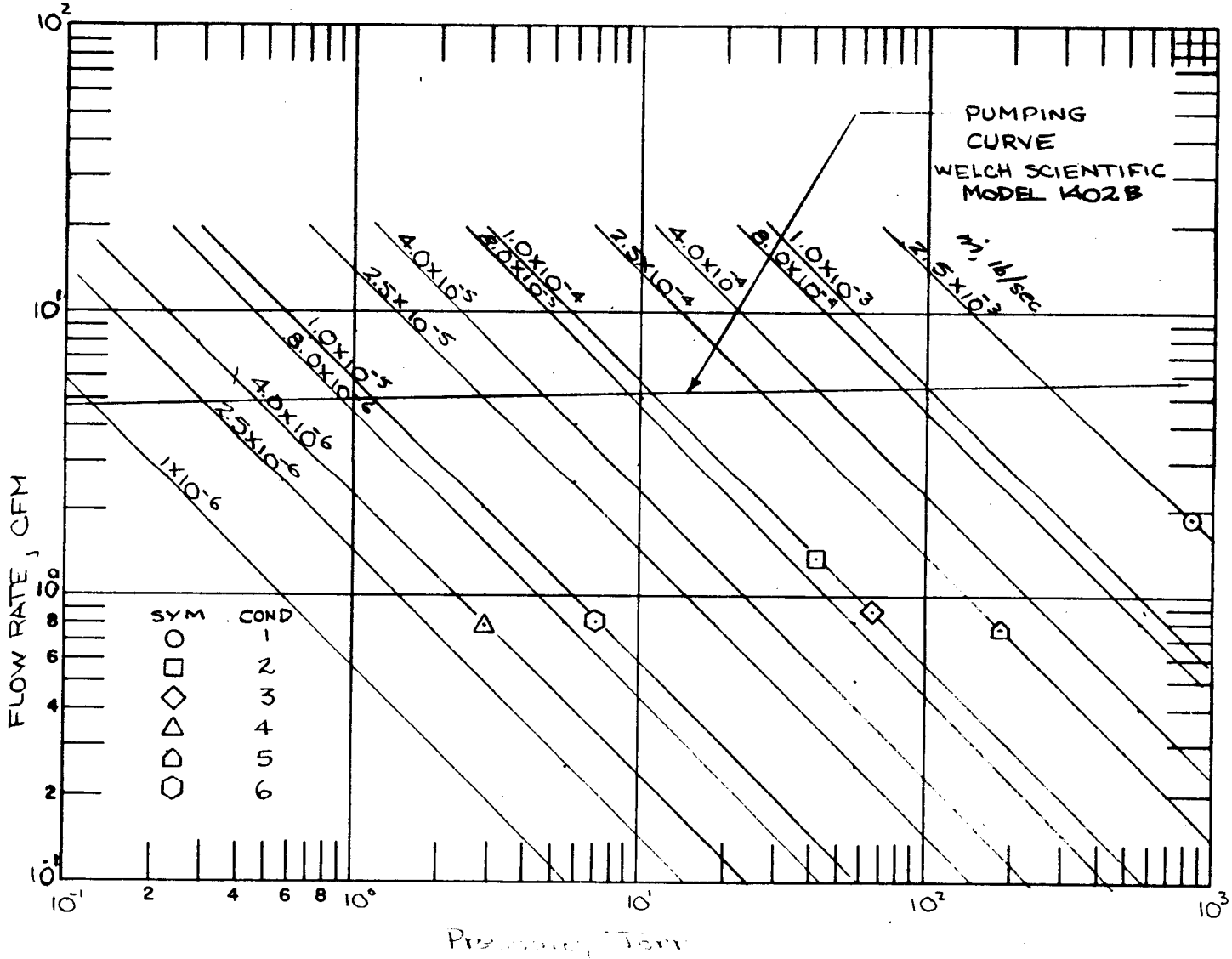

FIG 40 SONIC ORIFICE FLOW RATES

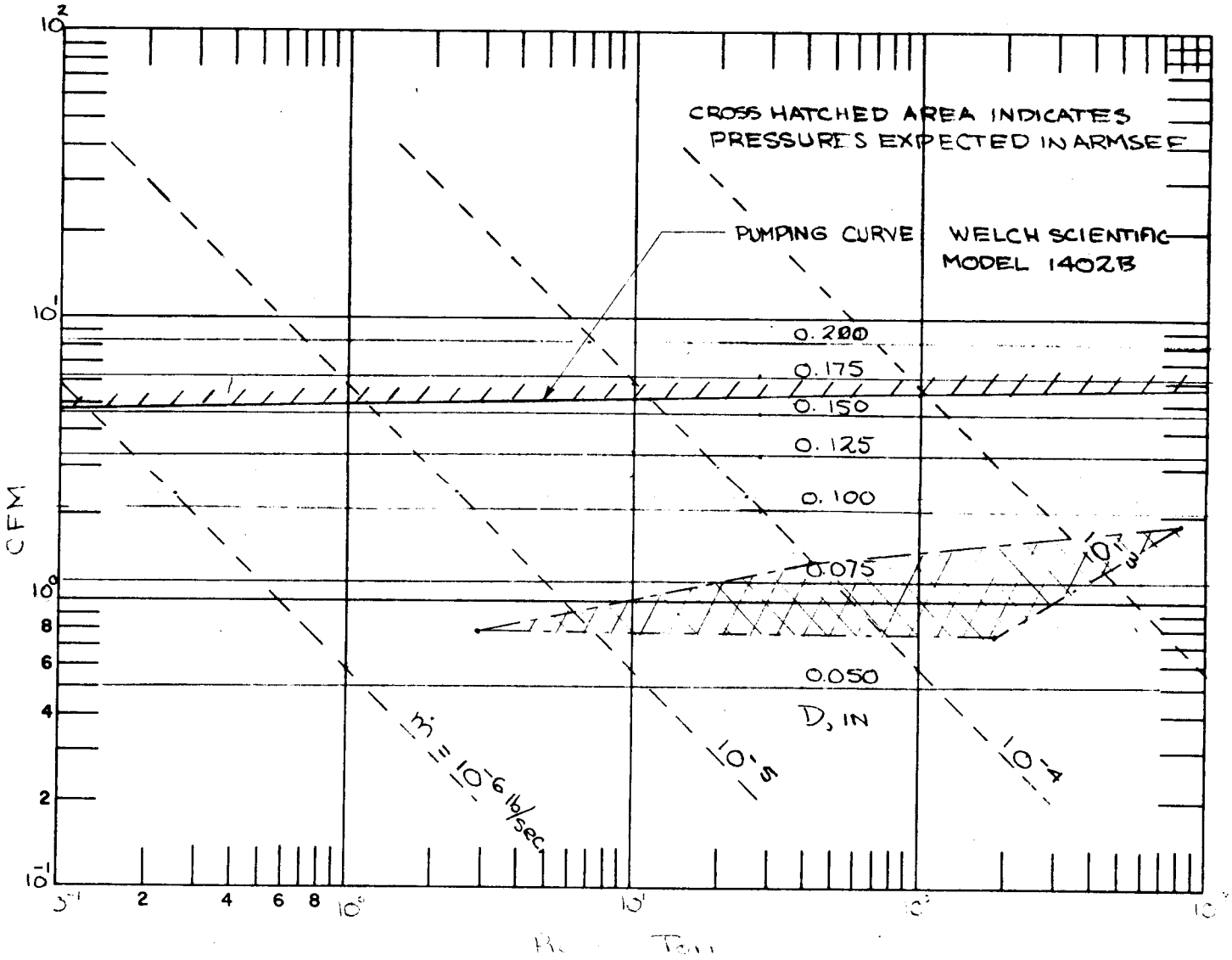

V. MASS FLOW CALIBRATION SYSTEM

In essence the calibration system (Figure 41) consists of two manifolded tanks of known volume each of which can be independently vented through a restrictive orifice plate to provide a mass flow through the flow meter being calibrated. The meter being investigated is positioned between the restrictive orifice and the system vacuum pump thereby allowing the meter to be calibrated at pressure levels comparable to those which will be encountered during operation of the probe system in the ARMSEF exhaust stream.

The basic procedure which is employed in calibration of the flow meters is as follows. With the exit valves of the two gas reservoirs closed, the two tanks are loaded to a specified pressure, P_o, at which time they are isolated from the gas supply. Gas is then allowed to flow from one tank (the other remaining isolated) for a measured time interval through the restrictive orifice and, in turn, through the flow meter being calibrated and to the vacuum pump. During this period the response of the meter is monitored and then it is once again isolated from the reservoirs. The total mass flow from the reservoir can then be calculated from variations in the pressure and temperature changes in the reservoir:

$$\Delta m = \frac{V}{R}\left\{\frac{P_o}{T_o} - \frac{P_1}{T_1}\right\} \tag{113}$$

where subscripts 0 and 1 refer to conditions immediately before and after the experiment. In order to provide an accurate measurement of the final pressure (P_1) in the reservoir, it is determined from the response of a differential pressure transducer between the two reservoirs, i.e.,

$$P_1 = P_o - \Delta P \tag{114}$$

therefore

$$\Delta m = \frac{P_o V}{R}\left\{\frac{1}{T_o} - \frac{1}{T_1} + \frac{\Delta P}{P_o T_1}\right\} \tag{115}$$

Now if the temperature changes within the system are small, this may be written as

$$\Delta m = \frac{P_o V}{R\bar{T}}\left\{\frac{\Delta P}{P_o}\right\} \tag{116}$$

Furthermore, with a volume large enough to limit the pressure change to less than 5 percent, the mass flow rate through the meter is simply

$$\dot{m} = \frac{\Delta m}{\Delta t} = \frac{V}{R\bar{T}}\left\{\frac{\Delta P}{\Delta t}\right\} \tag{117}$$

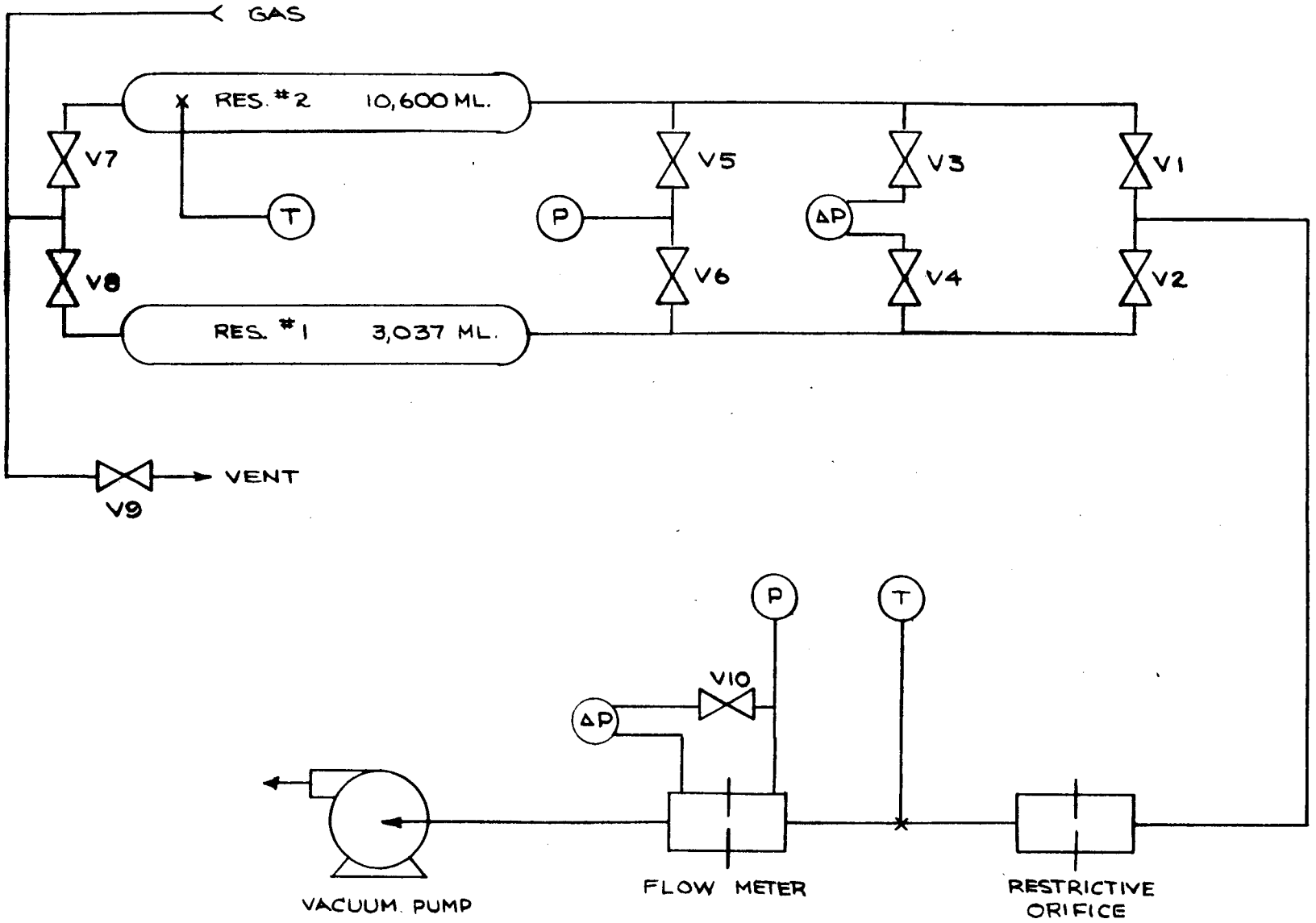

FIG 41 MASS FLOW CALIBRATION SYSTEM

The volume of the reservoir required to satisfy the stipulation the pressure changes are to be less than 5 percent is easily established from the relationship

$$\frac{\dot{m}_{max}\, \Delta t}{\rho V} = 0.05$$

which for a mass flow of 2.3×10^{-3} lb/sec for a 10 second period at 250 psia initial loading pressure results in a minimum reservoir volume of 0.34 cubic feet. This volume corresponds to a length of 10 feet of 2.50 inch inside diameter pipe. To provide some means of obtaining a substantial pressure change at very low rates, the volume of the second reservoir was chosen to be 0.10 ft^3. Actual reservoir volumes obtained in fabricating the system were 0.1075 ft^3 and 0.374 ft^3.

A series of calibration experiments were performed to determine the loading pressures required to obtain mass flow rates with the restrictive orifice plates that would be in the range expected in the ARMSEF. These orifice plates were calibrated by allowing gas (air) to flow from the larger volume to the smaller for a measured time period. The mass flow rate through these restrictive orifices was computed from equation 117 using both the pressure rise in the smaller volume and the pressure drop obtained in the larger tank. The resulting calibration curves are shown in Figure 42, as expected each orifice (in the range of pressures employed) acts as a sonic orifice with the mass flow being directly proportional to the pressure on the upstream side of the orifice. These orifice plates therefore provide a means of obtaining mass flow rates of the magnitude desired for the ARMSEF facility and hence can be used to calibrate the flow meters which are to be used during the actual probe experiments conducted in the facility exhaust jet. It is evident from the data presented in Figure 42 that the actual orifice diameters are considerably different from the nominal diameters, for example comparing the data for 0.004 inch and 0.020 inch orifices the ratio of the two mass flows is found to be 0.060. This is fifty percent greater than what would be expected from the ratio of the square of the nominal diameters (0.040).

Three orifices ranging in size from 0.0995 inch to 0.140 inch in diameter were calibrated in the manner discussed above with air in the system. The results of these calibration tests are illustrated in Figure 43 while similar data obtained with argon and a 0.120 inch diameter orifice plate are shown in Figure 44. The mass flow through the orifice plates were found to be linear in the pressure on the upstream side of the flow meter at pressures as low as 2 mm Hg. The range of calibration employed in these tests was from 10^{-5} lb/sec to 10^{-3} lb/sec with air and from 3×10^{-5} to 10^{-3} for argon. A comparison of argon and air data with the same orifice plate show that the data are in good agreement with the ratio of the two flow rates as predicted from sonic flow. For example, sonic flow indicates that at the same pressure the mass flow of argon should be 25 percent greater than the air flow rate; comparing the data in Figures 43 and 44 at 23.5 Torr the air flow is 1.0×10^{-4} while for argon it is 1.25×10^{-4} lb/sec.

FIG 42
RESTRICTIVE ORIFICE CALIBRATION

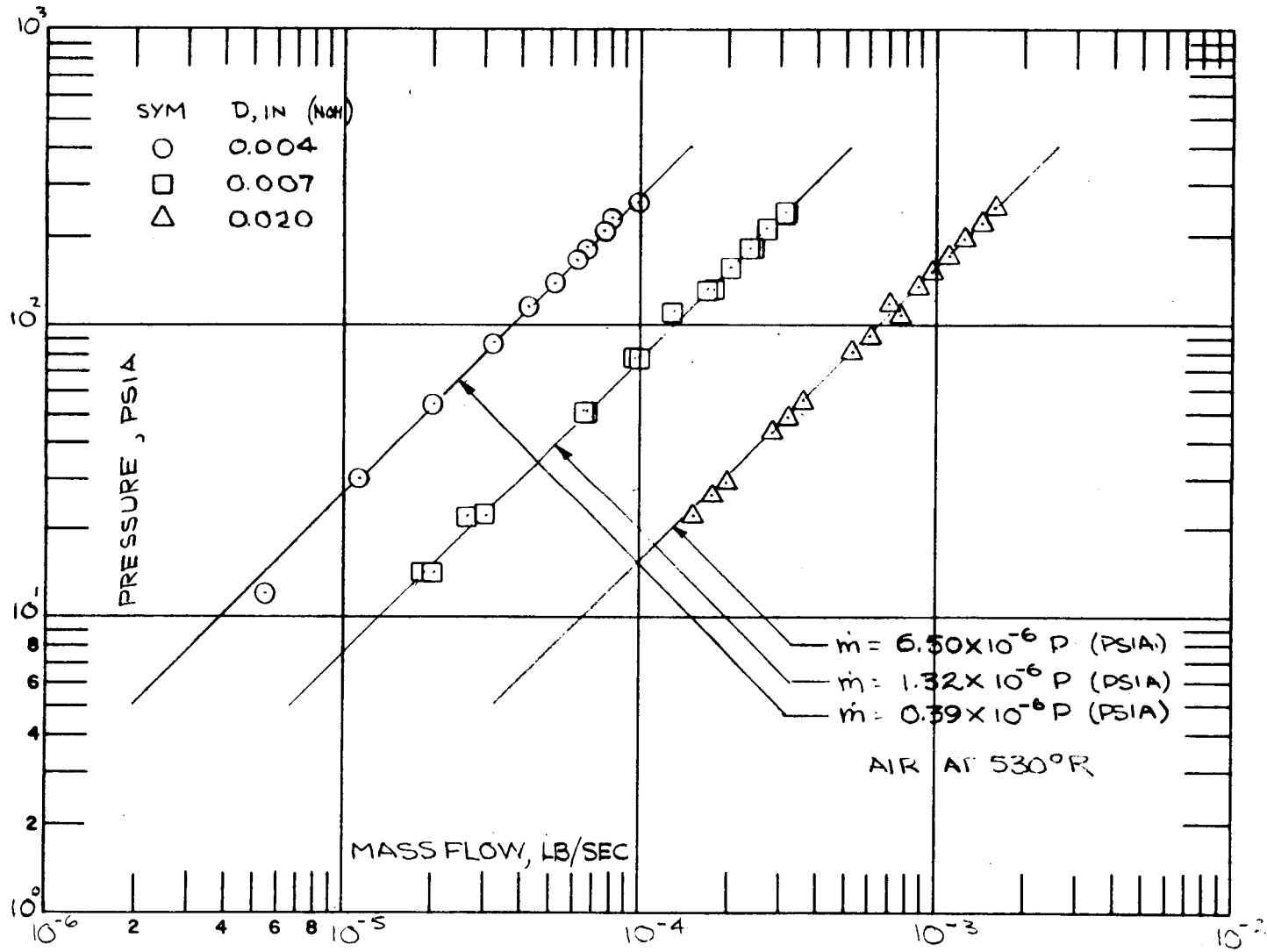

FIG 43 ORIFICE CALIBRATION CURVES (AIR)

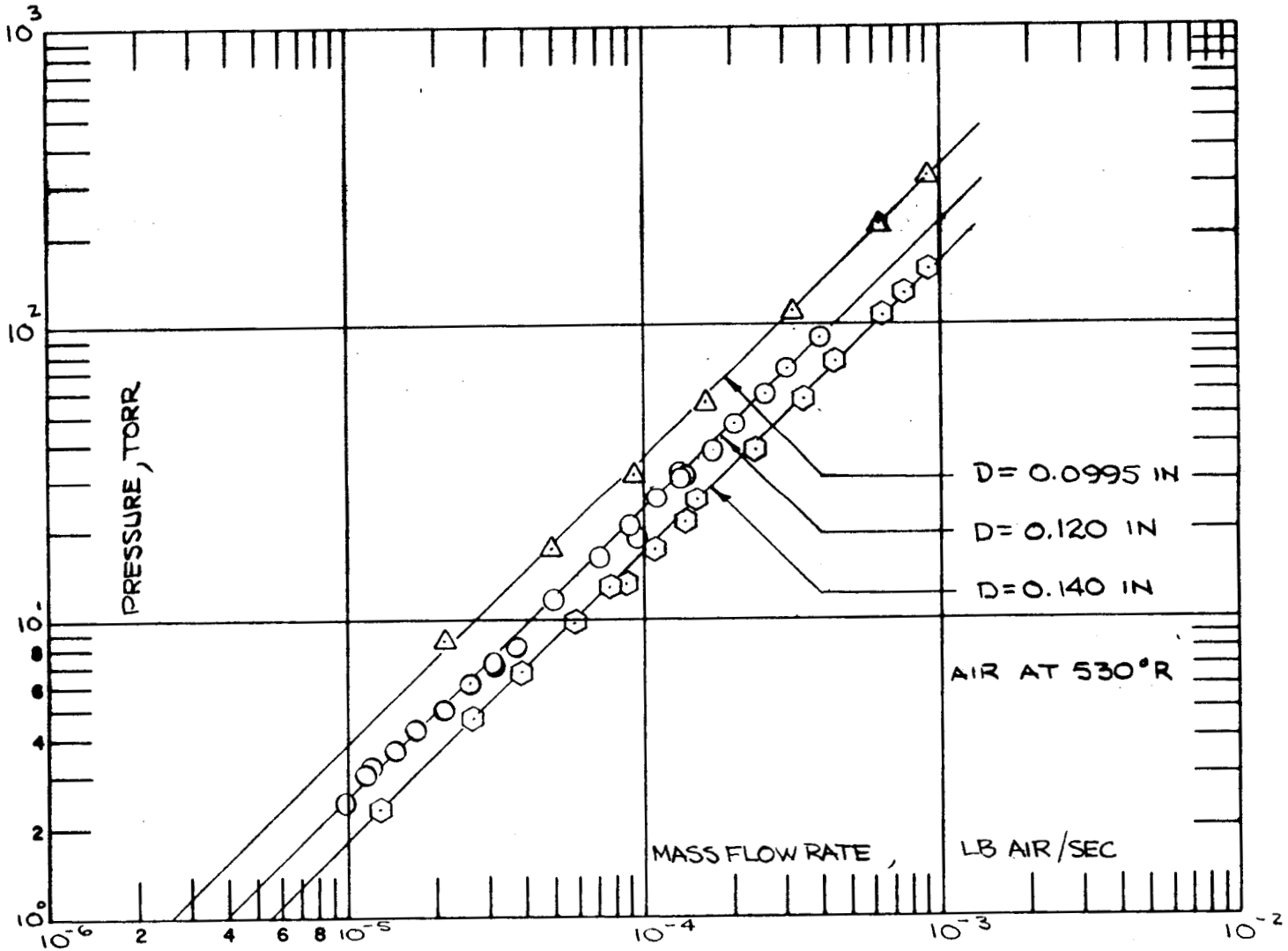

FIG 44 ORIFICE CALIBRATION (ARGON)

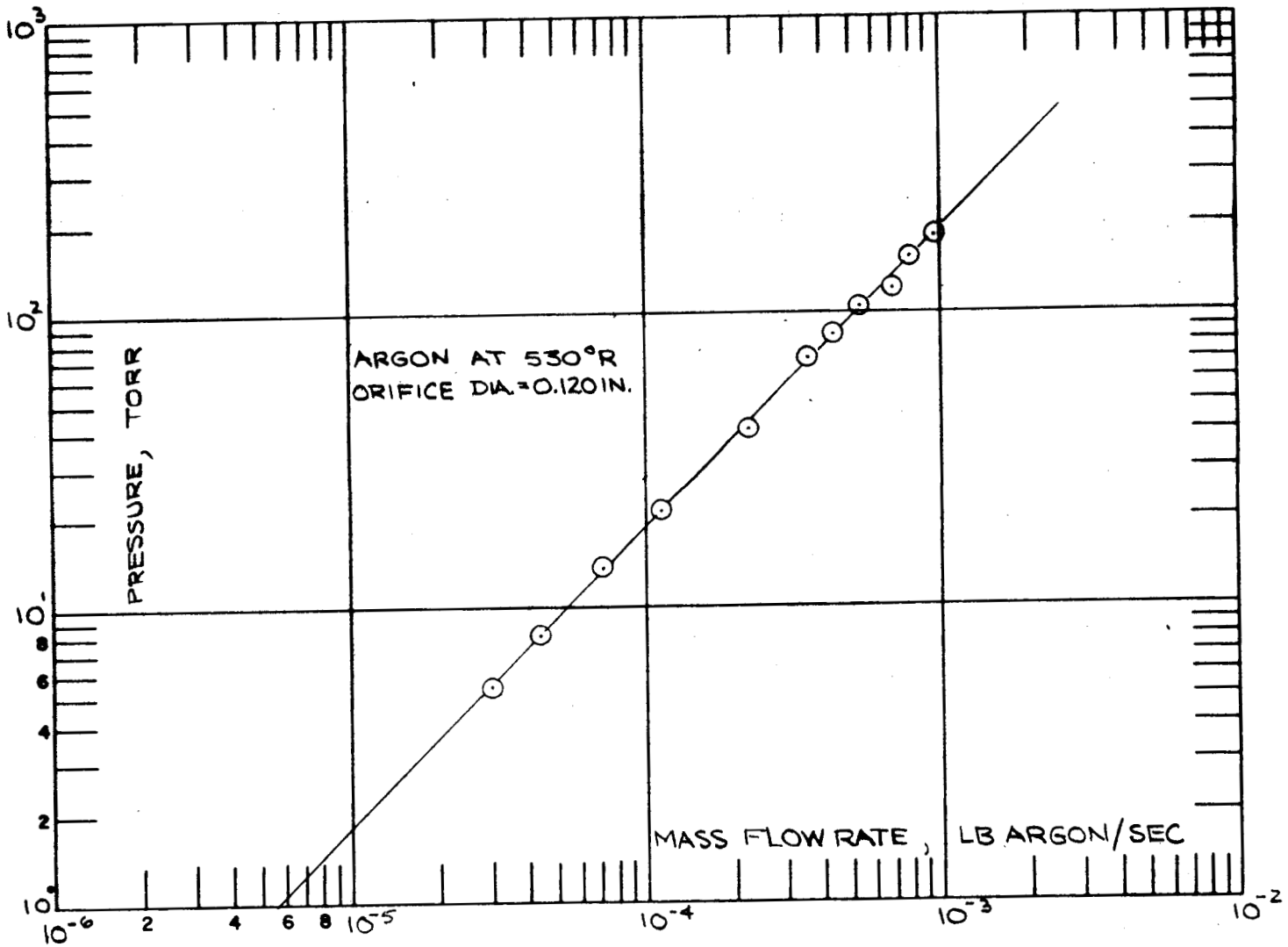

VI. PROBE EVALUATION

Evaluation of the probe system in highly heated gas streams was conducted in two phases. The first portion of the evaluation was performed in the Avco ROVERS[26] arc facility exhaust jet and was primarily designed to determine if the various portions of the probe system performed their desired functions. The second portion of the evaluation was conducted in the NASA/MSC ARMSEF facility to demonstrate the capability of the probe system.

ROVERS Arc Experiments

A number of experiments were conducted with the probe system in the supersonic exhaust jet produced by the Avco ROVERS arc facility (Figure 45) to provide a means of evaluating the probe design. The ROVERS facility consists of a constricted arc plasma generator which exhausts through a supersonic conical nozzle into a 6 feet diameter vacuum chamber. The arc heater employs a water-cooled tungsten cathode and a water cooled copper anode. High enthalpy air is produced by passing nitrogen through the arc discharge and mixing oxygen to the plasma in a plenum chamber prior to expanding the flow through the conical exit nozzle. Measurement of the total power input to the heater (i.e., current and voltage) as well as the energy absorbed in the arc cooling water allows the enthalpy of the plasma stream to be computed from an energy balance.

The conical exit nozzle has an area ratio of 9.0 and an exit diameter of 3.00 inches. For a specific heat ratio of 1.20 the area ratio corresponds to an exit Mach number of 3.20. The static pressure in the nozzle exit plane for this Mach number is 1.46 percent of the stagnation pressure of the flow measured in the arc heater plenum. However since the exit nozzle is conical in shape, the flow continues to diverge downstream of the nozzle even when the static pressure in the vacuum chamber is slightly in excess of the static pressure in the nozzle exit plane.

The enthalpy probe assembly was mounted in the ROVERS vacuum tank with the axis of the probe sampling tube coincident with the axis of the facility exhaust jet. The long length of the strut and associated mounting hardware made it necessary to place the base of the strut in the recessed viewing ports located on walls of the vacuum chamber. Hence axial and lateral movement of the probe within the exhaust jet was severely limited. The only positions which could be achieved were on the flow field axis at distances of 12.250 and 6.125 inches from the nozzle exit plane. A photograph of the probe during a typical experiment can be found in Figure 46.

A series of enthalpy probe measurements were performed at an axial distance of 12.250 inches from the nozzle exit plane. Arc heater parameters in these tests are listed in Table III. The enthalpy measurements made with the probe were considerably less than those calculated from the energy balance. The average being approximately 42 percent of the energy balance value. In one series of experiments (ROVERS Run No. 434-1) the coolant water flow to the inner calorimetric probe was varied from 0.21 gpm to 1.74 gpm while maintaining the outer probe cooling water flow rate at a constant value of 0.44 gpm. The variation in enthalpy measured in these tests was from 3800 Btu/lb to a maximum of 4150 Btu/lb with the mean value being 3985 Btu/lb. This amounts to a spread of ±4.5 percent about the mean value.

1 RADIANT LAMP (RADIATION SOURCE)
2 VIEW PORT FOR SURFACE TEMPERATURE MEASUREMENT AND / OR FRONT SURFACE MOTION PICTURES
3 LARGE MODEL INJECTOR
4 LARGE TEST MODEL
5 ENTHALPY PROBE & IMPACT PRESSURE PROBE
6 MODEL OR STEADY- STATE HEAT FLUX CALORIMETER
7 PROBE AND SAMPLE POSITIONING MECHANISM (THREE DEGREES OF FREEDOM)
8 OBSERVATION PORT
9 TRANSIENT HEAT FLUX CALORIMETER
10 ENVIRONMENTAL CHAMBER
11 CONVECTIVE ARC HEAD

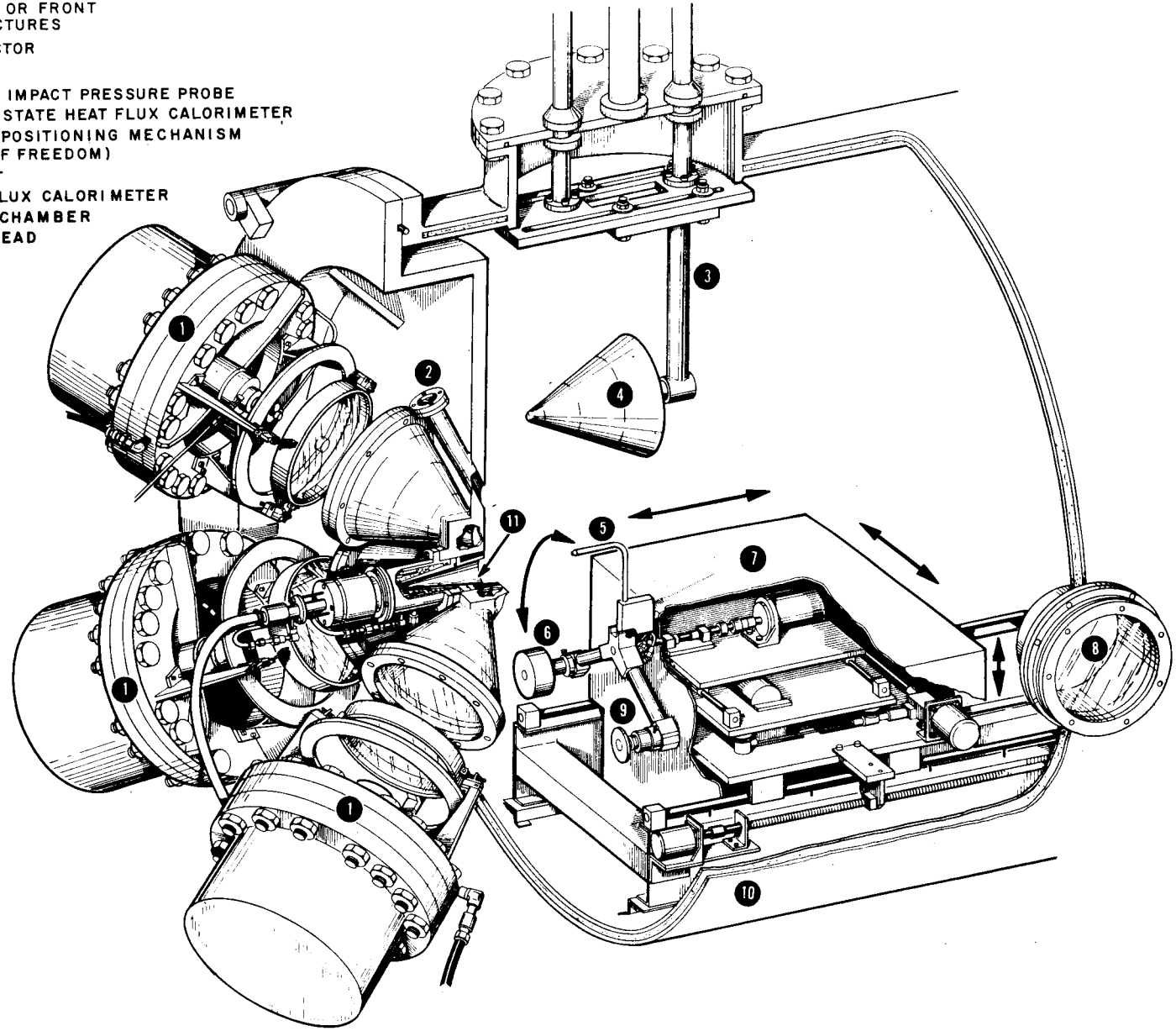

26-2500

FIGURE 45 SECTIONAL VIEW OF ROVERS FACILITY

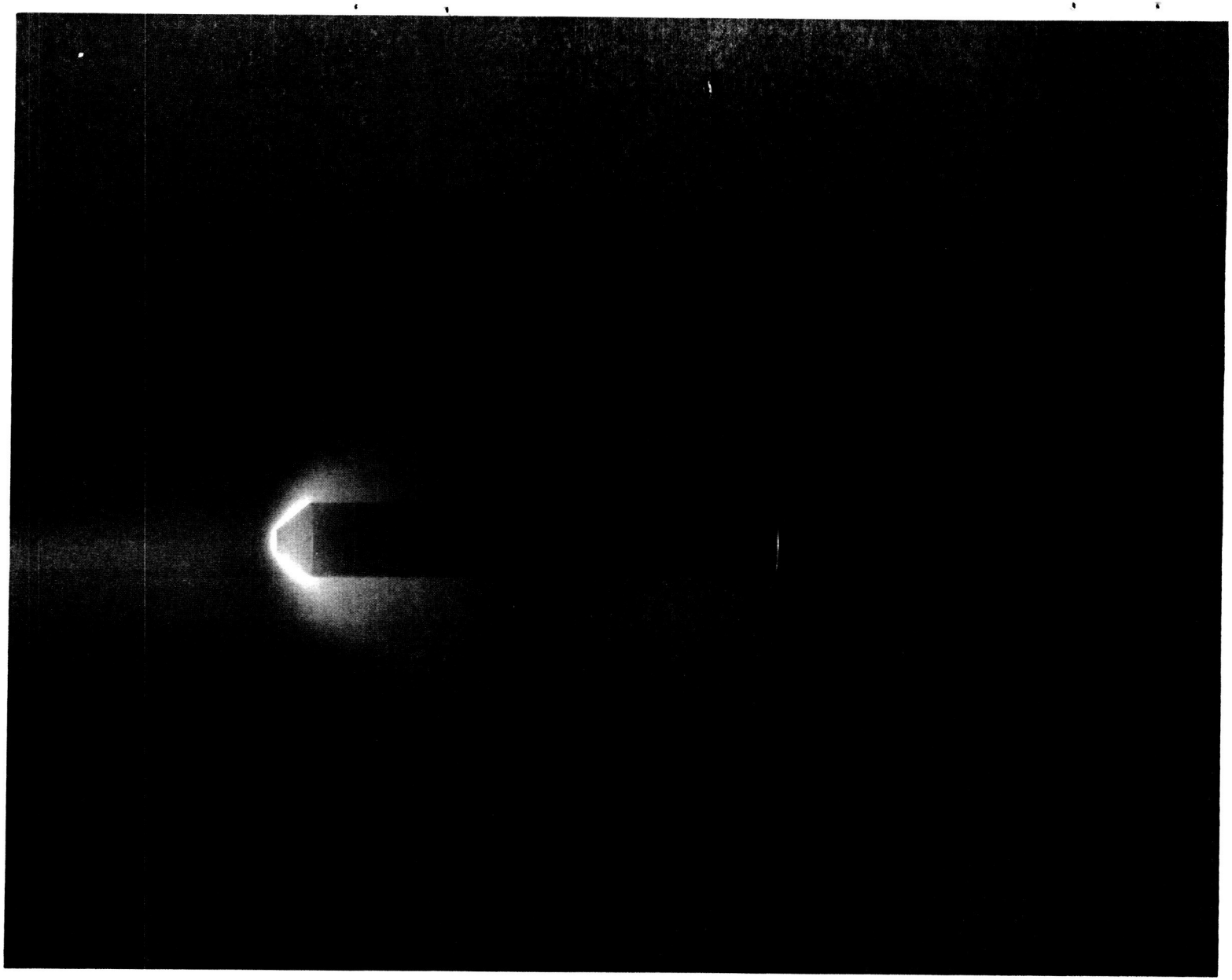

FIGURE 46 ENTHALPY PROBE IN ROVERS EXHAUST JET (Photo #29447D)

TABLE III

SUMMARY OF ENTHALPY PROBE MEASUREMENTS IN ROVERS ARC FACILITY

ROVERS RUN NO.	GAS FLOW RATE LB/SEC	PLENUM PRESSURE MM Hg	IMPACT PRESSURE MM Hg	STATIC PRESSURE MM Hg	ENERGY BALANCE ENTHALPY BTU/LB	PROBE POSITION INCH	PROBE RUN NO.	OUTER COOLANT FLOW GPM	INNER COOLANT FLOW GPM	ΔT °F	GAS FLOW RATE LB/SEC	ENTHALPY BTU/LB	AVERAGE ENTHALPY BTU/LB
434-1	4.0×10^{-3}	64.0	13.6	1.5	9,400	12.25	1	0.44	1.74	0.356	2.15×10^{-5}	4025	3985
							2	0.44	1.18	0.512	2.15×10^{-5}	3920	3985
							3	0.44	0.72	0.89	2.15×10^{-5}	4150	3985
							4	0.44	0.33	1.89	2.15×10^{-5}	4040	3985
434-2	4.0×10^{-3}	62.5	12.9	1.6	7,580	12.25	5	0.44	0.21	2.78	2.15×10^{-5}	3800	3985
							7	0.44	0.90	0.49	2.07×10^{-5}	2960	2920
434-3	4.0×10^{-3}	65.0	9.4	0.9	11,000	12.25	8	0.44	0.48	0.89	2.07×10^{-5}	2880	2920
							9	0.44	1.51	0.311	1.24×10^{-5}	5200	5390
							10	0.44	0.955	0.490	1.20×10^{-5}	5450	5390
							11	0.44	0.48	1.07	1.25×10^{-5}	5700	5390
							12	0.44	1.38	0.268	1.20×10^{-5}	4300*	5390
434-4	3.0×10^{-3}	48.0	9.05	1.2	10,900	12.25	13	0.44	0.65	0.712	1.24×10^{-5}	5200	5390
							14	0.44	1.27	0.290	1.15×10^{-5}	4450	4583
							15	0.44	0.84	0.443	1.10×10^{-5}	4700	4583
434-6	4.0×10^{-3}	65.0	13.6	1.6	9,400	12.25	16	0.44	0.43	0.888	1.16×10^{-5}	4600	4583
							17	0.44	1.16	0.489	2.15×10^{-5}	3700	3900
434-7	4.0×10^{-3}	62.5	13.1	1.0	7,350	12.25	18	0.44	0.77	0.822	2.15×10^{-5}	4100	3900
434-8	4.0×10^{-3}	65.0	9.4	1.0	10,800	12.25	19	0.44	0.91	0.467	2.10×10^{-5}	2820	--
435-2	4.0×10^{-3}	62.0	15.1	1.5	7,650	6.12	20	0.44	1.20	0.366	1.18×10^{-5}	5050	--
							21	0.44	1.02	0.800	2.50×10^{-5}	4570	4460
435-3	3.0×10^{-3}	48.0	12.2	1.3	11,100	6.12	22	0.44	0.76	1.020	2.50×10^{-5}	4350	4460
							23	0.44	1.23	0.556	1.75×10^{-5}	5450	5750
							24	0.44	0.88	0.845	1.75×10^{-5}	5950	5750
435-5	4.0×10^{-3}	64.0	14.6	1.5	9,200	6.12	25	0.44	0.59	1.250	1.75×10^{-5}	5850	5750
							26	0.44	1.18	1.130	2.75×10^{-5}	6800	6607
							27	0.44	0.85	1.530	2.75×10^{-5}	6620	6607
							28	0.44	0.49	2.580	2.75×10^{-5}	6400	6607

* Results are obviously in error and are not included in the average.

As is demonstrated by the results listed in Table III there is no consistent variation in the measured enthalpy with changes in the coolant flow rate. If there were energy transfer from the inner to the outer probe coolant streams, there would be a change in the heat exchange between the streams as the flow varied and hence a variation in gas enthalpy would be observed. Since essentially no variation in enthalpy was noticed even when the inner coolant flow was changed by a factor of 8 (Figure 47) it was concluded that there was no energy transfer between the two coolant streams.

This observation was substantiated by placing a Nichrom heating element within the probe sampling tube. When 40 watts of power was dissipated in the heater the energy absorbed by the inner probe cooling was measured to be 38 watts. This small discrepancy can be attributed to losses from the bare leads of the heater and the small portion of the heating element which was allowed to remain outside of the sampling tube.

A second series of experiments were performed with the probe tip located at an axial distance of 6.125 inches from the nozzle exit plane. The results of these tests are included in Table III. Each experiment conducted in this portion of the evaluation program was identical to experiements performed at 12.250 inches. In each case, higher values of enthalpy were measured closer to the nozzle exit plane. For example, in Run No. 434-1 and 435-5 enthalpies of 3985 Btu/lb and 6600 Btu/lb were measured at 12 and 6 inches, respectively, thereby further demonstrating that the discrepancy between measured and calculated enthalpies is due to jet mixing.

The difference between the enthalpy calculated from the facility energy balance and the measured value was therefore assumed to be caused by mixing of the exhaust jet with the external recirculatory flow within the vacuum chamber. This mixing process is considerably more rapid than that which occurs in a free jet since use of the relationships and experimental data of Warren quantities would have values identical to those in the nozzle exit plane. The reasons for the enhanced jet decay may be seen by considering the flow patterns in the two cases which are illustrated schematically in Figure 48. In the free jet case, the jet entrains fluid from the environment and the total mass flow within the jet increases with distance from the nozzle exit plane. Furthermore it is noted that the entrained fluid has an axial momentum which is identically zero. As is the case with all free shear layer mixing processes the total momentum and energy passing through any plane normal to the jet axis is conserved. However with a jet that issues into a chamber which is maintained at steady state conditions of pressure and temperature there are important differences which alters the rate of mixing. As with the free jet the conservation laws still apply and the total mass flow in the jet increases with distance downstream. Since the vacuum chamber is maintained at steady state, only that portion of the jet mass flow which entered the vacuum tank through the arc heater nozzle leaves the system at the far end of the chamber. The remainder of the flow recirculates along the outer wall of the tank to be re-entrained by the jet in the vicinity of the nozzle exit plane. Hence, when in the vacuum chamber, the jet leaving the nozzle mixes with an opposing external flow field. Furthermore, the recirculating external flow, when it reaches the forward end of the vacuum chamber is directed radially inward towards the exhaust jet and hence increases the amount of fluid entrained in the initial portion of the jet and increases the rate of jet decay.

FIG 47
VARIATION IN ENTHALPY WITH COOLANT FLOW RATE

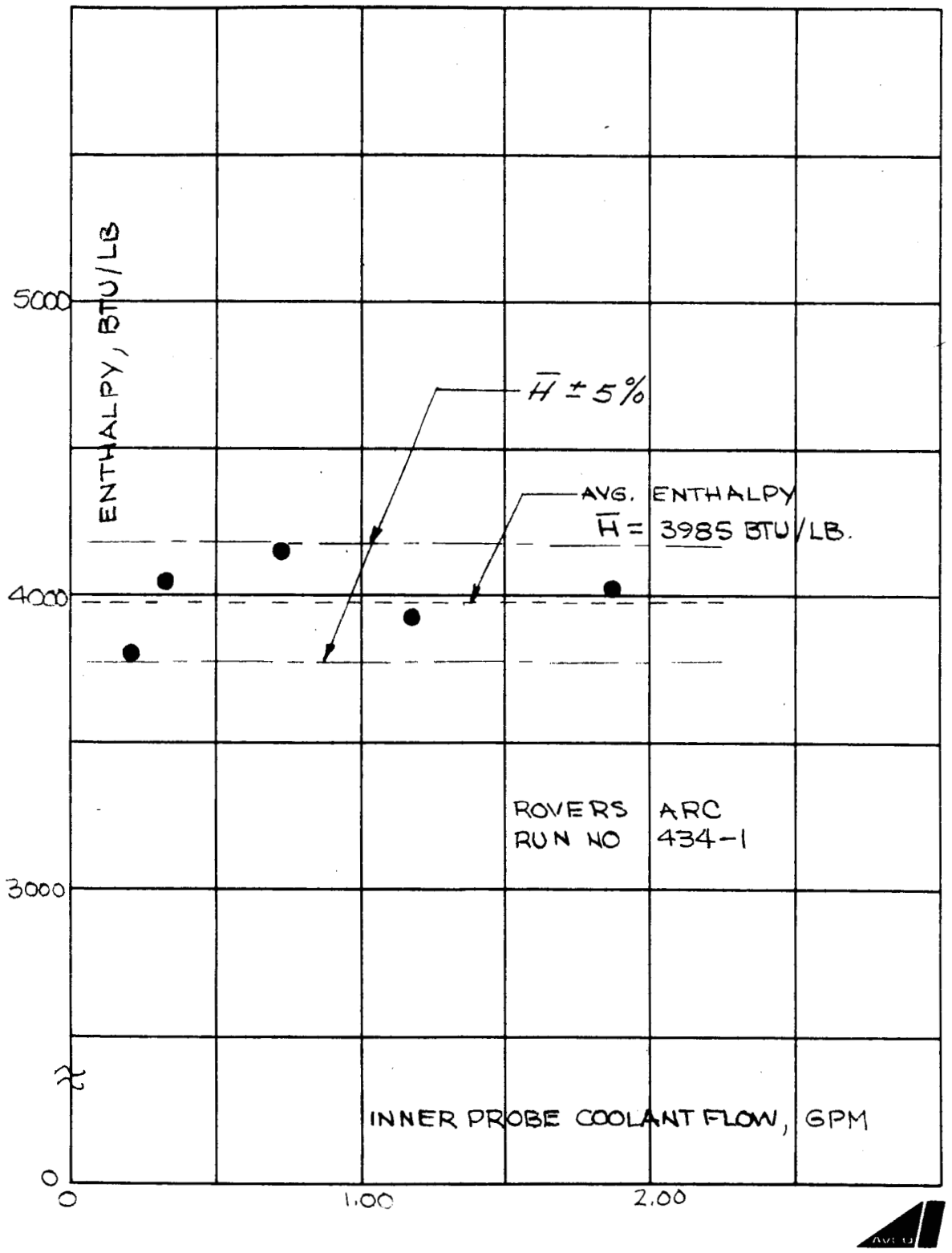

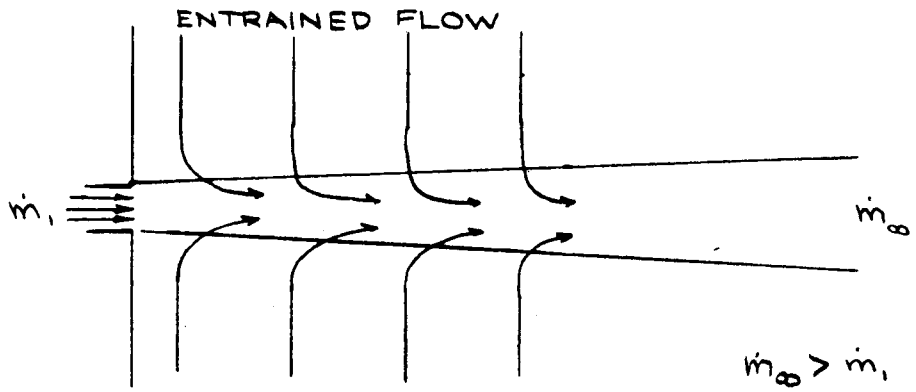

A. FREE JET MIXING

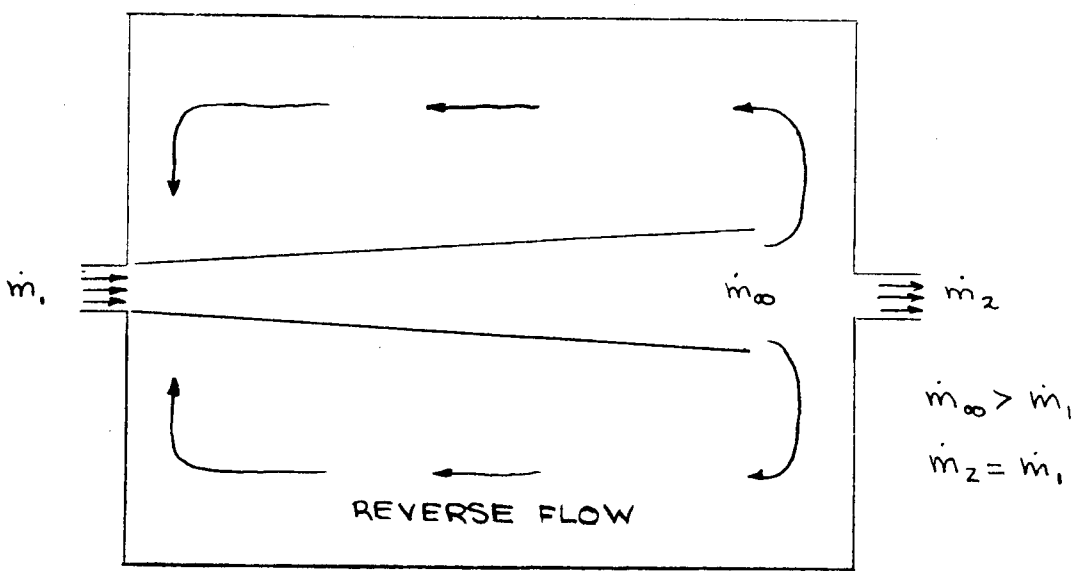

B. JET MIXING WITHIN A VOLUME

FIG.48 COMPARISON OF FREE AND ENCLOSED JET MIXING

In each run where more than three measurements of enthalpy were made each data point was compared to the mean value for each run. The results are included in Figure 49 as a function of cooling water flow rate. The average deviation of the data from the mean value in any experiment was found to be 2.6 percent further demonstrating the adequacy of the insulation between the inner and outer probe cooling systems.

ARMSEF Experiments

A similar series of tests were conducted in the NASA/MSC ARMSEF facility. The probe was located with its tip located at a distance of 4.25 inches downstream of the nozzle exit plane. During these experiments the probe was capable of being moved radially across the flow field so as to provide information concerning property variations within the free stream.

Facility operating conditions in the experiments are listed in Table IV. Notice that the enthalpy of the gas stream produced by the facility is obtained by three methods:

a) by an energy balance ($h_{e.b.}$) using power input to the facility, energy absorbed by the cooling water and the gas flow through the arc heater

b) by use of the sonic flow relationship ($h_{s.t.}$) which relates plenum pressure, throat area, gas mass flow rate, and gas enthalpy

c) by use of the relationships for stagnation point heating rates ($h_{F.R.}$) to calculate enthalpy from measured stagnation point heating rates and impact pressure.

Data were gathered with the enthalpy probe at each of the ARMSEF operating conditions. The gas flow measuring system employed in these tests was that described in the previous sections of this report with an orifice diameter of 0.120 inch. The enthalpy computed from the quantities measured with the probe are included in Table IV for comparison with enthalpy determined with the various techniques described above.

The gas enthalpy measured with the probe system was for the most part considerably greater than that determined by either the energy balance or sonic flow techniques. Since each of these methods provide some average value of the flow field properties, this comparison is as expected. When the enthalpy calculated from measured heating rates is compared with the value obtained with the probe, it is found that with the larger nozzle (larger free stream Mach number) the former value is considerably greater than the probe enthalpy. However, with the smaller nozzle, values measured with the probe are in good agreement with the enthalpy deduced from heat transfer rates. The reason for this variation is not understood at the present time.

The data gathered with the probe in Runs 337 and 338 clearly indicate the enthalpy variation across the nozzle exit plane are small. If the data gathered in Run number 339 is disregarded it is found that all data obtained at

FIG 49

ENTHALPY VARIATION WITH COOLANT FLOW RATE

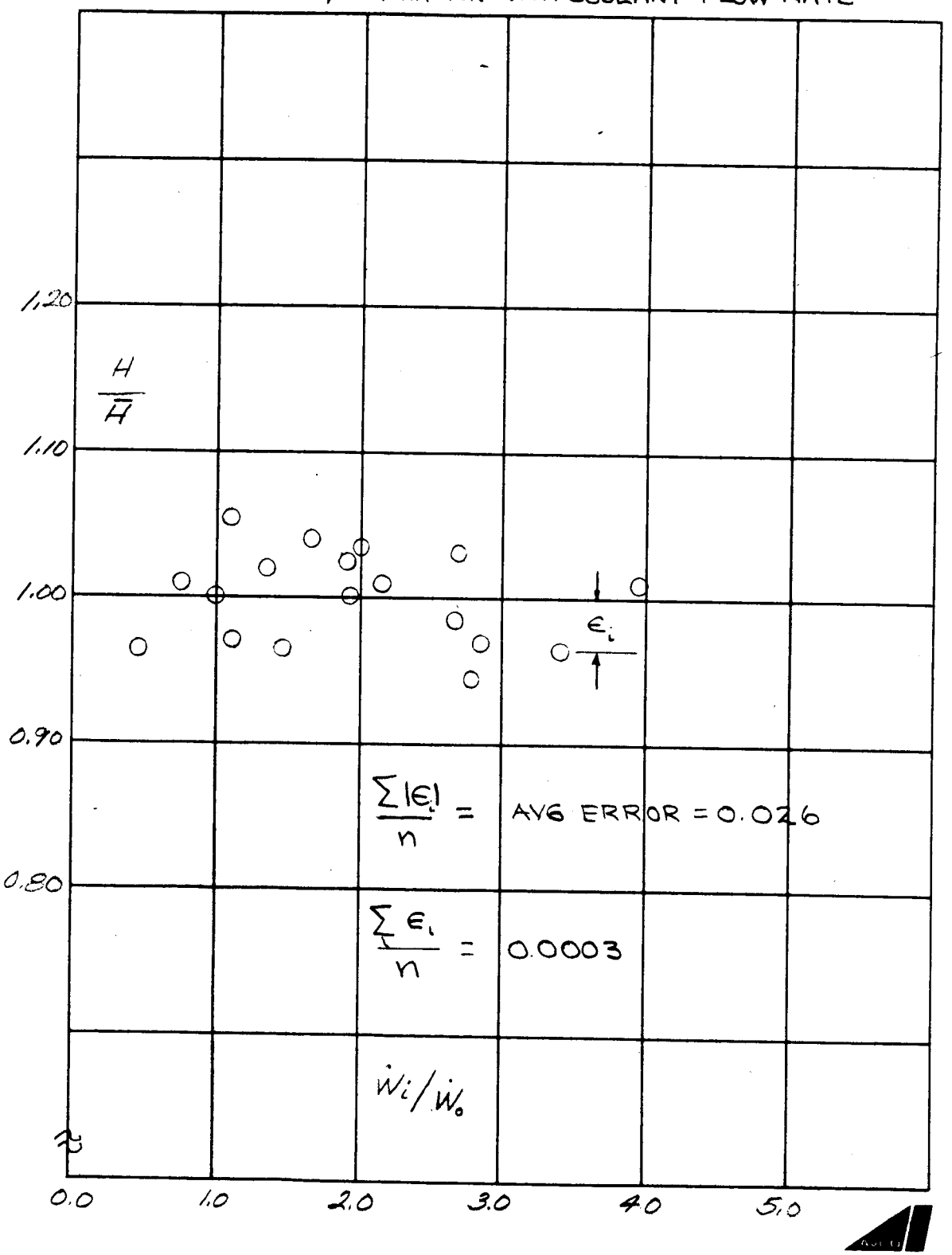

TABLE IV

SUMMARY OF ENTHALPY PROBE MEASUREMENTS IN ARMSEF FACILITY

RUN NO.	THROAT DIAMETER INCH	EXIT DIAMETER INCH	MASS FLOW RATE LB/SEC	PLENUM PRESSURE PSIA	h_{cb} BTU/LB	h_{CT} BTU/LB	h_{FR} BTU/LB	PROBE RADIAL POSITION INCH	INNER COOLANT FLOW LB/SEC	OUTER COOLANT FLOW LB/SEC	h_{probe} BTU/LB	PROBE MASS FLOW RATE LB/SEC
334-1	0.75	25.0	0.107	40.6	2655	3450	5820	0.0	0.0695	0.311	3971	3.5×10^{-6}
334-2			0.215	82.7	2928	2650	5230	0.0	0.0675	0.308	3185	8.7×10^{-6}
335-1	0.75	25.0	0.107	40.2	2579	3350	5820	0.0	0.0268	0.216	3530	3.7×10^{-6}
335-2			0.218	82.7	2802	2520	5295	0.0	0.0354	0.316	3470	9.0×10^{-6}
337-1	1.50	10.0	0.328	37.3	3524	3850	6202	0.0	0.2373	0.320	6296	7.6×10^{-5}
337-2			0.328	37.2	3490	3800		2.0	0.2399	0.319	6068	7.2×10^{-5}
337-3			0.329	37.2	3589	3950		4.0	0.2373	0.319	6210	3.6×10^{-5}
338-1	1.50	10.0	0.325	37.2	3499	3900	6052	0.0	0.1125	0.317	6186	7.5×10^{-5}
338-2			0.325	37.2	3502			0.0	0.1121	0.317	6200	6.4×10^{-5}
338-3			0.325	37.3	3518			2.0	0.1106	0.317	6676	9.0×10^{-5}
338-4			0.325	37.3	3529			4.0	0.1097	0.317	6458	3.6×10^{-5}
339-1	1.50	10.0	0.328	37.5	4121	3900	6120	0.0	0.342	0.315	6840	7.50×10^{-5}
339-2			0.330	37.6	4098			0.0	0.342	0.315	5333	7.60×10^{-5}
339-3			0.331	37.7	4095			2.0	0.342	0.315	5394	9.0×10^{-5}
339-4			0.331	37.8	4066			4.0	0.341	0.315	9186	3.6×10^{-5}
339-5			0.331	38.0	4085	3900		0.0	0.340	0.315	5828	7.0×10^{-5}

the same radial position with comparable arc parameters agree to within 6 percent with no apparent variation in calculated gas enthalpy with variations in inner probe coolant flow rate. The data obtained in Run 339 appears to be anamolous and is in poor agreement with results obtained in the previous two experiments. The cause of this discrepancy is unknown, since all probe data with the exception of the coolant temperature rise is in good agreement with previous results.

APPENDIX I

OPERATION OF THE ENTHALPY PROBE

The enthalpy probe is a simple, calorimetric device which allows one to measure the enthalpy of a gas sample drawn through an aspirating tube located on the axis of the instrument. As the sample travels down the aspirating tube energy is transferred to the tube walls and in turn to the cooling water flowing along the outer surface of the tube wall. Upon its exit from the sampling tube, the gas stream is at a temperature Tg and hence has some residual energy. From a simple energy balance it is obvious that

$$\dot{m}_g h_s = (\dot{m} C_p)_{H_2O} (T_2 - T_1) + (m C_p)_g (T_g - T_o) \qquad \text{(A-1)}$$

where T_1 and T_2 are the inlet and outlet coolant temperatures, T_o is the base temperature for computation of the gas enthalpy, and $\dot{m}_g$ and $\dot{m}_{H_2O}$ are the gas sampling rate and coolant flow rates, respectively. The gas sampling rate is measured by means of sonic orifice plates located in the vacuum line located between the probe and a vacuum pump and the coolant flow rate is measured by any of the commercially available flow meters. Inlet and outlet cooling water temperature and the gas temperature at the end of the sampling tube are obtained from the output of chromel-alumel thermocouples supplied with the probe system.

The probe system itself consists of an external probe, an internal calorimetric probe and a probe strut each of which is provided with a separate cooling system. The primary function of the external probe which completely surrounds, and is insulated from the inner calorimetric probe is to protect the inner probe from the external environment. The water cooled probe strut is of sufficient length to allow the probe sampling tube to be located with its axis on the axis of the flow field produced by the ARMSEF facility.

The amount of cooling water required to protect the probe system at various heating levels can be found from the analyses presented in the main body of this report. The minimum cooling requirements for the probe strut may be found in Figure A-1 as a function of environmental conditions ($\dot{q}_s \sqrt{R_N}$) and inlet coolant pressure to the base of the strut.

Minimum coolant requirements to protect the external probe from the environment are illustrated in Figure A-2 as a function of external heating while similar curves for the internal calorimetric probe are presented in Figure A-3. As discussed in those portions of this report dealing with the design of the probe system the minimum cooling flow rates are determined from the desire to prevent boiling within the system at particular heating rate. It is noted however that in the design the heat transfer correlations employed were those applicable to fully developed flow within channels. The critical heating area in the calorimetric probe is near the probe tip in a region where the coolant flow is in the process of negotiating a 165 degree change in direction. Hence the use of the heat transfer relationships employed in the analysis is open to question. In this situation the actual heat transfer coefficient would be considerably higher than those employed in establishing the minimum coolant flow rates. Hence it is expected that the information presented in Figure A-3 is conservative and that boiling can be prevented even at flow rate less than those shown in this illustration.

FIG A-1
MINIMUM COOLING REQUIREMENTS (STRUT)

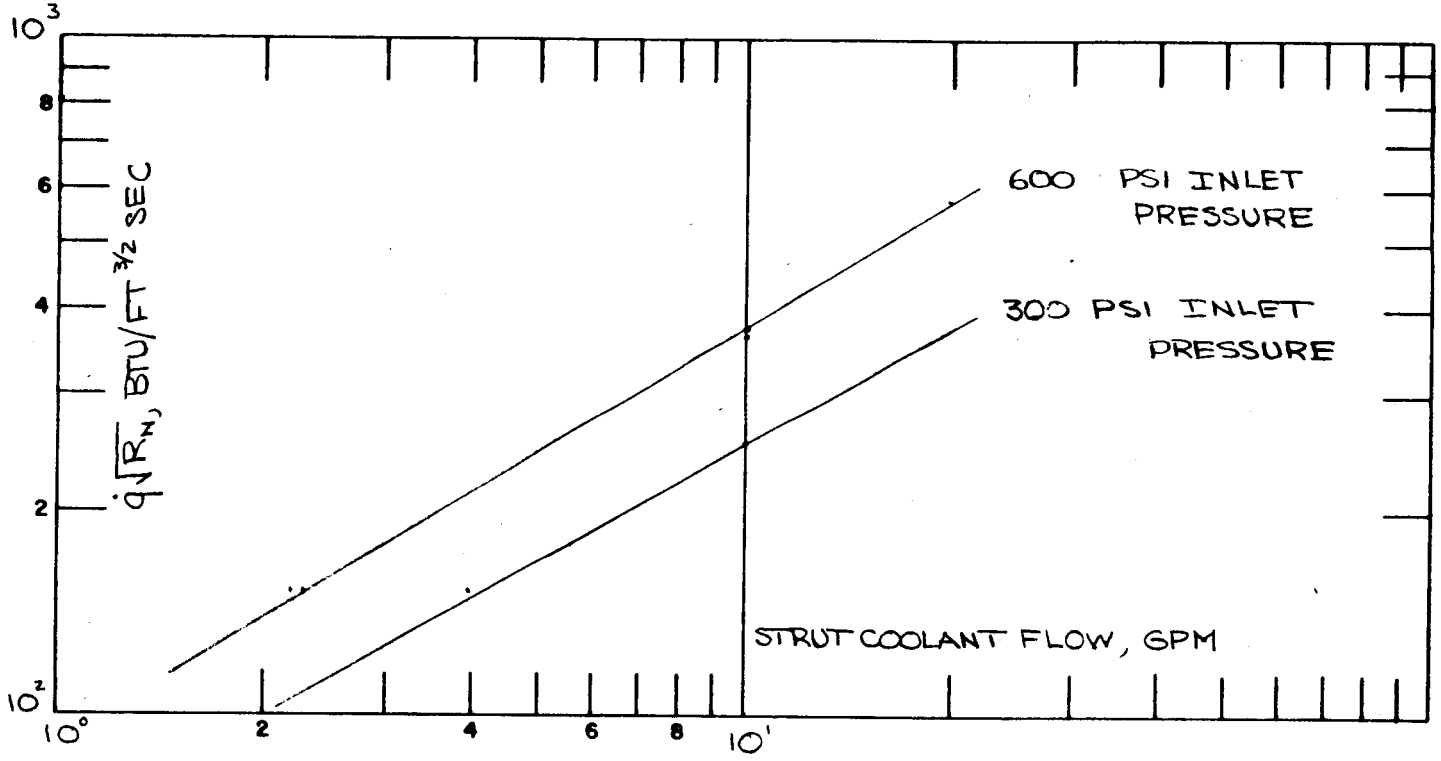

FIG. A-2
MINIMUM COOLANT FLOW RATES, OUTER PROBE

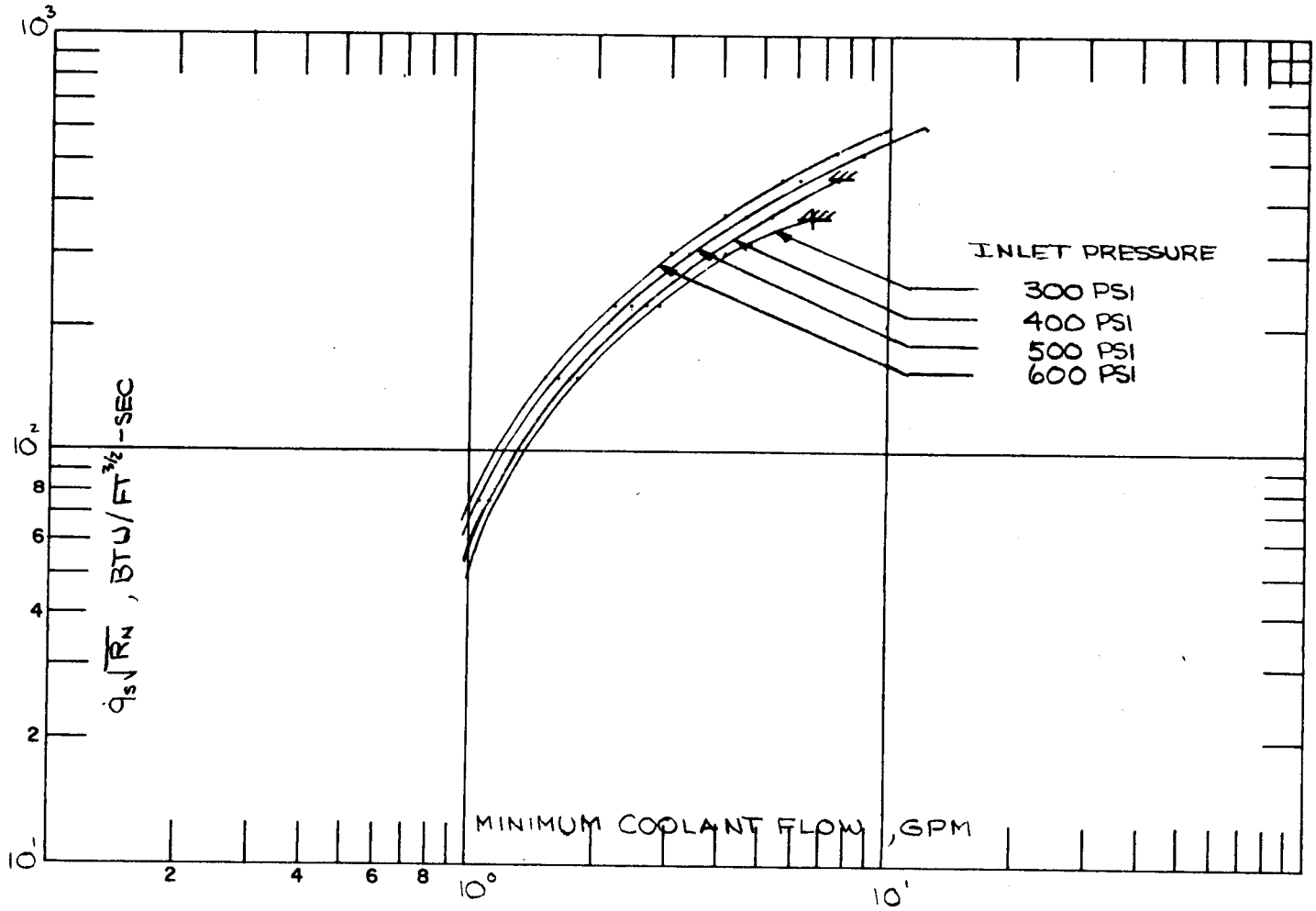

FIG A-3
MINIMUM COOLANT FLOW RATE (INNER PROBE)

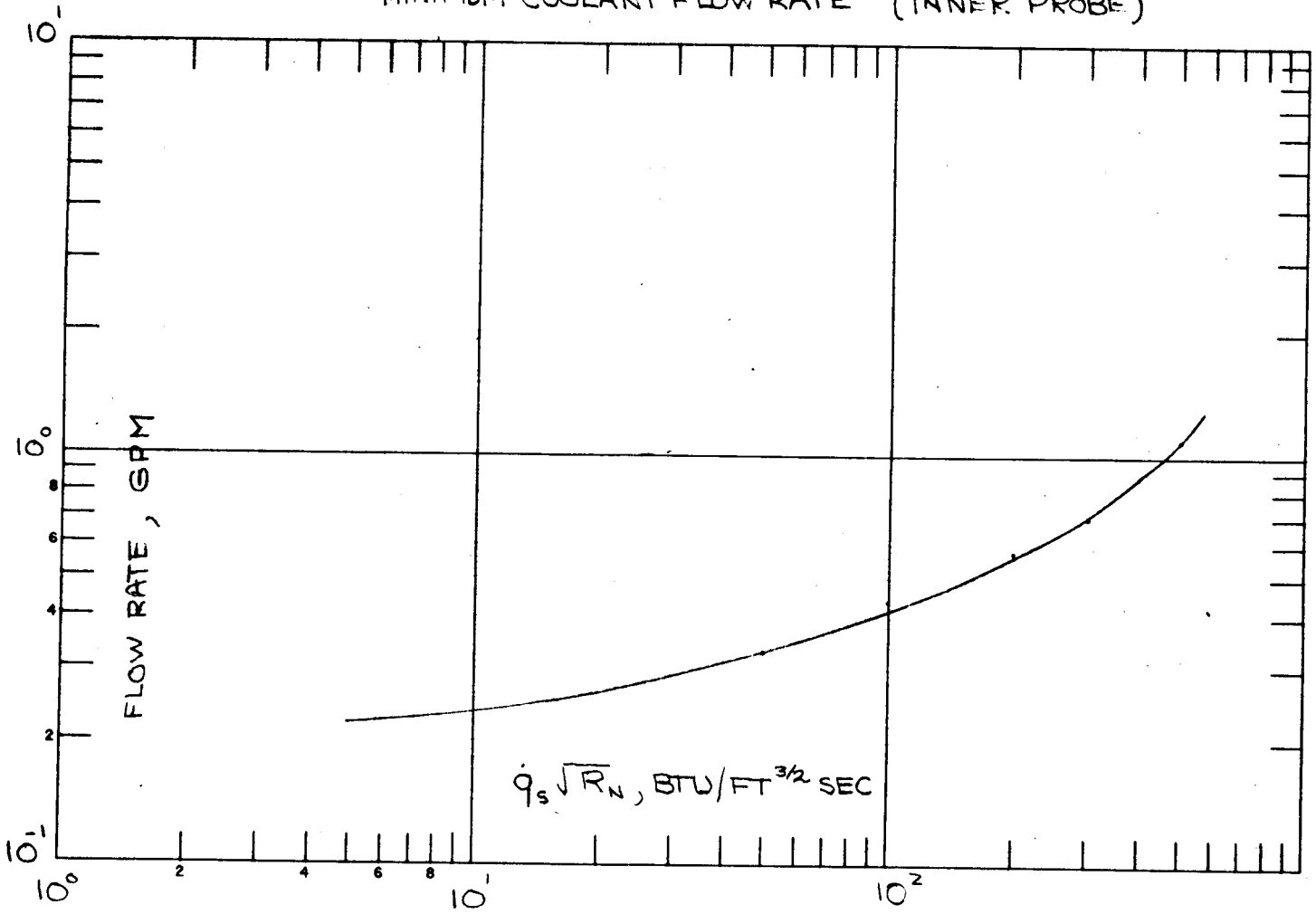

In addition to these data, the inner calorimetric probe coolant temperature rise which would be expected at various facility operating conditions is shown in Figure A-4. These results are based on the assumption that the stream leaving the nozzle of the ARMSEF facility is of uniform properties and that the probe acts as a mass flux measuring instrument.

Installation of the probe in the facility consists of providing coolant inlet and outlet lines (with flow meters) for the probe strut, the external probe, and the inner calorimeter probe. In addition, a vacuum line is provided between the gas sampling line and the vacuum pump which is located within the mass flow calibration system console. The vacuum line between the base of the probe should have as small a length-to-diameter ratio as possible in order to minimize frictional losses within the sampling train. A vacuum solenoid valve is included in the line to provide a means of sampling gas at will and when this valve is closed the impact pressure in the free stream can be measured by locating a pressure transducer between the valve and the probe tip. In addition a flow meter to measure the mass flow rate of the aspirated gas stream is placed in the vacuum line between the valve and the vacuum pump. A schematic diagram of the probe system is presented in Figure A-5.

The procedure followed in making a measurement of enthalpy in a flow field is discussed below. Following insertion of the probe into the stream with the sampling valve closed, the temperatures in the inner probe cooling water stream are observed until they come to steady state. At this time, the gas sampling valve is opened drawing gas through the probe until the calorimetric probe coolant temperatures reach steady state once again. During this period the output of the instrumentation associated with the flow meters for measuring sampling rate and coolant flow rate as well as the temperature of the gas leaving the inner calorimetric probe are monitored also. At this time the valve in the sampling line is closed ans the probe can then be moved to the next position where a measurement is desired.

The enthalpy of the gas sample drawn through the probe can then be calculated from an energy balance on the calorimetric probe:

$$h_s = \frac{(\dot{m}C_p)_{H_2O}(T_2 - T_1)}{\dot{m}_g} + C_{Pg}(T_g - T_o) \qquad \text{(A-2)}$$

and the mass flux in the external flow field is obtained by dividing the gas sampling rate by the cross-sectional area of 0.250 inch diameter sampling tube:

$$(\rho u)_\infty = \frac{4\dot{m}_g}{\pi D_p^2} \qquad \text{(A-3)}$$

FIG A-4
COOLANT TEMPERATURE RISE

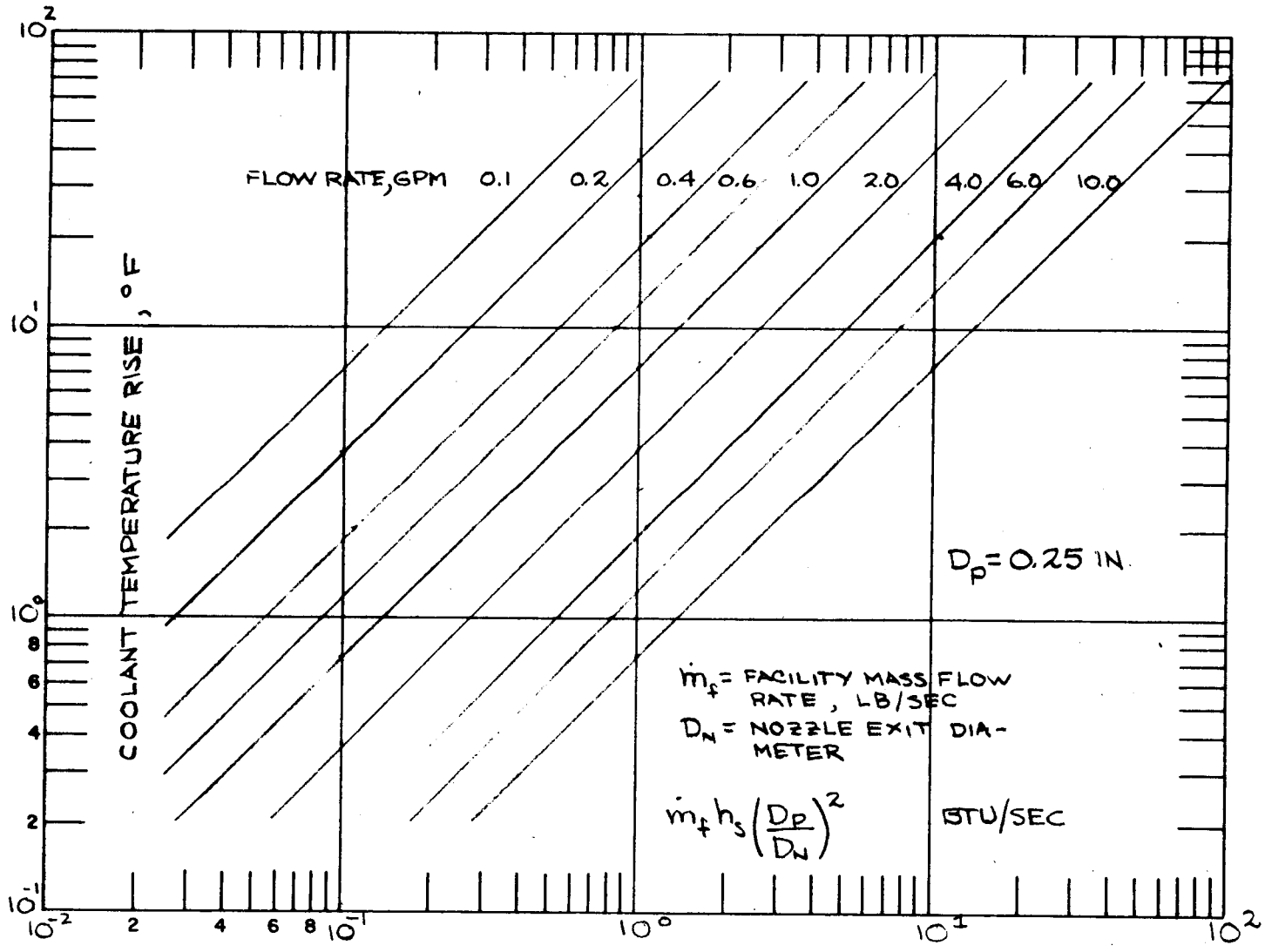

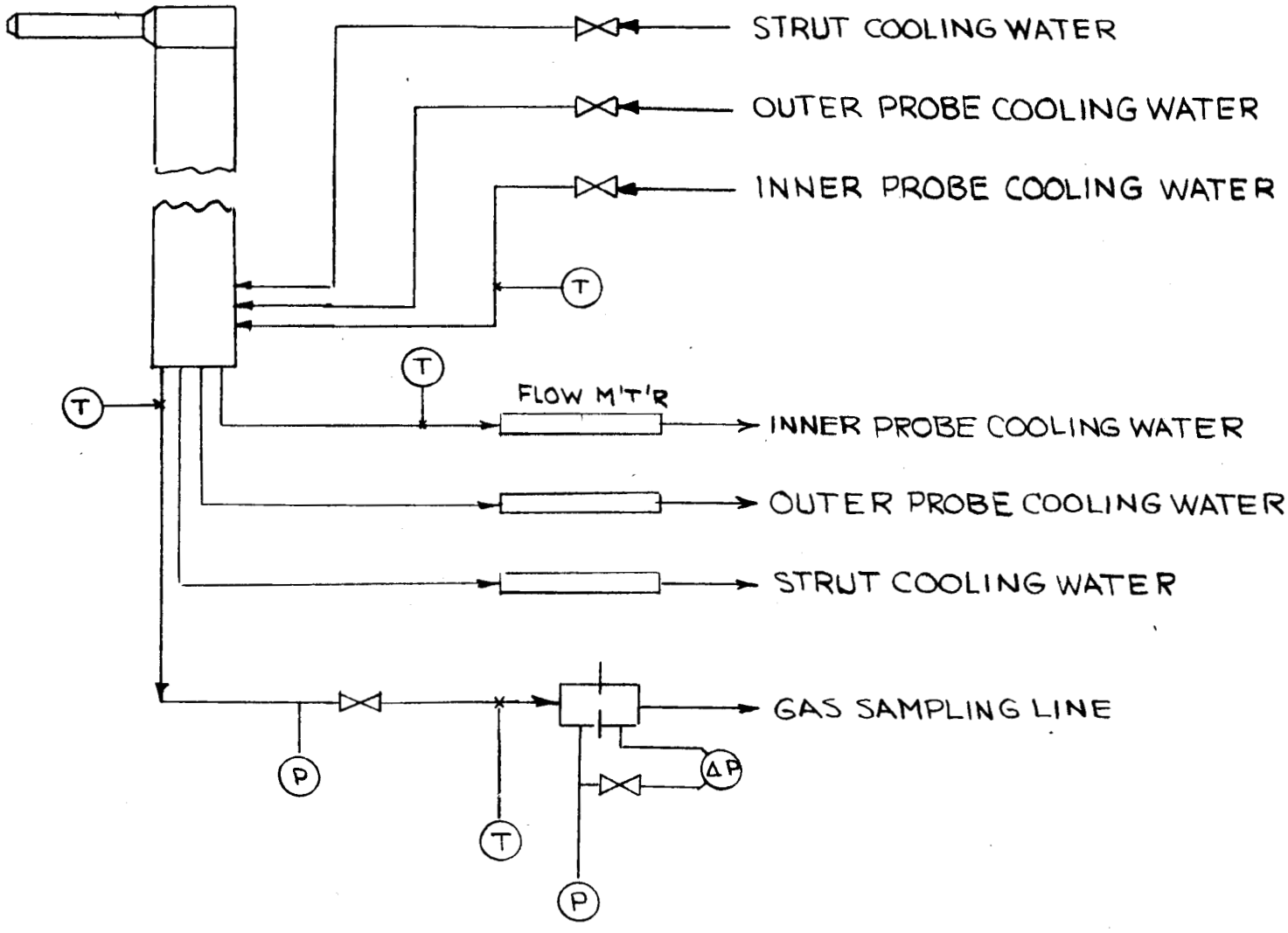

FIG A5 SCHEMATIC DIAGRAM OF PROBE INSTALLATION

APPENDIX II

OPERATION OF THE MASS FLOW CALIBRATING SYSTEM

The mass flow calibrating system consists of two manifoleded reservoirs having volumes of 0.374 ft^3 and 0.1075 ft^3 which are connected by appropriate valves and a restrictive orifice to the inlet of a 5.6 CFM vacuum pump. A flow meter being calibrated is positioned in the line between the restrictive orifice and the vacuum pump. The system is such that gas flows ranging from 4×10^{-6} to 4×10^{-3} lb air per second may be obtained by proper choice of initial pressure in the reservoirs and the diameter of the restrictive orifice plates. The restrictive orifices range in size from 0.004 inch to 0.020 inch. In the flow rate range of interest, the static line pressures in the system between the restrictive orifice and the vacuum pump are in the range expected during operation of the enthalpy probe in the ARMSEF facility. Hence the calibration system provides a means of calibrating flow meters at the pressures and flow rates expected during operation in the facility.

The procedure followed in various operations performed during calibration of a flow meter are described below.

a) Filling: With valves 3, 4, 5, 6, 7 and 8 opened and valves 1, 2 and 9 closed gas is introduced into the system through the fill line located in the console containing the system (see Figure A-6 for valve designation).

b) Venting of the gas inlet line: With valves 3, 4, 5, and 6 opened and valves 1, 2, 7, and 8 closed, the regulator valve on the gas supply is closed and the vent valve (Valve No. 9) is opened.

c) Isolating a reservoir as a constant pressure volume: To employ reservoir no. 1 as a constant pressure volume valves 1, 2, 5, 7 and 8 are maintained in the closed position and valves 3, 4, and 6 are kept open. If the other reservoir was selected as the standard volume the position of the valves would be identical except that valve 6 would be closed and valve 5 would be open

d) Equilizing the pressure in the two volumes: With valves 1, 2, 7 and 8 in the closed position, the pressure can be equalized by opening valves 3, 4, 5, and 6.

e) Gas flow from reservoir #2 with reservoir #1 maintained as a constant pressure volume: Valves 1, 2, 5, 7 and 8 maintained in the closed position and valves 3, 4, and 6 open, valve 1 is then opened to allow gas from reservoir 1 to flow through the restrictive orifice through the flow meter being calibrated and then to the vacuum pump.

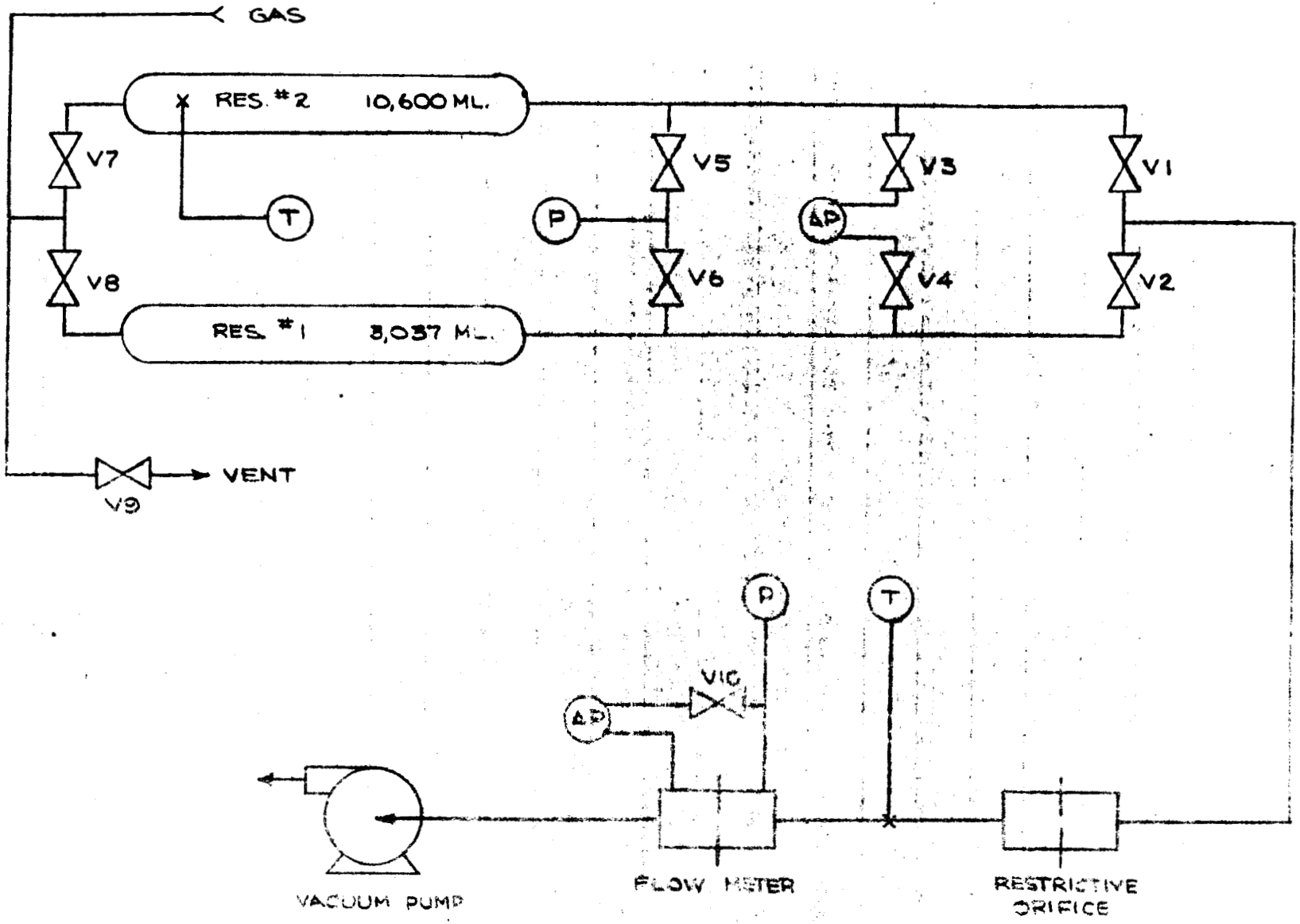

FIGURE A-6 SCHEMATIC DIAGRAM OF MASS FLOW CALIBRATION SYSTEM

f) Venting of entire system: With valves 1, 2, 7 and 8 initially closed and valves 3, 4, 5, 6 and 9 initially open, valves 7 and 8 are then opened.

These operations are summarized in Table A-I

During the calibration of a flow meter the following sequence of operations is followed:

1. Proper pressure transducers and restrictive orifice are selected based on the data presented in Figure A-7.

2. Pressure transducers and orifice plates are installed in the system.

3. The system is filled with gas to the correct pressure level.

4. The gas inlet line is vented.

5. One reservoir (usually the smaller of the two) is isolated from the remainder of the system.

6. Gas is allowed to flow from the larger reservoir for a measured time period. This flow passes through the restrictive orifice, the flow meter being calibrated, and then through the vacuum pump. During this period the output of the flow meter pressure transducers are recorded.

7. The valve between the larger reservoir and the restrictive orifice is then closed. It will be observed that immediately after closing this valve that the temperature in the tank begins to rise as the gas absorbs energy from the environment. At the end of this time period it will be noted that the pressure difference between the two reservoirs also comes to a steady state value at which time the pressure in the reference volume and the pressure difference between the two reservoirs is recorded. The total mass flow from the large reservoir during the period the valve was open is then

$$\Delta m = \frac{V}{RT} \Delta P \qquad \text{(A-4)}$$

and the average mass flow rate is

$$\overline{\dot{m}} = \frac{V}{RT}\left(\frac{\Delta P}{\Delta t}\right) \qquad \text{(A-5)}$$

which can be correlated with the output of the meter being calibrated.

8. The two reservoirs are allowed to come to the same pressure.

9. The entire system can then be vented (if desired) to some lower pressure.

TABLE A-I

SUMMARY OF CALIBRATION SYSTEM OPERATIONS

OPERATION	INITIAL VALVE POSITION OPEN	CLOSED	EXECUTION
1. Fill reservoirs	3, 4, 5, 6, 7, 8	1, 2, 9	
2. Vent inlet line	3, 4, 5, 6	1, 2, 7, 8, 9	OPEN 9
3. Isolate small reservoir	3, 4, 5, 6, 9	1, 2, 7, 8	CLOSE 5
4. Isolate large reservoir	3, 4, 5, 6, 9	1, 2, 7, 8	CLOSE 6
5. Flow from small reservoir	3, 4, 6, 9	1, 2, 5, 7, 8	OPEN 2
6. Flow from large reservoir	3, 4, 5, 9	1, 2, 6, 7, 8	OPEN 1
7. Equalization of reservoir pressures	3, 4, 9	1, 2, 5, 6, 7, 8	OPEN 5, 6
8. Vent entire system	3, 4, 5, 6, 9	1, 2, 7, 8	OPEN 7, 8
9. Evacuate reservoirs	3, 4, 5, 6, 9	1, 2, 7, 8	OPEN 1, 2

FIG. A7 CALIBRATION SYSTEM OPERATING PRESSURE

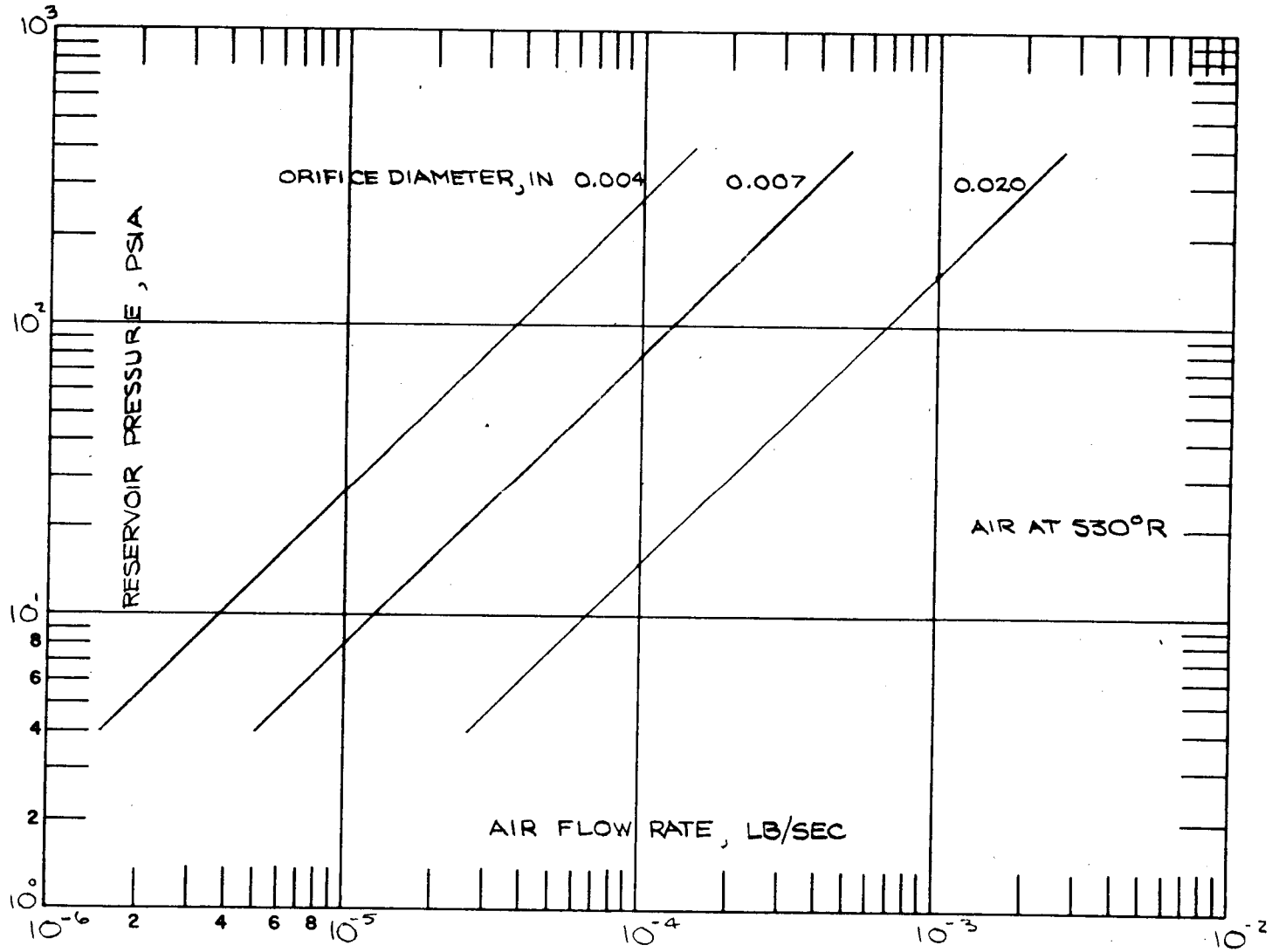

10. Steps 5 through 9 are then repeated to obtain the next calibration point.

Selection of the restrictive orifice plates and the operating pressure of the system reservoirs is made from the data presented in Figure A-7 at the desired gas flow rate. For gases other than air it is obvious that the data presented can be easily modified by use of the sonic flow relationships for choked orifices:

$$\dot{m} = PA \left\{ \frac{g\gamma}{RT} \left(\frac{2}{\gamma+1} \right)^{\frac{\gamma+1}{\gamma-1}} \right\}^{1/2} \qquad \text{(A-6)}$$

The length of time that gas may be allowed to flow from the large reservoir to obtain pressure drops of 1.0, 2.5, and 5.0 psia are illustrated in Figure A-8.

FIG A8 RESERVOIR PRESSURE DROP

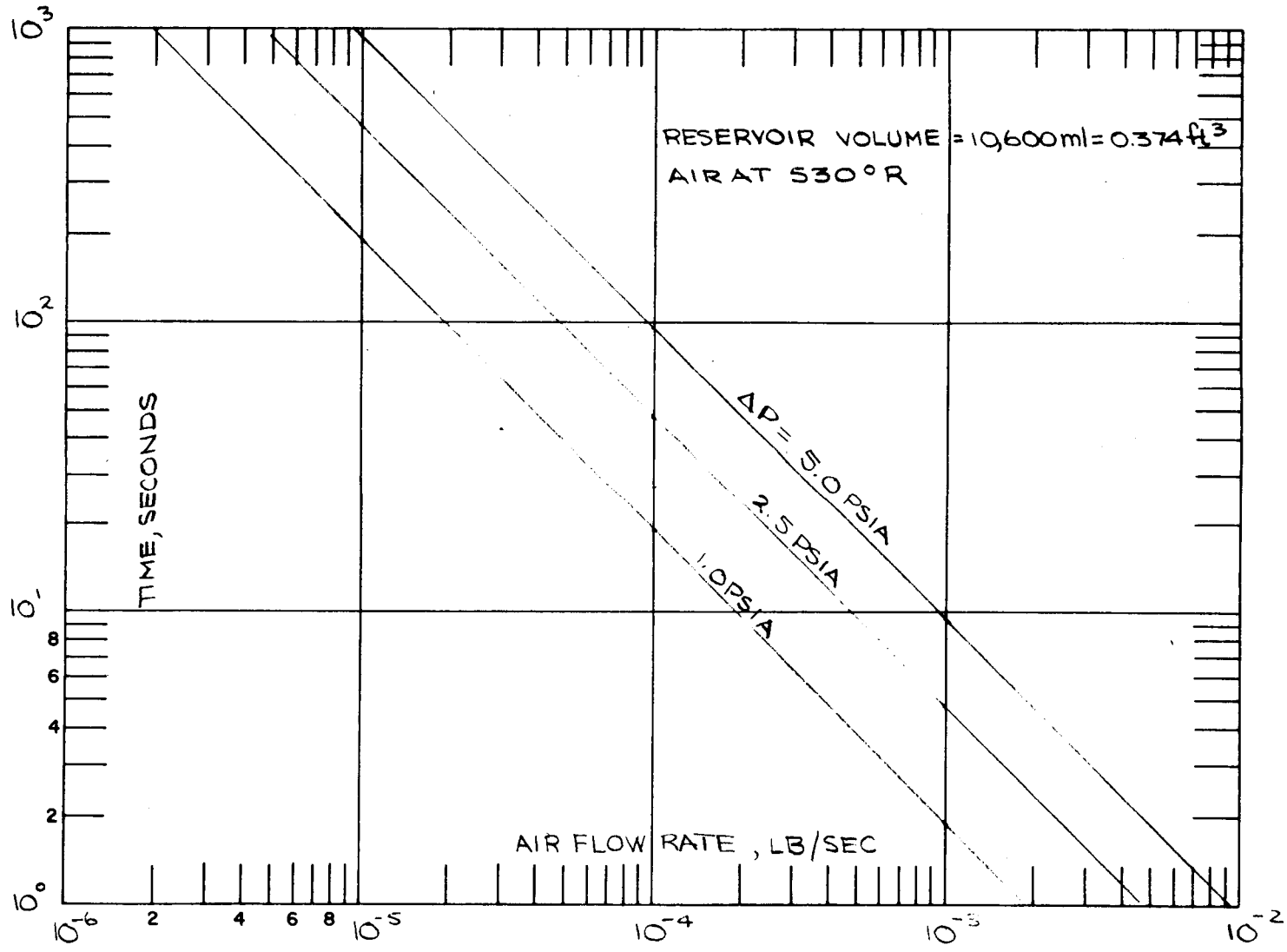

REFERENCES

1) Grey, J., "Thermodynamic Methods of High Temperature Measurements", ISA Transactions, Vol. 4, No. 2, pp. 102-115.

2) Grey, J., P. F. Jacobs and M. D. Sherman, "Calorimetric Probe for the Measurement of Extremely High Temperature", Princeton University Aeronautical Engineering Report No. 602, April 1962.

3) O'Connor, T. J., "A Split-Flow Enthalpy Probe for Measurement of Enthalpy in Highly Heated Subsonic Streams", ISA Preprint 68-539, October 1968.

4) O'Connor, T. J., E. H. Comfort and L. A. Cass, "Turbulent Mixing of Axisymmetric Jets of Partially Dissociated Nitrogen with Ambient Air", Avco RAD-TR-65-18, also AIAA Journal, 4, 11, pp. 2026-2032, November 1966.

5) Avco/RAD, Thirty-Kilowatt Plasma Jet Rocket Engine Development, Summary Report on Third Year Development Program", Avco RAD TR 64-42, July 1964, p. 200.

6) Chernyi, G. C., Introduction to Hypersonic Flow, Academic Press, New York, N. Y., pp. 136-159.

7) Thyson, N., "Aerodynamics Program 1475, Similar Solutions of the Laminar Boundary Layer Equations", Avco RAD Memo S210-TR-64-12, 5 February 1964.

8) Schurmann, E. E. H., "Engineering Methods for the Analysis of Aerodynamic Heating", Avco RAD-TM-63-68, 30 October 1963.

9) Faye-Petersen, R. "Theoretical Aerodynamic Studies of Missiles with Flared Skirts in Supersonic Upstream Flow", Proceedings of the Aerospace Forum II Session, IAS 30th Annual Meeting, New York, N. Y., January 22-24, 1962.

10) Kays, W. M., Trans., ASME 77, 1265, (1955).

11) Cohen, N. B., "Correlation Formulae and Tables of Density and Some Transport Properties of Equilibrium Dissociated Air for Use in Solutions of the Boundary Layer Equations", NASA TND-194, February 1960.

12) Perry, J. H. (Ed.) Chemical Engineers Handbook, Third Edition, McGraw-Hill, New York, N. Y., 1954, p. 388.

13) Ibid

14) McAdams, Heat Transmission, Third Edition, McGraw-Hill, New York, N. Y., 1954, p. 219.

15) Ibid, pg. 241.

16) Rohsenow, W. M. and H. Choi, Heat,Mass, and Momentum Transfer, Prentice-Hall, Englewood Cliffs, N. J., 1961, pg. 226.

17) Ibid, pg. 225.

18) Perry, J. H. (ed), Chemical Engineers Handbook, Third Edition, McGraw-Hill, New York, N. Y., pg. 390.

19) O'Connor, T. J. and E. H. Comfort, "Enthalpy-Mass Flux Impact Pressure Probe System", AFFDL-TR-68-137, December 1968.

20) Perry, J. H. (Ed), Chemical Engineers Handbook, Third Edition, McGraw-Hill, New York, N. Y., pg. 1241.

21) Shapiro, A. H., The Dynamics and Thermodynamics Of Compressible Fluid Flow, Volume I, Ronald Press, pg. 167.

22) Welch Scientific Company, Bulletin 129.

23) Perry, J. H. (Ed), Chemical Engineers Handbook, Third Edition, McGraw-Hill, New York, N. Y., pg. 403.

24) Ibid, pg. 407.

25) Streeter, V. L., Fluid Mechanics, Second Edition, McGraw-Hill, New York, N. Y., 1958, pg. 317.

26) AVCO Hyperthermal Simulation Capabilities, AVSD-0006-70-CA, 15 January 1970.